Selective Stimulation of the Subthalamic Nucleus

Daphne G.M. Zwartjes

SELECTIVE STIMULATION OF THE SUBTHALAMIC NUCLEUS

Daphne G.M. Zwartjes

This work was supported by BrainGain Smart Mix Programme of the Netherlands Ministery of Economic Affairs and the Netherlands Ministry of Education, Culture and Science.

The publication of this thesis was financially supported by the group Biomedical Signals & Systems, University of Twente and by Demcon Advanced Mechatronics.

Cover design:
Ardjan Zwartjes

Printed by:
Ipskamp drukkers, Enschede, the Netherlands

SELECTIVE STIMULATION OF THE SUBTHALAMIC NUCLEUS

PROEFSCHRIFT

ter verkrijging van
de graad van doctor aan de Universiteit Twente,
op gezag van de rector magnificus,
prof. Dr. H. Brinksma
volgens besluit van het College voor Promoties
in het openbaar te verdedigen
op vrijdag 31 mei 2013 om 14.45 uur

door

Daphne Geerke Maria Zwartjes
geboren op 25 augustus 1983
te Nijmegen

Dit proefschrift is goedgekeurd door de promotor en assistent promotor:

Prof. dr. ir. P.H. Veltink
Dr. ir. T. Heida

ISBN: 978-90-365-3530-4

Samenstelling promotiecommissie

Voorzitter/Secretaris:

Prof. dr. ir. A.J. Mounthaan	Universiteit Twente

Promotor:

Prof. dr. ir. P.H. Veltink	Universiteit Twente

Assistent promotor:

Dr. ir. T. Heida	Universiteit Twente

Leden:

Prof. dr. P.A. Tass	Research Center Jülich
Dr.ir. L.J. Bour	Academisch Medisch Centrum Amsterdam
Prof. dr. V. Subramaniam	Universiteit Twente
Prof. dr. R.J.A. van Wezel	Universiteit Twente

Paranimfen:

Peter Steenbergen

Eva C. Wentink

Contents

Chapter 1

General introduction

1.1. Parkinson's disease

Parkinson's disease (PD) is the second most common neurodegenerative disorder (Wirdefeldt et al. 2011). In 2008, about 30.000 PD patients were registered at hospitals in the Netherlands (van den Berg 2010). The number of PD patients is expected to increase by 47% from 2005 to 2025 (Speelman 2008). The median incidence of PD is estimated at 14 per 100.000, which increases to 160 when restricting the age range to 65 or 70 and older (Hirtz et al. 2007).
James Parkinson first described PD in 1817 (Parkinson 1817). PD is caused by degeneration of the substantia nigra creating a loss of dopamine. Dopamine is a neurotransmitter that acts on different types of receptors in the striatum, which is the main input station of the basal ganglia (BG) (Alexander and Crutcher, 1990). As the striatum and BG are involved in motor function, the loss of dopamine in PD impairs motor performance.
PD is characterized by several motor related symptoms including tremor, bradykinesia, i.e. reduced movement speed and amplitude, hypokinesia, i.e. poverty of movement, episodes of freezing, impaired balance and postural control, dyskinesia, i.e. overactivity of muscles, rigidity, and adaptive responses (Morris 2000). In the initial stage, PD is usually treated with Levodopa. This treatment is often very effective, but the efficacy of levodopa drops with time. The disease progressively becomes more severe and therefore it becomes increasingly difficult to treat in advanced stages. Surgical treatment in PD is usually employed when the patient responds well to medication, but experiences motor fluctuations and intolerable side effects as a result of high dosages (Limousin et al. 1998; Bronstein et al. 2011).

1.2. The basal ganglia

In the BG, five functionally different circuits run parallel to each other commencing in the cortex, going through the BG and thalamus and returning to the cortex. The motor circuit (Fig. 1A), limbic circuit, oculomotor circuit and two prefrontal circuits can be distinguished (Alexander and Crutcher 1990).
In the motor circuit, three pathways can be discerned, the hyperdirect, direct and indirect pathway (Alexander and Crutcher 1990; DeLong and Wichmann 2007). The hyperdirect pathway consists of a monosynaptic connection between the cortex and the subthalamic nucleus (STN). The STN is connected to the globus pallidus internus (GPi) and the substantia nigra pars reticulata (SNr) by an excitatory connection. Although the hyperdirect pathway has been well documented for rodents (Canteras et al. 1990), cats (Auer 1956) and primates (Petras 1969; Carpenter et al. 1981), its existence remains to be proven in human

(Marani et al. 2008). Recently, Brunenberg et al. (Brunenberg et al. 2012) were the first to support the existence of the hyperdirect pathway in human using high angular resolution diffusion imaging. The indirect pathway also originates in the cortex and is connected to the GPi/SNr via the STN, but by a polysynaptic corticosubthalamic connection: The cortex first gives rise to axons acting on D2 type dopamine receptors of striatal neurons. The striatum connects to the globus pallidus externus (GPe) providing an inhibitory input and the GPe connects to the STN also via an inhibitory pathway. The direct pathway surpasses the STN and consists of an excitatory corticostriatal connection, which acts on D1 type dopamine receptors of striatal neurons, and an inhibitory connection between the striatum and GPi/SNr. The cortico-BG-thalamocortical loop is completed by an inhibitory connection between the GPi/SNr and the thalamus and an excitatory thalamocortical connection.

For the control of voluntary limb movements, a center-surround-model has been proposed, which encompasses that the basal ganglia do not generate movement, but acts by inhibiting competing motor programs that would interfere with the desired movement (Mink 1996; Nambu et al. 2000; Nambu et al. 2002). The execution of a motor program involves the three main pathways, i.e. the hyperdirect, direct and indirect pathway. First, the hyperdirect pathway inhibits large areas of the thalamus and cortex, which are involved in the selected motor program but also in other programs. The direct pathway disinhibits only those areas involved in the selected motor program. Finally, the motor program is terminated by inhibition of the indirect pathway.

Dopamine acts on the D1 and D2 type receptors of the striatum, exciting and inhibiting these receptors respectively (Delong and Wichmann, 2007). Since the direct and indirect pathway are involved in respectively D1 and D2 type receptors, the loss of dopamine, present in PD, disrupts the balance between those pathways, and thereby disturbs the execution of motor programs. When we analyze what happens in the motor circuit in the cortico-BG-thalamocortical loop, we see the following. As the D1 type receptor is involved in the direct pathway, the loss of dopamine causes a decreased activity of the inhibitory connection between the striatum and GPi/SNr, resulting in an increased activity of the GPi/SNr. Vice versa, the D2 type receptors receive less inhibition from the decreased amount of dopamine resulting in an increased activity of the striatum-GPe connection in the indirect pathway (Alexander and Crutcher 1990)(Fig. 1B). The increased activation of the GPe causes a decreased inhibition of the STN and thereby an increased excitation of the GPi/SNr. Thus, although the loss of dopamine has opposing effects on D1 and D2 type receptors, the final effect is similar, i.e. increased GPi/SNr activity and thereby an increased inhibition of the thalamus. Because of this inhibition, signals involved in the execution of motor

programs are not properly transmitted through the thalamus, which results in impaired motor function as seen in PD.

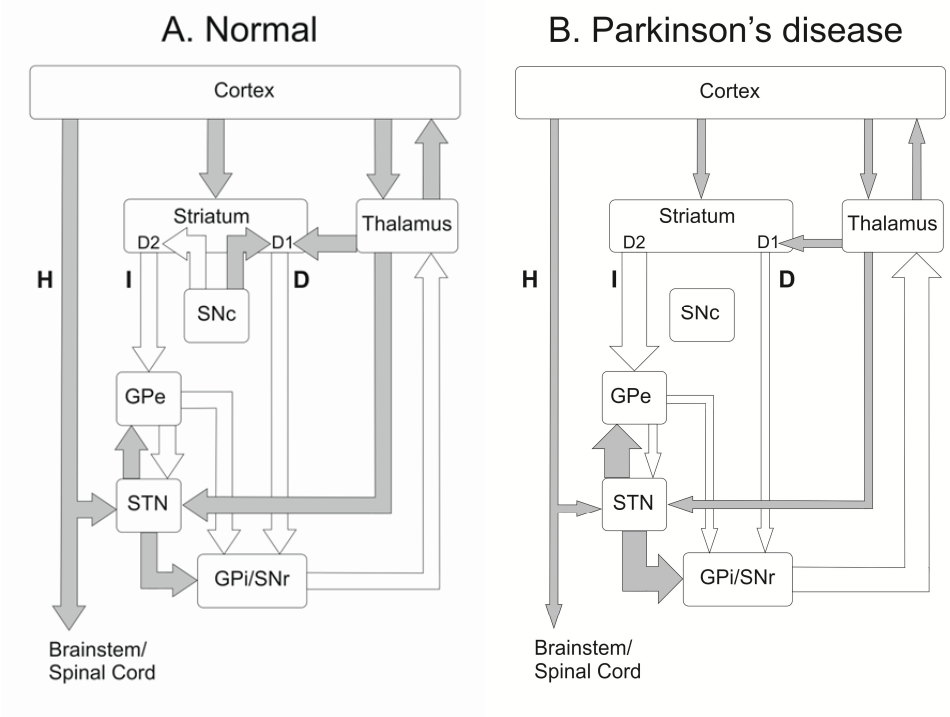

Figure 1. A schematic overview of the motor circuit. A. The circuit in the normal state. Shaded arrows are excitatory connections and white arrows are inhibitory connections. The cortex projects to the STN via the hyperdirect pathway (H). The direct pathway (D) originates in the cortex and goes via the Striatum and GPi/SNr to the Thalamus. The indirect pathway (I) consists of a cortico-striatal connection and then proceeds via an inhibitory connection to the GPe, which inhibits the STN. B. The circuit in the case of Parkinson's disease. The thickness of the arrows indicates the change in weight relative to the normal state. The loss of dopamine eventually results in an increased inhibition of the Thalamus.

The classical model described above is purely based on average firing frequencies. However, firing patterns also play an important role in PD, as a pathological bursting of neuronal discharges is observed in the STN of PD patients and animal models of PD (Bergman et al. 1994; Ni et al. 2001; Benazzouz et al. 2002; Janssen et al. 2012). This burst activity is associated with synchronized oscillations in the LFP beta frequency band (Brown 2007; Hammond et al. 2007). Recently, the role of oscillations in motor processing has been

emphasized. It has been suggested that beta oscillations in the cortico-BG-thalamocortical loop promote tonic activity at the expense of voluntary movement (Brown 2007). In an extended hypothesis, Jenkinson and Brown (Jenkinson and Brown 2011) propose that the levels of beta oscillations provide a measure of the likelihood that a new voluntary action will need to be activated. Dopamine levels modulate the beta oscillations, i.e. a high amount of dopamine suppresses beta activity, and they are modulated in response to salient internal and external cues. In PD, the loss of dopamine causes an increase in synchronized oscillatory activity in the beta band and thereby a suppression of voluntary movement.

1.3. Deep Brain Stimulation

Deep brain stimulation (DBS) is a form of neuromodulation used to treat PD. DBS improves motor function in PD-patients, which is observed in favorable effects on tremor, bradykinesia, akinesia, rigidity, postural stability, and gait disorders (Breit et al. 2004). During DBS, an electrode delivers high frequency stimulation to either the GPi, thalamus, or STN. Although DBS is being applied on all three sites, the literature tends to mark STN stimulation as the most efficient (Deuschl et al. 2006; Benabid et al. 2009; Weaver et al. 2009; Odekerken et al. 2012). Accordingly, STN stimulation has gained popularity in recent years. Although effective, the mechanisms of DBS are not yet fully understood (McIntyre et al. 2004). Currently, it is thought that DBS modulates the pathological network activity, i.e. the network becomes less susceptible to the pathological synchronized oscillations that are present in PD (McIntyre et al. 2004; Brown 2007; Hammond et al. 2007). To optimize DBS therapy new closed-loop techniques involving optimal desynchronization of networks of oscillatory neurons are emerging as well, and the first experiments on MPTP-treated nonhuman primates show favorable effects of these closed-loop stimulation techniques over conventional methods (Rosin et al. 2011; Tass et al. 2012). In the Netherlands it is estimated that up to 2011, 1000 patients have been treated with DBS (van Vugt 2011). This increase in the number of DBS interventions makes it crucial to reduce the costs of the intervention and improve the procedure.

Currently, the surgical procedure to implant the DBS electrode involves certain steps that vary between one centre to another. Generally, the procedure is carried out as follows (Machado et al.): Before surgery, imaging techniques such as magnetic resonance imaging (MRI) or computer tomography (CT) are performed. Together with a stereotactic head frame, imaging provides anatomical targeting of the STN. Frameless technologies, which do not make use of a

stereotactic frame, are emerging as well. After defining the target's location, the electrode's point of entry and the trajectory to reach the STN are defined. During surgery, the first step is the physiological mapping. This is done by either using micro-electrode recordings and subsequent microstimulation or by solely using macrostimulation (Gross et al. 2006). To study the effects of stimulation, the patient is awake during surgery. After the optimal implantation location is determined by physiological mapping, the DBS electrode is implanted in the brain and optimal stimulation settings are achieved. Stimulation is generally delivered at around 130 Hz with a pulse width of 60-210 μs and an amplitude of 1-3.5 V.

One of the major hurdles in using DBS as a therapeutic method is the occurrence of cognitive and limbic alterations (Temel et al. 2006; Witt et al. 2008). It is believed that this is caused by the fact that the STN is segregated into a sensorimotor, limbic and associative functional area (Fig. 2)(Parent and Hazrati 1995; Joel and Weiner 1997; Rodriguez-Oroz et al. 2001; Hamani et al. 2004; Lambert et al. 2012). Precise placement of the DBS electrode in the sensorimotor area is essential to avoid stimulation of the limbic or associative area, as stimulation of those areas is thought to be responsible for the side effects (Temel et al. 2005).

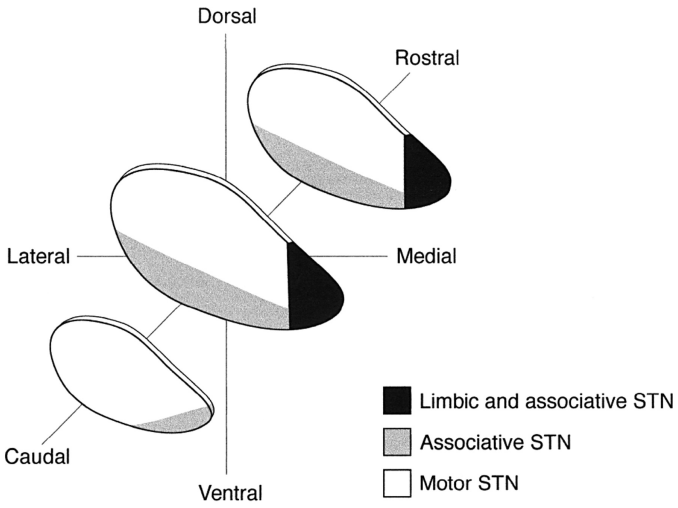

Figure 2. The STN has three functional modalities: Limbic, associative and motor (Source: Hamani et al. (Hamani et al. 2004)).

1.4. Electrophysiological measurements in the STN

The functional segregation of the STN, as depicted in Fig. 2, relates to the fact that the STN is involved in several functional circuits. Electrophysiological measurements of the motor circuit have first been performed in rats by Kitai et al. (Kitai and Deniau 1981). During this study, the motor cortical area for jaw and forearm was stimulated while simultaneous intracellular recordings were performed to sense the STN response. They reported an initial excitatory response, which was interrupted by a short inhibitory period, followed by a long inhibitory period. Several later electrophysiological studies reported the same responses to stimulation in a series of species (Fujimoto and Kita 1993; Maurice et al. 1998; Nambu et al. 2000; Kolomiets et al. 2001; Magill et al. 2004).
The first study on humans was performed by Strafella et al. (Strafella et al. 2004). They applied transcranial magnetic stimulation (TMS) of the human motor cortex and recorded the STN response. They observed the late response. Unfortunately, the existence of the early response could not be studied, because of a large stimulation artifact. Electrical stimulation of the motor cortex to locate the motor areas of the GPi and GPe has also been performed (successfully) by Nishibayashi et al. (Nishibayashi et al. 2011). MCS and subsequent STN recording has not yet been applied in human.

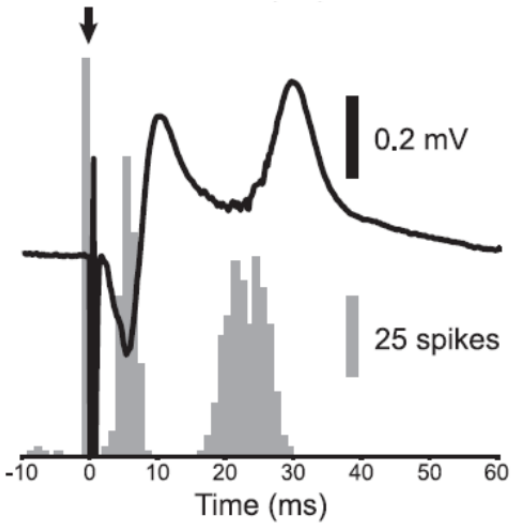

Figure 3: Typical response of the rostral STN in a rat to stimulation of the frontal cortex. The black line denotes the peristimulus local field potential, averaged over 200 sequential stimuli. The grey peristimulus time histogram of the summed unit responses to 200 sequential stimuli. (Source: Magill et al. (Magill et al. 2004))

Research on spontaneous electrophysiological measurements of the STN sensorimotor area is dominated by the analysis of local field potentials (LFPs). Recently, many studies have demonstrated the functional significance of oscillations in the STN. Different frequency bands can be distinguished: 8-13 Hz, the alpha-band, 13-30 Hz, the beta-band, and 30-80 Hz, the gamma-band. Beta oscillations have been investigated most widely. It has been shown that neural activity in the dorsolateral STN (supposedly the location of the STN sensorimotor area (Parent and Hazrati 1995; Hamani et al. 2004; Temel et al. 2005)) has elevated neural activity in the beta frequency band compared to the remaining part of the STN and regions outside the STN (Kühn et al. 2005; Chen et al. 2006; Weinberger et al. 2006; Trottenberg et al. 2007). Beta activity was found to be associated with bradykinesia and rigidity (Kühn et al. 2006; Eusebio et al. 2012). As described previously, beta oscillations promote tonic activity at the expense of voluntary movements and are modulated by dopamine (Brown 2007; Jenkinson and Brown 2011). Gamma oscillations have also been studied, but to a lesser extent (Jenkinson et al. 2012). It has been shown that gamma oscillations are promoted by dopaminergic therapy (Cassidy et al. 2002; Williams et al. 2002; Alegre et al. 2005; Fogelson et al. 2005; Androulidakis et al. 2007). Gamma oscillations are thought to be physiological rather than pathological (Brown 2003; Androulidakis et al. 2007; Jenkinson et al. 2012). Recently, Jenkinson et al. (Jenkinson et al. 2012) proposed that the function of gamma oscillations lies in the determination of response vigor, rather than arousal or determination of kinematic parameters. The spatial distribution of gamma oscillations has also been investigated. Unlike the beta oscillations, gamma oscillations were found to be increased prior to entering the STN in the zona incerta, namely 1 to 2 mm before the dorsal border of the STN (Trottenberg et al. 2006). The gamma oscillations reduced again 3 mm after the STN dorsal border. A third frequency band of interest is the alpha band. Alpha oscillations are believed to be related to rest and kinetic tremor (Brown 2003). It has been shown that alpha oscillations increase upon entering the STN and remain elevated throughout the entire STN (Trottenberg et al. 2007).

1.5. Objective assessment of motor function

In order to judge the success of a treatment dopaminergic as well as surgical interventions have to be well monitored. Currently, the golden standard are clinical examinations such as the unified Parkinson´s disease rating scale (UPDRS)(Fahn and Elton 1987) and Hoehn & Yahr scale (Hoehn and Yahr 1967), but in the last decades strategies providing objective and ambulant assessment have emerged (Dunnewold et al. 1997; Hoff et al. 2001; Salarian

2006; Someren et al. 2006). These methods generally use objective measurement equipment such as accelerometers and gyroscopes and allow for detailed and extensive monitoring of multiple PD symptoms.

1.6. Aim of the project

To optimize DBS of the STN in PD, we hypothesize that the STN sensorimotor area should be targeted. In this way, the effect of DBS treatment on motor function will be optimal and cognitive or limbic side effects will be reduced as stimulation of different functional areas is avoided. Different approaches can be undertaken to locate the STN sensorimotor area. One approach is to apply motor cortex stimulation (MCS) and measure the response in the STN. We hypothesize that in PD patients MCS evokes a specific response in the STN sensorimotor area, which can be seen in both the single unit activity and the LFP. A second approach to locate the STN sensorimotor area is through sensing of the spontaneous LFPs. In order to determine whether the novel methods to improve DBS have the anticipated effect, an objective ambulatory system to assess motor function in PD over long term is desirable. To study the effects of the therapy on different aspects of PD, such a system should be able to assess each individual aspect of motor performance in detail. This allows for optimal improvement of treatment strategies.

1.7. Thesis outline

First, I explore the approach to locate the STN sensorimotor area that involves the use of MCS. In chapter 2, the responses in the unit activity are presented, and chapter 3 reveals the LFP responses to cortical stimulation.
To evaluate what happens at a neuronal level in the motor cortex during stimulation, a model was created in chapter 4. The model focuses on selective stimulation of certain neuronal populations in the motor cortex in relation to chronic epidural stimulation for PD. It is, however, also usable for the purpose to improve selective stimulation of the cortical neuronal populations evoking the STN response, which may eventually also be applied as a therapeutic method.
In chapter 5, I study the functional segregation of the cortical neuronal input in the rat STN. Therefore, I use the inverse current source density (CSD) method to estimate the CSD from cortically evoked subthalamic local field potentials. In future, this is a potential approach for locating the STN sensorimotor area during DBS surgery in human.
The approach to find the STN sensorimotor area using spontaneous LFPs is introduced in chapter 6. In this chapter, I examine the spontaneous LFPs in the

sensorimotor STN, the non-sensorimotor STN and the area dorsal to the STN. It is assessed whether the supposed STN sensorimotor area shows distinctive LFP oscillations in the gamma frequency band.
In the 7th chapter, I introduce a method to objectively assess whether therapy improves certain aspects of motor function in PD in a quantitative manner during normal daily activities. In this way, I can determine which motor aspects are improved with certain therapies and study the effects in detail.

References

Alegre, M., F. Alonso-Frech, M. C. Rodriguez, J. Guridi, I. Zamarbide, M. Valencia, M. Manrique, J. A. Obeso and J. Artieda (2005). "Movement-related changes in oscillatory activity in the human subthalamic nucleus: ipsilateral vs. contralateral movements." Eur. J. Neurosci. 22: 2315-2324.

Alexander, G. E. and M. D. Crutcher (1990). "Functional architecture of basal ganglia circuits: neural substrates of parallel processing." Trends Neurosci. 13(7): 266-271.

Androulidakis, A. G., A. A. Kühn, C. C. Chen, P. Blomstedt, F. Kempf, A. Kupsch, G. H. Schneider, L. Doyle, P. Dowsey-Limousin, M. I. Hariz and P. Brown (2007). "Dopaminergic therapy promotes lateralized motor activity in the subthalamic area in Parkinson's disease." Brain 130: 457-468.

Auer, J. (1956). "Terminal degeneration in the diencephalon after ablation of the frontal cortex in the cat." J. Anat. 90: 30-41.

Benabid, A. L., S. Chabardes, J. Mitrofanis and P. Pollak (2009). "Deep brain stimulation of the subthalamic nucleus for the treatment of Parkinson's disease." Lancet Neurol. 8: 67-81.

Benazzouz, A., S. Breit, A. Koudsie, P. Pollak, P. Krack and A. L. Benabid (2002). "Intraoperative microrecordings of the subthalamic nucleus in Parkinson's disease." Mov. Disord. 17(Suppl 3): S145-149.

Bergman, H., T. Whichmann, B. Karmon and M. R. DeLong (1994). "The primate subthalamic nucleus. II. Neuronal activity in the MPTP model of parkinsonism." J. Neurophysiol. 72(2): 507-520.

Breit, S., J. B. Schulz and A.-L. Benabid (2004). "Deep brain stimulation." Cell and Tissue Research 318(1): 275-288.

Bronstein, J. M., M. Tagliati, R. L. Alterman, A. M. Lozano, J. Volkmann, A. Stefani, F. B. Horak, M. S. Okun, K. D. Foote, P. Krack, R. Pahwa, J. M. Henderson, M. Hariz, R. A. Bakay, A. Rezai, W. J. Marks, E. Moro, J. L. Vitek, F. M. Weaver, R. E. Gross and M. R. Delong (2011). "Deep Brain Stimulation for Parkinson Disease. An expert consensus and review of key issues." Arch. Neurol. 68(2): 165-171.

Brown, P. (2003). "Oscillatory nature of human basal ganglia activity: relationship to the pathophysiology of Parkinson's disease." Mov. Disord. 18: 357-363.

Brown, P. (2007). "Abnormal oscillatory synchronisation in the motor system leads to impaired movement." Curr. Opin. Neurobiol. 17: 656-664.

Brunenberg, E. L. J., P. Moeskops, W. H. Backes, C. Pollo, L. Cammoun, A. Vilanova, M. L. F. Janssen, V. Visser-Vandewalle, B. M. ter Haar Romeny, J. Thiran and B. Platel (2012). "Structural and Resting State Functional Connectivity of the Subthalamic Nucleus: Identification of Motor STN Parts and the Hyperdirect Pathway." PloS One 7(6): e39061.

Canteras, N. S., A.-L. Shammah-Lagnado, A. Silva and J. A. Ricardo (1990). "Afferentconnections of the subthalamic nucleus: a combined retrograde and anterograde horseradish peroxidase study in the rat." Brain Res. 513: 43-59.

Carpenter, M. B., S. C. Carleton, J. F. Keller and P. Conte (1981). "Connections of the subthalamic nucleus in the monkey." Brain Res. 224: 1-29.

Cassidy, M., P. Mazzone, A. Oliviero, A. Insola, P. Tonali, V. Di Lazzaro and P. Brown (2002). "Movement-related changes in synchronization in the human basal ganglia." Brain 125: 1235-1246.

Chen, C. C., A. Pogosyan, L. U. Zrinzo, S. Tisch, P. Limousin, K. Ashkan, T. Yousry, M. I. Hariz and P. Brown (2006). "Intra-operative recordings of local field potentials can help localize the subthalamic nucleus in Parkinson's disease surgery." Exp. Neurol. 198: 214-221.

DeLong, M. R. and T. W. Wichmann (2007). "Circuits and circuit disorders of the basal ganglia." Arch. Neurol. 64: 20-24.

Deuschl, G., C. Schade-Brittinger, P. Krack, J. Volkmann, H. Schafer, K. Botzel, C. Daniels, A. Deutschlander, U. Dillmann, W. Eisner, D. Gruber, W. Hamel, J. Herzog, R. Hilker, S. Klebe, M. Kloss, J. Koy, M. Krause, A. Kupsch, D. Lorenz, S. Lorenzl, H. M. Mehdorn, J. R. Moringlane, W. Oertel, M. O. Pinsker, H. Reichmann, A. Reuss, G. H. Schneider, A. Schnitzler, U. Steude, V. Sturm, L. Timmermann, V. Tronnier, T. Trottenberg, L. Wojtecki, E. Wolf, W. Poewe and J. Voges (2006). "A randomized trial of deep-brain stimulation for Parkinson's disease." N. Engl. J. Med. 355: 896-908.

Dunnewold, R. J. W., C. E. Jacobi and J. J. van Hilten (1997). "Quantitative assessment of bradykinesia in patients with parkinson'sdisease." J Neurosc Meth 74(1): 107-112.

Eusebio, A., H. Cagnan and P. Brown (2012). "Does suppression of oscillatory synchronisation mediate some of the therapeutic effects of DBS in patients with Parkinson's disease?" Front. Integr. Neurosci. 6(47): 1-9.

Fahn, S. and R. L. Elton (1987). Unified Parkinson's Disease Rating Scale development Committee: Unified Parkinson's Disease Rating Scale. Recent developments in Parkinson's disease. S. Fahn, C. D. Marsden and D. Calne. New York, Macmillan**:** 153-164.

Fogelson, N., A. Pogosyan, A. A. Kühn, A. Kupsch, G. van Bruggen, H. Speelman, M. Tijssen, A. Quartarone, A. Insola, P. Mazzone, V. Di Lazzaro, P. Limousin and P. Brown (2005). "Reciprocal interactions between oscillatory activities of different frequencies in the subthalamic region of patients with Parkinson's disease." Eur. J. Neurosci. 22: 257-266.

Fujimoto, K. and H. Kita (1993). "Response characteristics of subthalamic neurons to the stimulation of the sensorimotor cortex in the rat." Brain Res. 609: 185-192.

Gross, R. E., P. Krack, M. C. Rodriguez-Oroz, A. R. Rezai and A.-L. Benabid (2006). Electrophysiological mapping for the implantation of deep brain stimulators for Parkinson's disease and tremor. 21**:** S259-S283.

Hamani, C., J. A. Saint-Cyr, J. Fraser, M. Kaplitt and A. M. Lozano (2004). "The subthalamic nucleus in the context of movement disorders." Brain 127(1): 4-10.

Hammond, C., H. Bergman and P. Brown (2007). "Pathological synchronization in Parkinson's disease: networks models and treatments." Trends Neurosci. 30(7): 357-364.

Hirtz, D., D. J. Thurman, K. Gwinn-Hardy, M. Mohamed, A. R. Chaudhuri and R. Zalutsky (2007). "How common are the "common" neurologic disorders?" Neurology 69: 326-337.

Hoehn, M. and M. Yahr (1967). "Parkinsonism: onset, progression and mortality." Neurology 17: 427-442.

Hoff, J., E. A. Wagemans and J. J. van Hilten (2001). "Ambulatory objective assessment of tremor in Parkinson's disease." Clin. Neuropharmacol. 24(5): 280/283.

Janssen, M. L. F., D. G. M. Zwartjes, S. Tan, R. Vlamings, M. Jahanshahi, T. Heida, G. Hoogland, W. M. Steinbusch, V. Visser-Vandewalle and Y. Temel (2012). "Mild dopaminergic lesions are accompanied by robust changes in subthalamic nucleus activity." Neurosci. Lett. 508: 101-105.

Jenkinson, N. and P. Brown (2011). "New insights into the relationship between dopamine, beta oscillations and motor function." Trends Neurosci. 34(12): 611-618.

Jenkinson, N., A. A. Kühn and P. Brown (2012). "Gamma oscillations in the human basal ganglia." Exp Neurol.

Joel, D. and I. Weiner (1997). "The connection of the primate subthalamic nucleus: indirect pathways and the open-interconnected scheme of basal ganglia-thalamocortical circuitry." Brain Res. Rev. 23: 62-78.

Kitai, S. T. and J. M. Deniau (1981). "Cortical inputs to the subthalamus: intracellular analysis." Brain Research 214(2): 411-415.

Kolomiets, B. P., J. M. Deniau, P. Mailly, A. Menetrey, J. Glowinski and A. Thierry (2001). "Segregation and Convergence of Information Flow through the Cortico-Subthalamic Pathways " J. Neurosci. 21(15): 5764-5772.

Kühn, A. A., A. Kupsch, G. H. Schneider and P. Brown (2006). "Reduction in subthalamic 8–35 Hz oscillatory activity correlates with clinical improvement in Parkinson's disease." Eur. J. Neurosci. 23: 1956-1960.

Kühn, A. A., T. Trottenberg, A. Kivi, A. Kupsch, G. H. Schneider and P. Brown (2005). "The relationship between local field potential and neuronal discharge in the subthalamic nucleus of patients with Parkinson's disease " Exp Neurol 194: 212-220.

Lambert, C., L. Zrinzo, Z. Nagy, A. Lutty, M. Hariz, T. Foltynie, B. Draganski, J. Ashburner and R. Frackowiak (2012). "Confirmation of functional zones within

the human subthalamic nucleus: Patterns of connectivity and sub-parcellation using diffusion weighted imaging." Neuroimage 60: 83-94.

Limousin, P., P. Krack, P. Pollak, A. Benazzouz, C. Ardouin, D. Hoffmann and A. L. Benabid (1998). "Electrical Stimulation of the Subthalamic Nucleus in Advanced Parkinson's Disease." N. Engl. J. Med. 339: 1105-1111.

Machado, A., A. R. Rezai, B. H. Kopell, R. E. Gross, A. D. Sharan and A.-L. Benabid (2006). Deep brain stimulation for Parkinson's disease: Surgical technique and perioperative management. 21**:** S247-S258.

Magill, P. J., A. Sharott, M. D. Bevan, P. Brown and J. P. Bolam (2004). "Synchronous unit activity and local field potentials evoked in the subthalamic nucleus by cortical stimulation." Journal of Neurophysiology 92: 700-714.

Magill, P. J., A. Sharott, M. D. Bevan, P. Brown and J. P. Bolam (2004). "Synchronous unit activity and local field potentials evoked in the subthalamic nucleus by cortical stimulation." J. Neurophysiol. 92: 700-714.

Marani, E., T. Heida, E. A. J. F. Lakke and K. G. Usunoff (2008). The subthalamic nucleus. Part I: Development, Cytology, Topography and Connections. Berlin, Springer-Verlag.

Maurice, N., J. M. Deniau, J. Glowinski and A. Thierry (1998). "Relationships between the prefrontal cortex and the basal ganglia in the rat Physiology of the corticosubthalamic circuits." J. Neurosci. 18(22): 9539-9546.

McIntyre, C. C., M. Savasta, L. Kerkerian-Le Goff and J. L. Vitek (2004). "Uncovering the mechanisms of action of deep brain stimulation Activation inhibition or both." Clin. Neurophysiol. 115: 1239-1248.

Mink, J. W. (1996). "The basal ganglia: focused selection and inhibition of competing motor programs." Prog. Neurobiol. 50: 381-425.

Morris, M. E. (2000). "Movement disorders in people with Parkinson's disease: A model for physical therapy." Phys. Ther. 80: 578-597.

Nambu, A., H. Tokuno, I. Hamada, H. Kita, M. Imanishi, T. Akazawa, Y. Ikeuchi and N. Hasegawa (2000). "Excitatory cortical inputs to pallidal neurons via the subthalamic nucleus in the monkey." J. Neurophysiol. 84: 289-300.

Nambu, A., H. Tokuno and M. Takada (2002). "Functional significance of the cortico-subthalamo-pallidal 'hyperdirect' pathway." Neurosci. Res. 43: 111-117.

Ni, Z., R. Boualli-Benazzouz, D. Gao, A. L. Benabid and A. Benazzouz (2001). "Intrasubthalamic injection of 6-Hydroxydopamine induces changes in the firing rate and pattern of Subthalamic nucleus neurons in the rat." Synapse 40: 145-153.

Nishibayashi, H., M. Ogura, K. Kakishita, S. Tanaka, Y. Tachibana, A. Nambu, H. Kita and T. Itakura (2011). "Cortically Evoked Responses of Human Pallidal Neurons Recorded During Stereotactic Surgery." Mov. Disord. 26(3): 469-476.

Odekerken, V., T. van Laar, M. Staal, A. Mosch, C. Hoffmann, P. Nijssen, G. Beute, J. van Vugt, M. Lenders, M. F. Contarino, M. Mink, L. Bour, P. van den Munckhof, B. Schmand, R. de Haan, P. Schuurman and R. de Bie (2012). "Subthalamic nucleus versus globus pallidus bilateral deep brain stimulation for

advanced Parkinson's disease (NSTAPS study): a randomised controlled trial." Lancet Neurol.

Parent, A. and L. Hazrati (1995). "Functional anatomy of the basal ganglia. II. The place of the subthalamic nucleus and external pallidum in basal ganglia circuitry." Brain Res. Rev. 20: 128-154.

Parkinson, J. (1817). An essay on the shaking palsy. London, Whittingham and Rowland.

Petras, J. M. (1969). "Some efferent connections of the motor and somatosensory cortex of simian primates and felid, canid and procyonid carnivores." Annals of the New York Academy of Sciences 167(1): 469-505.

Rodriguez-Oroz, M. C., M. Rodriguez, J. Guridi, K. Mewes, V. Chockkman, J. L. Vitek, M. R. DeLong and J. A. Obeso (2001). "The subthalamic nucleus in Parkinson's disease: somatotopic organization and physiological characteristics." Brain 124: 1777-1790.

Rosin, B., M. Slovik, R. Mitelman, M. Rivlin-Etzion, S. N. Haber, Z. Israel, E. Vaadia and H. Bergman (2011). "Closed-Loop Deep Brain Stimulation Is Superior in Ameliorating Parkinsonism." Neuron 72(2): 370-384.

Salarian, A. (2006). Ambulatory monitoring of motor functions in patients with Parkinson's disease using kinematic sensors, Ecole polytechnique federale de Lausanne.

Someren, E. J. W., M. Pticek, J. D. Speelman, P. R. Schuurman, R. Esselink and D. F. Swaab (2006). "New actigraph for long-term tremor recording." Mov. Disord. 21(8): 1136-1143.

Speelman, J. D. (2008). "Ziekte van Parkinson samengevat." from <http://www.nationaalkompas.nl> Nationaal Kompas Volksgezondheid\Gezondheid en ziekte\Ziekten en aandoeningen\Zenuwstelsel en zintuigen\Ziekte van Parkinson.

Strafella, A. P., Y. Vanderwerf and A. F. Sadikot (2004). "Transcranial magnetic stimulation of the human motor cortex influences the neuronal activity of subthalamic nucleus " European Journal of Neuroscience 20(8): 2245-2249.

Tass, P. A., L. Qin, C. Hauptmann, S. Dovero, E. Bezard, T. Boraud and W. G. Meissner (2012). "Coordinated reset has sustained aftereffects in Parkinsonian monkeys." Ann Neurol 72(5): 816-820.

Temel, Y., A. Blokland, W. M. Steinbusch and V. Visser-Vandewalle (2005). "The functional role of the subthalamic nucleus in cognitive and limbic circuits." Prog. Neurobiol. 76: 393-413.

Temel, Y., A. Kessels, S. Tan, A. Topdag, P. Boon and V. Visser-Vandewalle (2006). "Behavioural changes after bilateral subthalamic stimulation in advanced Parkinson disease: A systematic review." Parkinsonism & Related Disorders 12(5): 265-272.

Trottenberg, T., N. Fogelson, A. A. Kühn, A. Kivi, A. Kupsch, G. H. Schneider and P. Brown (2006). "Subthalamic gamma activity in patients with Parkinson's disease." Exp Neurol 200: 56-65.

Trottenberg, T., A. Kupsch, G. H. Schneider, P. Brown and A. A. Kühn (2007). "Frequency-dependent distribution of local field activity within the subthalamic nucleus in Parkinson's disease " Exp Neurol 205(1): 287-291.

van den Berg, B. (2010). De ziekte van parkinson en parkinsonisme in nederland. Een schatting van de prevalentie en incidentie op basis van data uit het DBC Informatie Systeem. Amsterdam, Regioplan Beleidsonderzoek. 1951.

van Vugt, J. P. P. (2011). "Een stimulerend ritme tegen chorea?" Tijdschr Neurol Neurochir 112: 175-176.

Weaver, F. M., K. Follett, M. Stern, K. Hur, C. Harris, W. J. Marks, J. Rothlind, O. Sagher, D. Reda, C. S. Moy, R. Pahwa, K. Burchiel, P. Hogarth, E. C. Lai, J. E. Duda, K. Holloway, A. Samii, S. Horn, J. M. Bronstein, G. Stoner, J. Heemskerk and G. D. Huang (2009). "Bilateral deep brain stimulation vs best medical therapy for patients with advanced Parkinson disease: a randomized controlled trial." JAMA 301: 63-73.

Weinberger, H., N. Mahant, W. D. Hutchison, L. A.M., E. Moro, M. Hodaie, A. E. Lang and J. O. Dostrovsky (2006). "Beta oscillatory activity in the subthalamic nucleus and its relation to dopeminergic response in Parkinson's disease " J Neurophysiol 96: 3248-3256.

Williams, D., M. Tijssen, G. van Bruggen, A. Bosch, A. Insola, V. Di Lazzaro, P. Mazzone, A. Oliviero, A. Quartarone, H. Speelman and P. Brown (2002). "Dopamine-dependent changes in the functional connectivity between basal ganglia and cerebral cortex in humans." Brain 125: 1558-1569.

Wirdefeldt, K., H. Adami, P. Cole, D. Trichopoulos and J. Mandel (2011). "Epidemiology and etiology of Parkinson's disease: a review of the evidence." Eur. J. Epidemiol. 26: S1-S58.

Witt, K., C. Daniels, J. Reiff, P. Krack, J. Volkmann, M. O. Pinsker, M. Krause, V. Tronnier, M. Kloss, A. Schnitzler, L. Wojtecki, K. Botzel, A. Danek, R. Hilker, V. Sturm, A. Kupsch, E. Karner and G. Deuschl (2008). "Neurophysiological and psychiatric changes after deep brain stimulation for Parkinson's disease: a randomised, multicentre study." Lancet Neurol. 7: 605-614.

Chapter 2

Subthalamic neuronal responses to cortical stimulation

Marcus L.F. Janssen
Daphne G.M. Zwartjes
Yasin Temel
Vivianne van Kranen-Mastenbroek
Annelien Duits
Lo J. Bour
Peter H. Veltink
Tjitske Heida
Veerle Visser-Vandewalle

Mov Dis, 2012, 27(3): 435-438

Abstract

Objective
Deep brain stimulation of the subthalamic nucleus alleviates motor symptoms in Parkinson's disease patients. However, some patients suffer from cognitive and emotional changes. These side effects are most likely caused by current spread to the cognitive and limbic territories in the subthalamic nucleus. The aim of this study was to identify the motor part of the subthalamic nucleus to reduce stimulation-induced behavioral side effects, by using motor cortex stimulation.

Methods
We describe the results of subthalamic nucleus neuronal responses to stimulation of the hand area of the motor cortex and evaluate the safety of this novel technique.

Results
Responses differed between regions within the subthalamic nucleus. In the anterior and lateral electrode at dorsal levels of the subthalamic nucleus, an early excitation (~5–45 ms) and subsequent inhibition inhibition (45–105 ms) were seen. The lateral electrode also showed a late excitation (~125–160 ms). Focal seizures were observed following motor cortex stimulation.

Conclusions
To prevent seizures the current density should be lowered, so that motor cortex stimulation evoked responses can be safely used during deep brain stimulation surgery.

2.1. Introduction

Deep brain stimulation (DBS) of the subthalamic nucleus (STN) alleviates motor symptoms in Parkinson's disease (PD) patients (Rodriguez-Oroz et al. 2004; Deuschl et al. 2006; Weaver et al. 2009). However, in a substantial number of patients the improvement of motor symptoms is accompanied by cognitive and/or limbic alterations (Berney et al. 2002; Piasecki and Jefferson 2004; Smeding et al. 2006; Temel et al. 2006; Witt et al. 2008). These behavioral side effects are thought to be caused by stimulation of the associative and limbic areas in the STN (Temel et al. 2005). Therefore, the optimal target is the dorsolateral part of the STN, supposedly the STN motor area (Hamani et al. 2004). Optimization, to identify the motor part, is currently done by intra-operative neurophysiological measurements, such as spontaneous neuronal firing, neuronal kinesthetic responses and beta-power in the local field potential (Chen et al. 2006; Gross et al. 2006; de Solages et al. 2011). Earlier, Nishibayashi et al. (Nishibayashi et al. 2011) applied subdural motor cortex stimulation (MCS) in humans in order to identify the motor area of the globus pallidus internus and externus. This report will provide insight in the cortically evoked responses of the human STN neurons. The aim of the study was to identify the STN motor area by using MCS in order to reduce stimulation induced behavioral side effects. In this study, we tested the feasibility of identifying the STN motor part by motor cortex stimulation and evaluated the safety of this novel approach.

2.2. Methods

Patients

The study was approved by the Medical Ethical Committee of the Maastricht University Medical Center and all patients gave written informed consent. Patients were informed about the additional burr hole, subdural placement of the stimulation electrode and its additional potential complications, like the risk of a bleeding or a seizure. In- and exclusion criteria were the same as for standard DBS STN. In total, five PD patients with an age ranging between 55 and 70 years old were enrolled in this study.

Procedure

The procedure and results described below are from the fifth patient, because the stimulation protocols used in the other patients did not result in a STN response due to saturation of the amplifier in the first two patients and suboptimal MCS protocols in the remaining two patients (table 1). The day before the DBS procedure transcranial magnetic stimulation (TMS) was performed to localize the

hand area of the motor cortex. The stereotactic procedure was performed under local anesthesia. Preoperatively, the patient was loaded with 15 mg/kg Diphantoine intravenously in ninety minutes. A strip of four electrodes (AD-Tech, model TS04R-SP10X-000; Racine, USA) was placed in the subdural space through a burr hole posterolateral to the hand area (identified by TMS). The strip electrode position was verified by performing a motor evoked potential (MEP) registration at the contralateral hand and arm and the stimulation amplitude threshold was obtained. Subsequently, five micro-electrodes (InoMed, MicroMacroElectrode) were simultaneously inserted towards the STN through a precoronal burr hole. After baseline recordings, cortical evoked neuronal activity was measured using a multiple channel registration system (InoMed, ISIS MER System; stimulation settings: bipolar, monophasic, 0.2 ms, 15mA). After acquiring the cortically evoked responses, surgery was continued according to the standard procedure (Medtronic, Columbia Heights, Minneapolis, USA, model 3389) (Temel et al. 2007). On the left side, the standard surgical procedure was performed without cortical stimulation. Three to four days after surgery, the electrodes were connected to an internal pulse generator (Medtronic, Kinetra, Model 7428).

Table 1. The different motor cortex stimulation protocols used in all patients and the responsiveness of the subthalamic neurons to the applied protocol.

Monopolar/ bipolar	Anodal/ cathodal	Amplitude (times MEP level)	STN response
Monopolar	Anodal	0.33	No
		0.5	No
		0.67	No
		1	No
		1.5	No
	Cathodal	0.5	No
		1	No
Bipolar		0.33	No
		0.67	No
		1	Yes (partial)
		2	Yes

The stimulation protocols that evoked a STN response were only used in the fifth patient. MEP, motor-evoked potential; STN, subthalamic nucleus.

Data analysis

Data analysis was performed in Matlab (MathWorks, Natick, MA, USA). First, offset and drift were removed from the signal by a high-pass butterworth filter at 5 Hz. Subsequently, the stimulation artifact was removed. To assess multi/single unit activity, each epoch was digitally filtered between 350 and 5000 Hz. Spike detection was performed using the envelope method (Dolan et al. 2009). To

obtain single unit activity, spike sorting was performed by computing the principal components, which were clustered using either K-means or the Gaussian mixture model and the expectation maximization algorithm (Lewicki 1998). After spike detection, peristimulus time histograms (PSTHs) from 100 ms before until 200 ms after stimulation were constructed from 200 sweeps, grouping all trials with a specific stimulation setting. Bins of 1 ms were used and bins 1 ms before and 2 ms after cortical stimulation were set to zero to avoid any remaining stimulation artifact to be mistaken for spikes. To determine significant excitatory and inhibitory responses from the PSTHs, changing points indicating increases and decreases of the PSTH were detected using the change point analyzer software (Taylor 2000; Magill et al. 2004). The periods between two changing points were tested for having a significantly different firing rate compared to the 100 ms preceding stimulation. This was done using a two-tailed t-test with a 5% significance level. STN borders were determined by the intra-operative observations of the neurophysiologist and the post-operative analysis of the micro electrode recordings (MER).

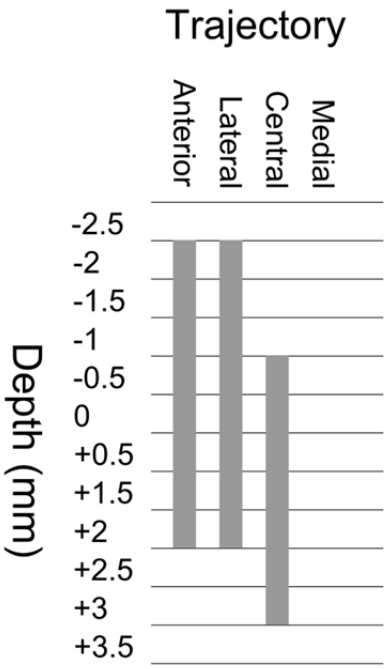

Figure 1. An overview of the depths at which the trajectories were inside the STN. A depth of 0 mm corresponds to the pre-operatively determined target.

2.3. Results

The STN was entered at a depth of 2 mm above target and left at 2.5 mm below target on the anterior and lateral trajectories (Fig. 1). The central trajectory was within the STN from 0.5 mm to 3.5 mm below target, while the medial trajectory did not go through the STN. The posterior channel was defect and could not be analyzed. We measured 8 neurons inside the STN at various locations in this patient. The neurons had an average firing rate of 47±25 Hz. Four neurons had a bursting pattern, three neurons showed a random pattern and one neuron showed a regular firing pattern (Kaneoke and Vitek 1996; Benazzouz et al. 2002). Statistically significant responses in the STN were observed when MCS was performed with a single monophasic pulse (0.2 ms duration) at 15 mA and bipolar settings. Excitations ranged from a 30% to a 103% increase in firing rate relatively to the 100 ms period preceding stimulation, while the inhibitory periods ranged from an 11% to a 76% decrease in firing rate (Fig. 2). After each cortical stimulus, a clear contraction of the contralateral hand musculature was observed. Both spontaneous unit activity and unit responses to cortical stimulation were recorded from target -1.5 until target +2.5 mm. Inside the STN, responses to MCS were found, while outside of the STN no responses were observed except for the medial electrode at 2.5 mm from target (Fig. 2). Responses varied between different depths and between different locations in the anterior-posterior and medio-lateral plane within the STN.
A focal seizure was seen in the first two patients; therefore Diphantoine was given pre-operatively in the three following patients with approval of the Medical Ethical Committee. No seizures were present in patients 3 and 4. Unfortunately, the fifth patient also had a focal seizure. In all patients, the seizure started in the contralateral hand area corresponding with the cortical stimulation side, with repetitive twitching. The seizure did not occur during stimulation, but with a latency period of more than one hour. The seizure could be controlled by acute application of additional i.v. anti-epileptic drugs. The anti-epileptics were stopped before discharge from the hospital. In the follow-up, no recurrent seizures occurred.

2.4. Discussion

The goal of this study was to provide insight in the cortically evoked responses of the human STN and evaluate the safety of this approach. We observed significant excitations and inhibitions as a response to MCS. Responses varied between different depths and between different locations in the anterior-posterior and medio-lateral plane within the STN. These responses can be used

to identify the motor area of the STN. Selective DBS of the motor part of the STN has the potential to prevent unwanted behavioral side effects.

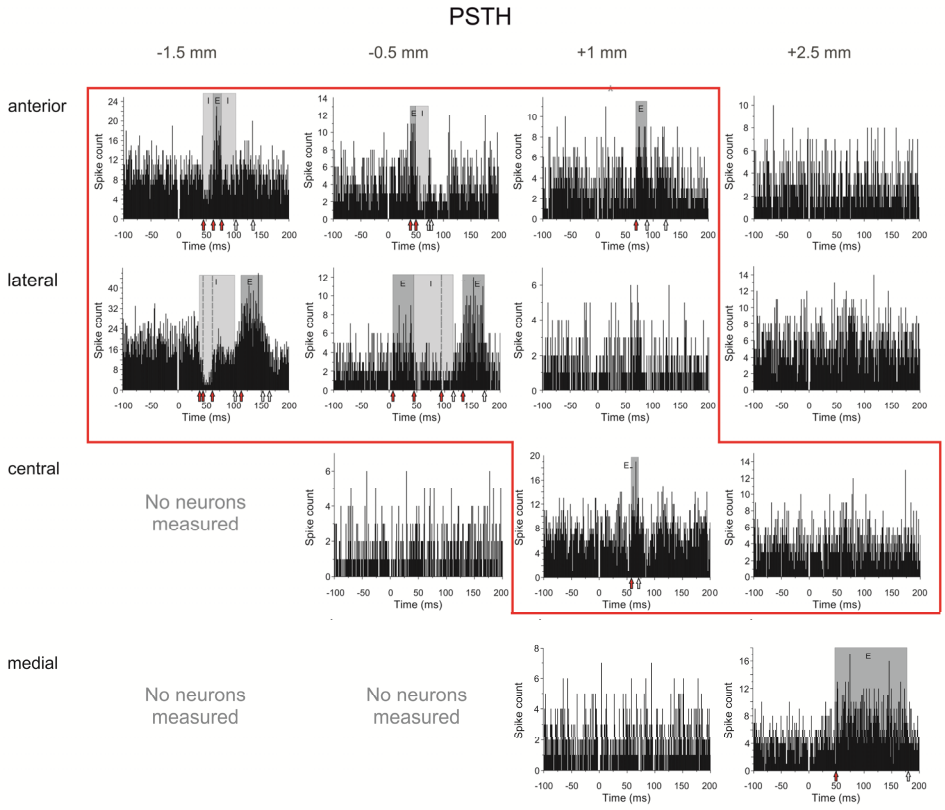

Figure 2. PSTHs of neuronal recordings starting 0.5 mm after the electrode first enters the STN (1.5 mm above target) until the last electrode leaves the STN (2.5 mm below target). Recordings inside the STN are enclosed with a red window. MCS was performed with a bipolar electrode configuration using a monophasic pulse with an amplitude of 15 mA and a duration of 0.2 ms. The arrows at the x-axis indicate the significant changes that were identified with the change point analysis. The red arrows specify changes after which a significant increase or decrease in firing rate relatively to the 100-ms preceding stimulation was found. These periods are also indicated with shaded areas in which "I" denotes a period of inhibition, while "E" represents a period of excitation. When 2 periods of inhibition occurred after each other, a change is indicated with a dashed line. The white arrows signify a change after which no significant increase or decrease in firing was found. No results at −1.5 mm on the medial and central electrode are shown, as no neurons were measured on these locations. MCS, motor cortex stimulation; PSTH, peristimulus time histogram; STN, subthalamic nucleus.

Studies in rats and primates showed typical triphasic responses, consisting of an initial excitation, a subsequent inhibition and a second excitation (Fujimoto and Kita 1993; Maurice et al. 1998; Nambu et al. 2000; Magill et al. 2004). In contrast to intra-cortical stimulation electrodes in animal studies, we used flat stimulation electrodes placed on the cortical surface. It is likely that the difference in methodology is responsible for the lack of clear tri-phasic responses in human studies (Strafella et al. 2004). On the other hand, a contraction of the contralateral hand musculature was observed after each cortical stimulus, which indirectly proved that a significant number of pyramidal neurons in the hand area of the MC were excited. A new finding is that in all electrode trajectories at different ventro-dorsal locations an "intermediate" excitation (starting from ~63-79 ms) was present in the period of the long lasting inhibition. The most reasonable explanation for this third excitation is a sensory response of the STN to the muscular contraction induced by the MCS (Hanajima et al. 2004).
We believed that the burden of the affective and cognitive side effects outweighed the risks of the MCS procedure (additional burr hole, cortical stimulation). An important limitation of subdural MCS in our study is the occurrence of partial seizures. The risk of a seizure is related to the applied current and current density. In our stimulation protocol (settings: bipolar, monophasic, 0.2 ms, 15mA, 1.1 Hz), the current density was ±72 μC/cm2, which might have been too high and thereby causing seizures. A second important consideration is the application of charge-balanced stimulation, which is achieved by biphasic instead of monophasic stimulation. Seizures also occur in other intra-operative procedures during which the cortex is stimulated repetitively (incidence of 1.2 %) (Szelenyi et al. 2007). Interestingly, subdural MCS has been applied with a similar stimulation protocol without inducing epileptic seizures (Nishibayashi et al. 2011). The main difference between the stimulation protocols is that Nishibayashi et al. applied a lower number of stimuli and the electrode contact size was larger. To prevent seizures the current density should be lowered, so that MCS evoked responses can be safely used during DBS surgery.

References

Benazzouz, A., S. Breit, A. Koudsie, P. Pollak, P. Krack and A. L. Benabid (2002). "Intraoperative microrecordings of the subthalamic nucleus in Parkinson's disease." Mov. Disord. 17(Suppl 3): S145-149.

Berney, A., F. Vingerhoets, A. Perrin, P. Guex, J. G. Villemure, P. R. Burkhard, C. Benkelfat and J. Ghika (2002). "Effect on mood of subthalamic DBS for

Parkinson's disease: a consecutive series of 24 patients." Neurology 59: 1427-1429.

Chen, C. C., A. Pogosyan, L. U. Zrinzo, S. Tisch, P. Limousin, K. Ashkan, T. Yousry, M. I. Hariz and P. Brown (2006). "Intra-operative recordings of local field potentials can help localize the subthalamic nucleus in Parkinson's disease surgery." Exp. Neurol. 198: 214-221.

de Solages, C., B. C. Hill, H. Yu, J. M. Henderson and H. Bronte-Stewart (2011). "Maximal subthalamic beta hypersynchrony of the local field potential in Parkinson's disease is located in the central region of the nucleus." J Neurol Neurosurg Psychiatry 82: 1387-1389.

Deuschl, G., C. Schade-Brittinger, P. Krack, J. Volkmann, H. Schafer, K. Botzel, C. Daniels, A. Deutschlander, U. Dillmann, W. Eisner, D. Gruber, W. Hamel, J. Herzog, R. Hilker, S. Klebe, M. Kloss, J. Koy, M. Krause, A. Kupsch, D. Lorenz, S. Lorenzl, H. M. Mehdorn, J. R. Moringlane, W. Oertel, M. O. Pinsker, H. Reichmann, A. Reuss, G. H. Schneider, A. Schnitzler, U. Steude, V. Sturm, L. Timmermann, V. Tronnier, T. Trottenberg, L. Wojtecki, E. Wolf, W. Poewe and J. Voges (2006). "A randomized trial of deep-brain stimulation for Parkinson's disease." N. Engl. J. Med. 355: 896-908.

Dolan, K., H. C. Martens, P. R. Schuurman and L. J. Bour (2009). "Automatic noise-level detection for extra-cellular micro-electrode recordings." Medical and Biological Engineering and Computing 47: 791-800.

Fujimoto, K. and H. Kita (1993). "Response characteristics of subthalamic neurons to the stimulation of the sensorimotor cortex in the rat." Brain Res. 609: 185-192.

Gross, R. E., P. Krack, M. C. Rodriguez-Oroz, A. R. Rezai and A. L. Benabid (2006). "Electrophysiological mapping for the implantation of deep brain stimulators for Parkinson's disease and tremor." Mov. Disord. 21(S14): S259-S283.

Hamani, C., J. A. Saint-Cyr, J. Fraser, M. Kaplitt and A. M. Lozano (2004). "The subthalamic nucleus in the context of movement disorders." Brain 127(1): 4-10.

Hanajima, R., R. Chen, P. Ashby, L. A.M., W. D. Hutchison, K. D. Davis and J. O. Dostrovsky (2004). "Very fast oscillation evoked by median nerve stimulation int eh human thalamus and subthalamic nucleus." J. Neurophysiol. 92: 3171-3182.

Kaneoke, Y. and J. L. Vitek (1996). "Burst and oscillation as disparate neuronal properties." J. Neurosci. Methods 68(2): 211-223.

Lewicki, M. S. (1998). "A review of methods for spike sorting: the detection and classification neural action potentials." Network: Computation in Neural Systems 9(4): R53-78.

Magill, P. J., A. Sharott, M. D. Bevan, P. Brown and J. P. Bolam (2004). "Synchronous unit activity and local field potentials evoked in the subthalamic nucleus by cortical stimulation." J. Neurophysiol. 92: 700-714.

Maurice, N., J. M. Deniau, J. Glowinski and A. Thierry (1998). "Relationships between the prefrontal cortex and the basal ganglia in the rat Physiology of the corticosubthalamic circuits." J. Neurosci. 18(22): 9539-9546.

Nambu, A., H. Tokuno, I. Hamada, H. Kita, M. Imanishi, T. Akazawa, Y. Ikeuchi and N. Hasegawa (2000). "Excitatory cortical inputs to pallidal neurons via the subthalamic nucleus in the monkey." J. Neurophysiol. 84: 289-300.

Nishibayashi, H., M. Ogura, K. Kakishita, S. Tanaka, Y. Tachibana, A. Nambu, H. Kita and T. Itakura (2011). "Cortically Evoked Responses of Human Pallidal Neurons Recorded During Stereotactic Surgery." Mov. Disord. 26(3): 469-476.

Piasecki, S. D. and J. W. Jefferson (2004). "Psychiatric complications of deep brain stimulation for Parkinson's disease." J. Clin. Psychiatry 65: 845-849.

Rodriguez-Oroz, M. C., I. Zamarbide, J. Guridi, M. R. Palmero and J. A. Obeso (2004). "Efficacy of deep brain stimulation of the subthalamic nucleus in Parkinson's disease 4 years after surgery: double blind and open label evaluation." J. Neurol. Neurosurg. Psychiatry 75: 1382-1385.

Smeding, H. M., J. D. Speelman, M. Koning-Haanstra, P. R. Schuurman, P. Nijssen, T. van Laar and B. Schmand (2006). "Neurophysiological effects of bilateral STN stimulation in Parkinson disease: a controlled study." Neurology 66: 1830-1836.

Strafella, A. P., Y. Vanderwerf and A. F. Sadikot (2004). "Transcranial magnetic stimulation of the human motor cortex influences the neuronal activity of subthalamic nucleus " Eur. J. Neurosci. 20(8): 2245-2249.

Szelenyi, A., B. Joksimovic and V. Seifert (2007). "Intraoperative risk of seizures associated with transient direct cortical stimulation in patients with symptomatic epilepsy." J. Clin. Neurophysiol. 24: 39-43.

Taylor, W. A. (2000). Change-Point Analyzer. Illinois, USA, Taylor Enterprises, Inc.

Temel, Y., A. Blokland, W. M. Steinbusch and V. Visser-Vandewalle (2005). "The functional role of the subthalamic nucleus in cognitive and limbic circuits." Prog. Neurobiol. 76: 393-413.

Temel, Y., A. Kessels, S. Tan, A. Topdag, P. Boon and V. Visser-Vandewalle (2006). "Behavioural changes after bilateral subthalamic stimulation in advanced Parkinson disease: A systematic review." Parkinsonism & Related Disorders 12(5): 265-272.

Temel, Y., P. Wilbrink, A. Duits, P. Boon, S. Tromp, L. Ackermans, V. Van Kranen-Mastenbroek, W. Weber and V. Visser-Vandewalle (2007). "Single electrode and multiple electrode guided electrical stimulation of the subthalamic nucleus in advanced Parkinson's disease." Neurosurgery 61: 346-355; discussion 355-357.

Weaver, F. M., K. Follett, M. Stern, K. Hur, C. Harris, W. J. Marks, J. Rothlind, O. Sagher, D. Reda, C. S. Moy, R. Pahwa, K. Burchiel, P. Hogarth, E. C. Lai, J. E. Duda, K. Holloway, A. Samii, S. Horn, J. M. Bronstein, G. Stoner, J. Heemskerk and G. D. Huang (2009). "Bilateral deep brain stimulation vs best medical therapy for patients with advanced Parkinson disease: a randomized controlled trial." JAMA 301: 63-73.

Witt, K., C. Daniels, J. Reiff, P. Krack, J. Volkmann, M. O. Pinsker, M. Krause, V. Tronnier, M. Kloss, A. Schnitzler, L. Wojtecki, K. Botzel, A. Danek, R. Hilker, V. Sturm, A. Kupsch, E. Karner and G. Deuschl (2008). "Neurophysiological and psychiatric changes after deep brain stimulation for Parkinson's disease: a randomised, multicentre study." Lancet Neurol. 7: 605-614.

Chapter 3

Cortically evoked potentials in the human subthalamic nucleus

Daphne G.M. Zwartjes
Marcus L.F. Janssen
Tjitske Heida
Vivianne van Kranen-Mastenbroek
Lo J. Bour
Yasin Temel
Veerle Visser-Vandewalle
Peter H. Veltink

Neurosci Lett, 2013, 539: 27-31

Abstract

Deep brain stimulation (DBS) of the subthalamic nucleus (STN) alleviates motor symptoms in Parkinson's disease (PD) patients. However, in a substantial number of patients the beneficial effects of STN DBS are overshadowed by psychiatric side effects. We hypothesize that stimulation of the STN motor area will provide the optimal effect on the motor symptoms without inducing these side effects, and expect that motor cortex stimulation (MCS) evokes a spatially specific response within the STN, which identifies the STN motor area. We previously showed that MCS evokes responses in the unit activity specifically within certain areas of the STN. Unit activity is generally considered a measure of the output activity. To gain more insight into the neuronal input into the STN, we describe the results of cortically evoked subthalamic local field potentials (LFPs). We show that the cortically evoked LFPs follow a certain temporal and spatial pattern. The significant peaks of the evoked LFPs coincide with the timing of some of the inhibitions and excitations present in the unit responses. The spatial resolution of responses measured in the LFP to MCS is not high enough to identify the STN motor region. However, we believe that optimizing targeting techniques and the development of novel DBS electrodes will improve STN DBS therapy for PD patients.

3.1. Introduction

Neuronal recordings from the human subthalamic nucleus (STN) have become possible due to the surgical treatment for advanced Parkinson's disease (PD), such as deep brain stimulation (DBS) of the STN. STN DBS provides a remarkable improvement in the motor function of PD patients (Deuschl et al. 2006). Unfortunately, STN DBS also induces unwanted behavioral changes, such as emotional disturbances and cognitive alterations (Temel et al. 2006). These unwanted side-effects can be explained by the involvement of the STN in motor, associative and limbic behavior. Current spread to the associative area, which is located ventrolaterally, and to the limbic area in the most ventromedial tip of the nucleus is responsible for the psychiatric side effects (Parent and Hazrati 1995; Hamani et al. 2004; Temel et al. 2005). Therefore, electrophysiological unit recordings are utilized to identify the STN and optimize electrode placement. Also local field potentials (LFPs) are often measured from the implanted DBS electrodes. The LFP shows pathologic ß oscillatory activity (12-30 Hz) in the STN of PD patients. This pathologic increase in ß activity is mainly observed within the dorsolateral motor region of the STN (Kuhn et al. 2005; Trottenberg et al. 2007; Moran et al. 2008). The LFP represents the summed postsynaptic potentials of a group of neurons (Buzsaki 2004), therefore it can be considered as the input activity. In contrast, the unit activity is a measure of the output activity. In humans, the cortex is classically connected to the STN via the indirect pathway, which not only passes through the striatum and globus pallidus externa to the STN (Parent et al. 1995), but also via a monosynaptic pathway (Brunenberg et al. 2012). Previously, we have shown in humans that motor cortex stimulation (MCS) evoked responses in the unit activity, which were not present outside the STN and differed spatially within the STN (Janssen et al. 2012). Strafella et al. (Strafella et al. 2004) had similar findings when measuring subthalamic unit activity during transcranial magnetic stimulation. Considering the different neuronal origin of the LFP, a more detailed study of the response in the LFP to MCS will provide more insight into the subthalamic input activity and the pathways involved (Magill et al. 2004). We hypothesized that the LFP is specifically responsive to MCS in the dorsolateral region of the STN, as this is the area believed to be involved in motor function (Hamani et al. 2004). Therefore, in this study we present the cortically evoked potentials in the LFP signal in the subthalamic region. As the LFP is believed to represent the neural input activity, it could provide an interesting tool for locating the STN motor area during stereotactic surgery. This potential use was studied by determining the temporal and spatial extent of the evoked LFPs. These results were also

compared to the unit responses, which show a specific response to cortical stimulation in the dorsal STN (Janssen et al. 2012).

3.2. Methods

Patients were enrolled based on the same criteria used for standard STN DBS. Five patients (ages 52-70 years) were included, but only the procedure and results of the last patient are described. The stimulation protocols used in the other patients did not result in an STN response due to saturation of the amplifier in the first two patients and suboptimal MCS protocols in the remaining two patients. The study, including five patients, was approved by the Medical Ethical Committee of the Maastricht University Medical Centre and all the patients gave written informed consent.

The procedure has been previously described in detail by Janssen et al. (Janssen et al. 2012). In short, subdural MCS with a strip of four electrodes (Model TS04R-SP10X-000; ADTech, Racine, WI, USA) was performed on the hand area of the motor cortex (stimulation settings: bipolar, monophasic, 0.2 ms, 7 or 15 mA, 200 stimuli). Concurrently, neuronal activity in and around the STN was measured using five microelectrodes (MicroMacroElectrode; InoMed, Emmendingen, Germany). Only local anesthesia was used. The stimulation amplitudes were determined based on the amplitude needed to obtain a motor evoked potential (MEP, 7mA).

In order to obtain LFPs from the raw signals, the signals were filtered using a non-causal second order band pass Butterworth filter between 3 and 95 Hz; 50 Hz noise was removed using a notch filter. Subsequently, the signals were divided into epochs from 100 ms before stimulation until 200 ms after stimulation. All epochs belonging to the same location and resulting from the same stimulation settings were averaged. Significant deflections in the average LFPs were determined when five successive samples exceeded a threshold of plus or minus two times the standard deviation of the signal measured during 15 mA stimulation. LFP responses were compared to the responses in the unit activity. The unit responses were evaluated by peri-stimulus time histograms (PSTHs) in which significant changes were found by the change point analysis. A detailed description of the analysis of the unit activity is previously described (Janssen et al. 2012).

3.3. Results

LFP recordings in the anterior and lateral trajectories were made from 1.5 and 0.5 mm above the target until 1 and 2.5 mm below the target. These trajectories were inside the STN from 2 mm above the target until 2.5 mm below the target. Fig. 1 shows the LFPs and peri-stimulus time histograms (PSTHs) constructed using the responses in the unit activity (Janssen et al. 2012) after cortical stimulation. The LFPs show a positive deflection around 43±3 ms. This peak is present at all heights in the lateral trajectory and at -1.5 and -0.5 mm in the anterior trajectory. Subsequently, negative peaks are present at 78 ms in the anterior trajectory and at 81 ms in the lateral trajectory at a height of -1.5 mm. At -0.5 mm above the calculated target, this negative peak has disappeared. At +1 mm in the anterior and lateral trajectory and at +2.5 mm in the lateral trajectory, a positive peak is seen at ~75 ms after stimulation. Finally, a significant negative peak is visible in the anterior trajectory at +2.5 mm. In the central and medial trajectory, the LFP response did show some significant peaks, but no specific pattern was visible. The LFP results did not correspond with the changes in the PSTH, which showed little to no response to stimulation (Janssen et al. 2012).
Responses were only visible in the LFPs when 15 mA stimulation was applied, but not when a stimulus amplitude of 7 mA was used; except for the responses shown at +2.5 mm. This was in agreement with the fact that no significant responses to MCS were visible in the PSTHs while using an amplitude of 7 mA for MCS (Janssen et al. 2012).
The positive peak at 43 ms corresponds with the start of the first inhibitory period found in the PSTHs at heights -1.5 and -0.5 mm. The negative peaks at 78 and 81 ms at a height of -1.5 mm in the anterior and lateral trajectory are within the period of increased firing rate in the PSTHs from about 63-100 ms after stimulation. The positive peaks in the anterior and lateral trajectories at ~75 ms are not seen in the PSTHs at these levels.

3.4. Discussion

In this study, for the first time evoked LFPs in the STN region following MCS in a PD patient, have been described. We showed that evoked LFPs follow a specific pattern in the dorsal STN, namely first a positive deflection around 43 ms followed by a negative deflection around 80 ms. The positive deflection is seen in the entire STN, but the negative deflection seems specific to the dorsolateral STN region. Some of the evoked LFP peaks are temporally and spatially linked to the unit responses to MCS.

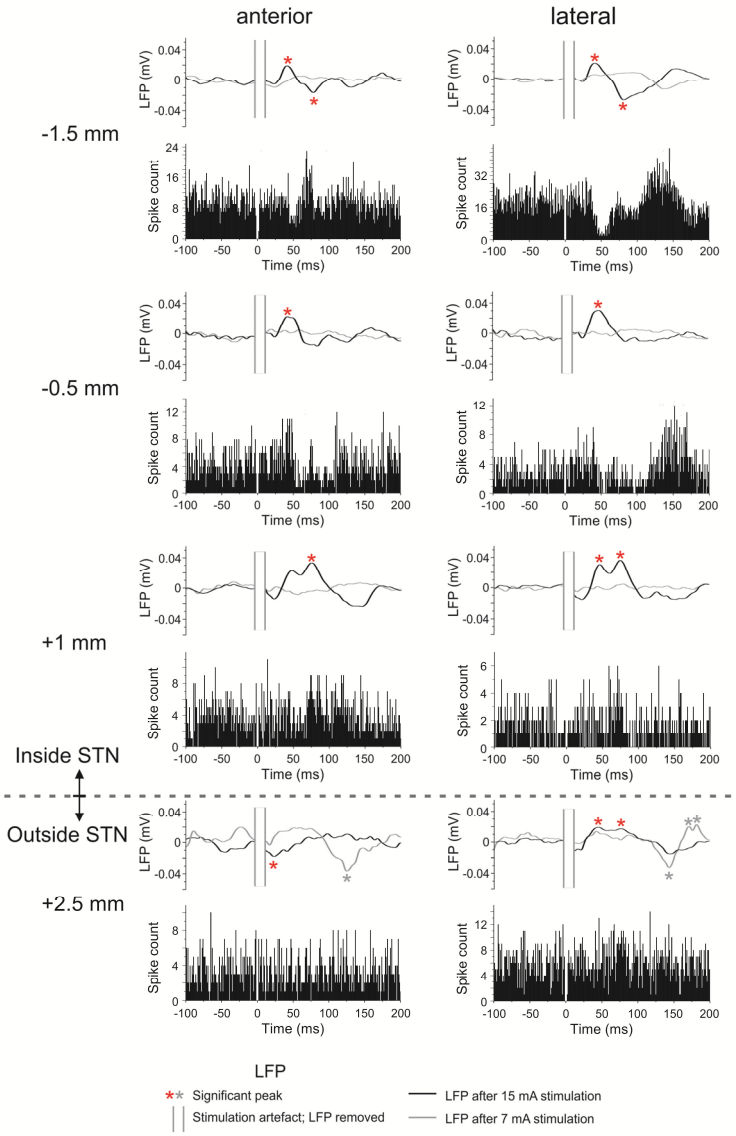

Figure 1. The cortically evoked LFPs using a stimulation amplitude of 7 and 15 mA are plotted as well as the PSTHs of the anterior and lateral electrode starting 0.5 mm after the electrode first enters the STN (1.5 mm above target) until it leaves the STN (2.5 mm below target). The PSTHs using 7 mA stimulation did not show any significant responses, therefore only the PSTHs obtained with 15 mA are plotted. LFP: LFPs were averaged over all trials. An asterisk indicates a significant LFP peak, which is determined by exceeding a threshold of ± 2 times the standard deviation from the signal during 15 mA stimulation. The PSTHs are partially adapted from Janssen et al. (Janssen et al. 2012).

We showed that the cortical input to the human STN can be visualized in the LFP. However, the temporal response in the LFP is not as clear-cut as in the rodent, although the LFP was averaged over many stimuli, which was not necessary in rodents (Magill et al. 2004). In contrast to the animal data, the deflections in the LFP caused by the mono-synaptic cortico-subthalamic pathway and the indirect cortico-striato-pallido-subthalamic pathway were not found. This could be due to difference in the size of the dendritic fields between species and a prominent lower cell density in the human compared to the rodent STN (Hammond and Yelnik 1983; Marani et al. 2008). Nonetheless, a clear positive deflection around 43 ms and a negative deflection around 80 ms were observed. The positive deflection was seen through the full ventro-dorsal axis of the STN and has a similar latency as observed in the rodents, which is the start of the long-lasting inhibitory period that may be caused by cortical disfacilitation (Magill et al. 2004). The negative deflection, which was only observed in the dorsal region of the STN, can be explained as a sensor response caused by muscular contraction induced by MCS (Hanajima et al. 2004). Movement related neuronal activity of the STN has earlier been described (Hutchison et al. 1998; Abosch et al. 2002).

Magill et al. (Magill et al. 2004) showed that a negative deflection in the LFP (input) coincides with an excitation shown in the PSTH (output) and vice versa. We clearly see that the positive peaks in the averaged LFP coincided with the long lasting inhibitory periods found in the PSTH. This positive LFP peak was also present at a height of +1 mm, at which the inhibition was no longer present in the PSTH. In this PD patient, the LFPs, thus, extended to a broader area than the unit responses. There can be different reasons for this. First, it should be considered that the LFP reflects the summed postsynaptic potentials of a group of neurons (Buzsaki 2004), while multi-unit activity reflects the action potentials measured in one or just a few neurons. Changes in the synaptic activity do not always lead to an action potential. Furthermore, LFPs exhibit strong low-pass filtering properties (Bédard et al. 2006), which could account for a larger responsive region of the low frequency LFP signal as compared to the high frequency spike signal. It has been argued that LFPs are volume conducted over a radius of 0.25 mm (Katzner et al. 2008). As the measurement at +2.5 mm was just outside of the STN (+2 mm was still inside of the STN), it might be that the LFPs originating from STN activity were volume conducted outside the STN. The negative peak in the LFPs at a height of -1.5 mm around 80 ms coincided with an increased firing rate shown in the PSTHs. However, the remaining PSTH was not reflected in the LFP. Additionally, we found significant deflections in the LFPs when no significant changes in the PSTH were found (Fig. 1: +2.5 mm).

These were probably caused by a low signal to noise ratio outside the STN, since also at 7 mA significant peaks were found.
Finally, we only observed a response after MCS while using a stimulation amplitude of 15 mA, but not after 7 mA stimulation. Moreover, in the LFP no excitatory monosynaptic response could be observed. This is not in line with what we expected, as our modeling study shows activation of pyramidal axons at 7 mA (Zwartjes et al. 2012). A reason for this discrepancy could be suboptimal placement of the stimulation electrode or it could be that the synaptic strength from the cortical afferents is less strong than thus far assumed. To our knowledge no quantitative studies exist on the number of synapses in the STN with a cortical origin. This would imply that a STN response is only present when a high number of pyramidal neurons is activated. On the other hand a strong coherence is present between the prefrontal cortex and the STN, which implicates a strong cortico-subthalamic connectivity (Litvak et al. 2011). Furthermore, the duration of the stimulation artifact overlapped with the expected timing of the monosynaptic response, which could have made this response invisible. We believe, despite the small sample size, that our results are important from a clinical perspective. In literature, it is being debated whether additional invasive procedures are warranted to improve the quality of the DBS procedure (Alegre et al. 2012). We believe that neurophysiological recordings can be helpful to increase the accuracy of the implantation of DBS electrodes. Accurate targeting is the limiting step in achieving maximal benefit on motor symptoms and minimizing side effects on behavior and cognition. Here we showed that the evoked LFPs were not restricted to a certain area of the STN and also extended beyond STN borders. Thus, the evoked LFPs did not have a spatial resolution high enough to locate the STN motor area. Further adaptation of the stimulation and recording protocol will decrease surgery time and will be of additional value to the standard used intra-operative tests to define the optimal site of implantation. To achieve this goal, computational models of cortical stimulation should be made to predict the optimal cortical stimulation site, electrode size and stimulation parameters (Zwartjes et al. 2012). Moreover, since MCS had an unexpectedly high risk of inducing seizures (Janssen et al. 2012) other electrophysiological markers, such as the ß activity, should be further investigated to explore their possibilities to target the motor part of the STN (Zaidel et al. 2010; Lambert et al. 2012). Imaging techniques can be combined with intra-operative electrophysiological information providing a more precise indication of which area of the STN should be stimulated. The next step then would be to develop DBS electrodes that are able to stimulate a selective area (Martens et al. 2011). Combining the improved identification of the STN motor region and the development of DBS electrodes with a higher spatial resolution

will optimize DBS therapy for PD patients. Butson et al. (Butson et al. 2011) describe volumes with a diameter as low as 1.5 mm and 2.5 mm giving 75% clinical improvement for bradykinesia and rigidity respectively, lying right next to each other. Based on these findings, electrode contacts and configurations could be optimized to target each functionally different volume selectively.

References

Abosch, A., W. D. Hutchison, J. A. Saint-Cyr, J. O. Dostrovsky and A. M. Lozano (2002). "Movement-related neurons of the subthalamic nucleus in patients with Parkinson disease." J Neurosurg 97(5): 1167-1172.

Alegre, M., M. Hallett, C. W. Olanow and J. A. Obeso (2012). "Technical advances in deep brain stimulation: How far is enough?" Mov Disord 27(3): 341-342.

Bédard, C., H. Kröger and A. Destexhe (2006). "Model of low-pass filtering of local field potentials in brain tissue." Physical Review E 73(5): 051911.

Brunenberg, E. J., P. Moeskops, W. H. Backes, C. Pollo, L. Cammoun, A. Vilanova, M. L. Janssen, V. E. Visser-Vandewalle, B. M. Ter Haar Romeny, J. P. Thiran and B. Platel (2012). "Structural and Resting State Functional Connectivity of the Subthalamic Nucleus: Identification of Motor STN Parts and the Hyperdirect Pathway." PLoS One 7(6): e39061.

Butson, C. R., S. E. Cooper, J. M. Henderson, B. Wolgamuth and C. C. McIntyre (2011). "Probablistic analysis of activation volumes during deep brain stimulation." NeuroImage 54: 2096-2104.

Buzsaki, G. (2004). "Large-scale recording of neuronal ensembles." Nat. Neurosci. 7(5): 446-451.

Deuschl, G., C. Schade-Brittinger, P. Krack, J. Volkmann, H. Schafer, K. Botzel, C. Daniels, A. Deutschlander, U. Dillmann, W. Eisner, D. Gruber, W. Hamel, J. Herzog, R. Hilker, S. Klebe, M. Kloss, J. Koy, M. Krause, A. Kupsch, D. Lorenz, S. Lorenzl, H. M. Mehdorn, J. R. Moringlane, W. Oertel, M. O. Pinsker, H. Reichmann, A. Reuss, G. H. Schneider, A. Schnitzler, U. Steude, V. Sturm, L. Timmermann, V. Tronnier, T. Trottenberg, L. Wojtecki, E. Wolf, W. Poewe and J. Voges (2006). "A randomized trial of deep-brain stimulation for Parkinson's disease." N. Engl. J. Med. 355: 896-908.

Hamani, C., J. A. Saint-Cyr, J. Fraser, M. Kaplitt and A. M. Lozano (2004). "The subthalamic nucleus in the context of movement disorders." Brain 127(1): 4-10.

Hammond, C. and J. Yelnik (1983). "Intracellular labelling of rat subthalamic neurones with horseradish peroxidase: computer analysis of dendrites and characterization of axon arborization." Neuroscience 8(4): 781-790.

Hanajima, R., J. O. Dostrovsky, A. M. Lozano, W. D. Hutchison, K. D. Davis, R. Chen and P. Ashby (2004). "Somatosensory evoked potentials (SEPs) recorded from deep brain stimulation (DBS) electrodes in the thalamus and subthalamic nucleus (STN)." Clin Neurophysiol 115(2): 424-434.

Hutchison, W. D., R. J. Allan, H. Opitz, R. Levy, J. O. Dostrovsky, A. E. Lang and A. M. Lozano (1998). "Neurophysiological identification of the subthalamic nucleus in surgery for Parkinson's disease." Ann Neurol 44(4): 622-628.

Janssen, M. L. F., D. G. M. Zwartjes, Y. Temel, V. Van Kranen-Mastenbroek, A. Duits, L. J. Bour, P. H. Veltink, T. Heida and V. Visser-Vandewalle (2012). "Subthalamic neuronal responses to cortical stimulation." Mov. Disord. 27(3): 435-438.

Katzner, S., I. Nauhaus, A. Benucci, V. Bonin, D. L. Ringach and M. Carandini (2008). "Local origin of field potentials in visual cortex." Neuron 61(1): 35-41.

Kuhn, A. A., T. Trottenberg, A. Kivi, A. Kupsch, G. H. Schneider and P. Brown (2005). "The relationship between local field potential and neuronal discharge in the subthalamic nucleus of patients with Parkinson's disease." Exp Neurol 194(1): 212-220.

Lambert, C., L. Zrinzo, Z. Nagy, A. Lutty, M. Hariz, T. Foltynie, B. Draganski, J. Ashburner and R. Frackowiak (2012). "Confirmation of functional zones within the human subthalamic nucleus: Patterns of connectivity and sub-parcellation using diffusion weighted imaging." Neuroimage 60: 83-94.

Litvak, V., A. Jha, A. Eusebio, R. Oostenveld, T. Foltynie, P. Limousin, L. Zrinzo, M. I. Hariz, K. Friston and P. Brown (2011). "Resting oscillatory cortico-subthalamic connectivity in patients with Parkinson's disease." Brain : a journal of neurology 134(Pt 2): 359-374.

Magill, P. J., A. Sharott, M. D. Bevan, P. Brown and J. P. Bolam (2004). "Synchronous unit activity and local field potentials evoked in the subthalamic nucleus by cortical stimulation." J. Neurophysiol. 92: 700-714.

Marani, E., T. Heida, E. A. J. F. Lakke and K. G. Usunoff (2008). The subthalamic nucleus. Part I: Development, Cytology, Topography and Connections. Berlin, Springer-Verlag.

Martens, H. C., E. Toader, M. M. J. Decre, D. J. Anderson, R. Vetter, D. R. Kipke, K. B. Baker, M. D. Johnson and J. L. Vitek (2011). "Spatial steering of deep brain stimulation volumes using a novel lead design." Clin. Neurophysiol. 122(3): 558-566.

Moran, A., H. Bergman, Z. Israel and I. Bar-Gad (2008). "Subthalamic nucleus functional organization revealed by parkinsonian neuronal oscillations and synchrony." Brain 131(Pt 12): 3395-3409.

Parent, A. and L. Hazrati (1995). "The functional anatomy of the basal ganglia. I. The cortico-basal ganglia-thalamo-cortical loop." Brain Res. Rev. 20: 91-127.

Strafella, A. P., Y. Vanderwerf and A. F. Sadikot (2004). "Transcranial magnetic stimulation of the human motor cortex influences the neuronal activity of subthalamic nucleus " Eur. J. Neurosci. 20(8): 2245-2249.

Temel, Y., A. Blokland, W. M. Steinbusch and V. Visser-Vandewalle (2005). "The functional role of the subthalamic nucleus in cognitive and limbic circuits." Prog. Neurobiol. 76: 393-413.

Temel, Y., A. Kessels, S. Tan, A. Topdag, P. Boon and V. Visser-Vandewalle (2006). "Behavioural changes after bilateral subthalamic stimulation in advanced

Parkinson disease: A systematic review." Parkinsonism & Related Disorders 12(5): 265-272.

Trottenberg, T., A. Kupsch, G. H. Schneider, P. Brown and A. A. Kuhn (2007). "Frequency-dependent distribution of local field potential activity within the subthalamic nucleus in Parkinson's disease." Exp Neurol 205(1): 287-291.

Zaidel, A., A. Spivak, B. Grieb, H. Bergman and Z. Israel (2010). "Subthalamic span of beta oscillations predicts deep brain stimulation efficacy for patients with Parkinson's disease." Brain 133(7): 2007-2011.

Zwartjes, D. G. M., T. Heida, H. K. P. Feirabend, M. L. F. Janssen, V. Visser-Vandewalle, H. C. F. Martens and P. H. Veltink (2012). "Motor cortex stimulation for Parkinson's disease: a modelling study " J Neural Eng 9(5): 056005.

Chapter 4

Motor cortex stimulation for Parkinson´s disease: a modelling study

Daphne G.M. Zwartjes
Tjitske Heida
Hans K.P. Feirabend
Marcus L.F. Janssen
Veerle Visser-Vandewalle
Hubert C.F. Martens
Peter H. Veltink

J Neural Eng, 2012, 9(5): 056005

Abstract

Chronic motor cortex stimulation (MCS) is currently investigated as a treatment method in Parkinson's disease (PD). Unfortunately, the underlying mechanisms of this treatment are unclear and there are many uncertainties regarding the most effective stimulation parameters and electrode configuration. In this paper, we present a MCS model with a 3D representation of several axonal populations. The model predicts that the activation of either the Basket cell or pyramidal tract (PT) type axons is involved in the clinical effect of MCS. We propose stimulation protocols selectively targeting one of these two axon types. To selectively target the Basket cell axons, our simulations suggest to use either cathodal or bipolar stimulation with the electrode strip placed perpendicular rather than parallel to the gyrus. Furthermore, selectivity can be increased by using multiple cathodes. PT type axons can be selectively targeted with anodal stimulation using electrodes with large contact sizes. Placing the electrode epidurally is advisable over subdural placement. These selective protocols, when practically implemented, can be used to further test which axon type should be activated for clinically effective MCS and can subsequently be applied to optimize treatment. In conclusion, this paper increases insight into the neuronal population involved in the clinical effect of MCS on PD and proposes strategies to improve this therapy.

4.1. Introduction

Stimulation of the brain is increasingly used to treat Parkinson's disease (PD) and stimulation of the basal ganglia, deep brain stimulation (DBS), has become a widely accepted therapy for PD (Benabid 2003). Chronic motor cortex stimulation (MCS) is a less invasive therapy, which was initially used for the treatment of chronic pain (Tsubokawa et al. 1991), but has now also been studied as a PD treatment, especially for patients who are not eligible for DBS or refuse this treatment (Pagni et al. 2005; Cioni 2007).

From a review of the literature and their own clinical data, Cioni et al. (Cioni et al. 2009) conclude that MCS may relieve all three main symptoms of PD (akinesia, rigidity, tremor), but results vary widely. Currently, MCS protocols for PD either comprise cathodal or bipolar stimulation (Canavero and Paolotti 2000; Drouot et al. 2004; Pagni et al. 2005; Cioni 2007; Arle et al. 2008; Arle and Shils 2008; Fasano et al. 2008; Cioni et al. 2009; Gutierrez et al. 2009; Meglio and Cioni 2009). There are, however, many uncertainties about the most effective stimulation parameters and electrode configuration. It is, for example, not known whether subdural or epidural stimulation should be used (Arle et al. 2008; Arle and Shils 2008; Gutierrez et al. 2009) and which electrode orientation relative to the gyrus is optimal (Cioni 2007; Cioni et al. 2007; Arle et al. 2008; Arle and Shils 2008; Gutierrez et al. 2009; Meglio and Cioni 2009).

Since the mechanisms of MCS in the treatment of PD are not clear, information on how to optimize treatment is lacking. Several theories exist about the neuronal populations that are involved: 1) The involvement of the axons projecting to the hyperdirect pathway from the cortex to the Subthalamic nucleus (STN) through which STN activity can be modulated (Fig. 1a) (Pagni et al. 2005). In cats, it has been shown that these axonal projections originate from the pyramidal tract (PT) type cells (Giuffrida et al. 1985) (Fig. 1b), but this has not been studied in rats and monkeys yet (Mathai and Smith 2011). 2) The axons projecting to the direct and indirect pathway (Fig. 1a) can also modulate basal ganglia activity (Pagni et al. 2005; Cioni 2007; Cioni et al. 2007; Meglio and Cioni 2009) . These pathways presumably originate from intratelecenphalic (IT) type pyramidal cells in the motor cortex (Ballion et al. 2008; Mathai and Smith 2011) and project to the striatum, or more particularly the lateral putamen (Takada et al. 1998), and then to the STN (Fig. 1b). 3) The involvement of the inhibitory axonal population (Hanajima et al. 2002; Cioni et al. 2007; Arle and Shils 2008; Meglio and Cioni 2009), i.e. the Basket cells, which have long axons running parallel to the pial surface (Nieuwenhuys 1994) (Fig. 1b). As the Basket cells have multiple synaptic contacts on the pyramidal neurons (Nieuwenhuys 1994), they can strongly inhibit this population and thereby modulate the

cortico-basal ganglia loops. Additional networks in the cortex are formed by excitatory projections from the pyramidal neurons to the Basket cells and other pyramidal neurons in different cortical layers (Nieuwenhuys 1994). Based on these theories, activation of three axonal populations has been suggested to play a role in MCS treatment for PD, namely Basket cell axons, PT and IT type pyramidal axons.

To optimize treatment, it is important to know which axonal population is primarily involved in the clinical effect of MCS on PD. We propose a modelling approach using a finite element volume conduction model in combination with an axon model, similar to previously developed models for MCS (Manola et al. 2005; Manola and Holsheimer 2007; Manola et al. 2007; Silva et al. 2008; Wongsarnpigoon and Grill 2008; Wongsarnpigoon and Grill 2012) and DBS (McIntyre et al. 2004; Sotiropoulos and Steinmetz 2007; Butson and McIntyre 2008; Frankemolle et al. 2010). We extended previous MCS models by: Considering axons with different orientations and at different depths in the grey matter (Fig. 1b); Including new anatomical data on the diameters of the myelinated fibre populations (personal communication Feirabend, H.K.P.); Using realistic models of PT and IT type pyramidal axons including axon collaterals (Nieuwenhuys 1994; Salvador et al. 2011); Modelling axons in 3D space.

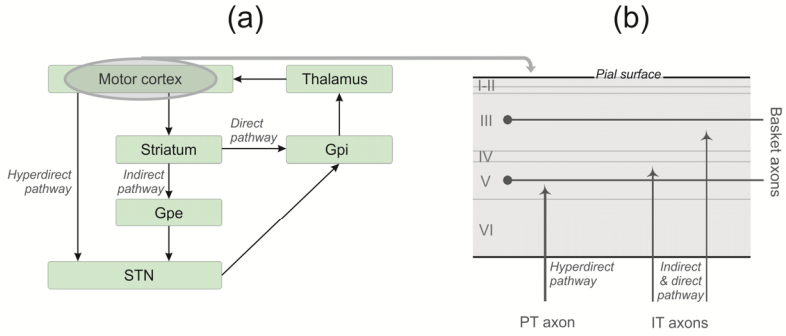

Figure 1. (a) The neuronal pathways from the cortex through the basal ganglia and thalamus back to the cortex. (b) A schematic representation of the axonal populations that have been suggested to play a role in the mechanisms of MCS for PD treatment: Basket cell axons, which have inhibitory properties, are mainly located in layer III and V; PT type pyramidal axons, being excitatory and composing the hyperdirect pathway, originate from deep layer V (Reiner et al. 2003); IT type pyramidal axons, which are also excitatory and compose the direct and indirect pathway. Their soma's are located in layer III, superficial and deep layer V (Reiner et al. 2003) (those located in deep layer V are not considered, since their relatively small diameter makes them less excitable than PT type axons at similar locations).

The aim is to determine which axonal populations are activated during clinically effective MCS treatment for PD using this computational model. Secondly, we will employ the model to determine protocols that selectively target these populations.
Although this paper is aimed at chronic MCS for PD, the outcome can also be useful for other applications, such as MCS for pain and stroke treatment and acute MCS to target the STN or GPi motor regions during DBS surgery (Nishibayashi et al. 2011; Janssen et al. 2012)

4.2. Methods

Volume conduction model
A 3D finite element volume conduction model of the MC including a current controlled stimulation electrode was developed using Comsol Multiphysics (v3.4, COMSOL, Inc., Burlington, MA, USA). In addition, an axon model was developed in Matlab (MathWorks, Natick, MA, USA), using a finite impedance single cable model, which was virtually positioned in the MC.
The modelled MC geometry included the scalp, skull, dura mater, cerebrospinal fluid, grey matter and white matter (Fig. 2, table 1). Since quasi-static conditions can be assumed (Plonsey and Heppner 1967), the electrical potential field was calculated by solving Poisson's equation. Boundary conditions were based on a realistic head model (Grant and Lowery 2009), since Grant and Lowery showed that it is inadequate to use a simple cubic block grounded on the exterior boundaries for the representation of distant tissue. They propose a realistic model with electric insulation at the exterior boundaries and a ground located at the approximate location of the reference electrode. As only relative voltage values are of concern for the cable models of the axon, the reference electrode was set to zero volts. Their head model has an ellipsoid shape and incorporates a two-layered representation of the scalp, a three-layered representation of the skull and the cerebrospinal fluid. We replicated this model and added the dura mater. Subsequently, the realistic model was simplified by converting the ellipsoid shape of the head to a block (Fig. 2). Furthermore, outside the area of interest, which is an area of ca. 30 mm around the electrode, the different shells representing the scalp, skull, dura mater and cerebrospinal fluid were converted to one layer. The effective conductivity of this layer was chosen such that the electric potential (in the grey matter right beneath the stimulation electrode) and impedance in the simplified model differed less than 2% from the electric potential and impedance in the realistic version. The boundary conditions in the realistic model and simplified model were similar, i.e. exterior boundaries were electrically insulated and the reference electrode was set to zero volts. During monopolar stimulation,

the reference electrode was located on the case of the implantable pulse generator (IPG; Fig. 2) (Canavero and Paolotti 2000; Drouot et al. 2004; Pagni et al. 2005; Cioni 2007; Arle et al. 2008; Fasano et al. 2008; Gutierrez et al. 2009). During bipolar stimulation, one of the remaining electrode contacts was used as a reference. Like Manola et al. (Manola et al. 2005), we set the conductance of the dura mater to a value that gives an impedance matching to the mean empirical value of ~1000 ohm during bipolar stimulation. This resulted in a conductance of 0.055 S/m, which is in between the values of 0.065 S/m proposed by Manola *et al.* (Manola et al. 2005) and 0.03 S/m used by Struijk *et al.* (Struijk et al. 1993). The conductance of the 'distant tissue' representing tissue in between the brain and clavicle, where the case of the IPG is located, was determined by matching the model impedance during monopolar stimulation to the mean empirical value of ~750 ohm (Manola et al. 2005). The finite element model was 19x16x17 cm and it was solved for $9.2x10^4$ tetrahedral elements using a linear solver, conjugate gradients, with preconditioning of an algebraic multigrid solver. The finest mesh is located in the electrode contact where the mesh elements had an average volume of 0.041 mm^3. The mesh element volume increased to an average of 412 mm^3 in the roughest meshed structure; the brain tissue. Increasing the overall resolution approximately twofold resulted in a less than 2% difference of the electric potential in the grey matter beneath the stimulation electrode.

Table 1. Parameters volume conduction model.

Geometry	dimensions (mm)	Conductivity (S/m)
Skin	y = 2.4 (Scheufler et al. 2003)	0.00087 (Gabriel et al. 1996)
Fat	y = 3.1 (Scheufler et al. 2003)	0.042 (Gabriel et al. 1996)
Skull inner layer	y = 3 (Snyder 1975)	0.076 (Gabriel et al. 1996)
Skull outer layers	y = 0.8 & y=0.8 (Snyder 1975)	0.02 (Gabriel et al. 1996)
Dura mater	0.36 (Hanajima et al. 2002)	0.055
Electrode insulation	xyz = 8x1.8x44	0.0001 (Manola et al. 2005)
Electrode contact	diameter = 2.3 or 4; height = 0.4	$6{\cdot}10^7$
Cerebrospinal fluid	y = 3.1 (Manola et al. 2005)	1.6 (Baumann et al. 1997)
Grey matter	y = 3.7 (Manola et al. 2005)	0.36 (Manola et al. 2005)
Precentral gyrus	x = 11.7 (Manola et al. 2005)	
Central sulcus	xy = 2.3x16.4 (Manola et al.	
Precentral sulcus	xy = 2.7x15.6 (Manola et al.	
White matter	xyz = 54x30.4x50	x = 0.083; y = 0.6; z = 0.083
Layer around the brain	xyz = 192.1x157.1x167.1	0.0004
Distant tissue	xyz= 40x13.56x40	0.048
Brain tissue	xyz = 165x130x140	0.27 (Ranck and BeMent

Axon model

Instead of an entire neuron, only the axon was modelled since axons are the key neuronal components responding to MCS, i.e. the component that primarily causes the output activity of the stimulated structure (Nowak and Bullier 1998a; Nowak and Bullier 1998b; Manola and Holsheimer 2007). The axon was modelled as a single cable model with the myelin having a finite resistance and capacitance; details can be found in (McNeal 1976; Richardson et al. 2000). The parameters applied in the axon model are listed in table 2. Details on the ion channel and leakage conductances are presented in the appendix.

The following boundary conditions were used in the axon model: At the start and end of the axons, the next 'virtual' compartment was assumed to have the same membrane potential value as the boundary compartment. This ensures that no action potentials will be generated by boundary effects. Activation of an axon was defined when the membrane potential of one of the nodes was raised by 70 mV from the rest potential.

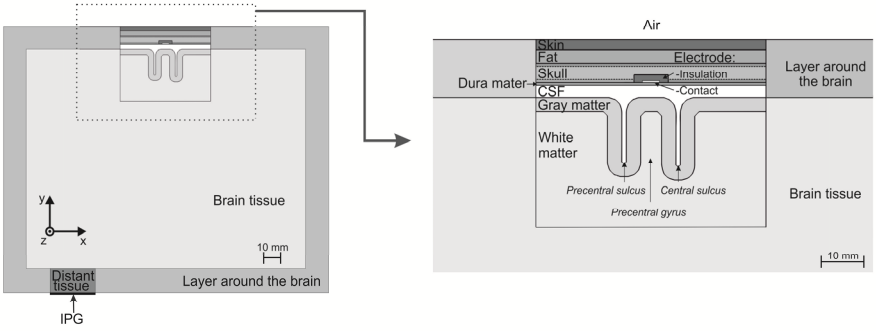

Figure 2. The finite element volume conduction model of the motor cortex with surrounding structures during epidural stimulation when the case of the IPG is used as a reference. On the left, the entire model, which is derived from a realistic head model, is shown. The area around the electrode, encompassed by dashed lines, is shown in more detail on the right. The layer around the brain represents the scalp, skull, dura mater and cerebro spinal fluid. The distant tissue represents the tissue in between the brain and clavicle, where the IPG is located. The entire model has the following dimensions: 192.1x157.1x167.1 mm.

Table 2. Parameters axon model.

Parameter	Value
Neuron resting potential	-0.084 V (Schwarz et al. 1995)
Intracellular resistivity	0.4 Ωm (Foster et al. 1976)
Membrane capacitance	0.028 F/m^2 (Wesselink et al. 1999)
Myelin membrane capacitance	0.0005 F/m^2 (Huxley and Stämpfli 1949)
Myelin membrane conductance	5 S/m2 (Huxley and Stämpfli 1949)

Different types of axons are located in the motor cortex. Since we are interested in those that might be involved in the clinical effect of MCS on PD, we modelled the Basket cell, PT and IT type axons (Fig. 1). We assume that the direct and indirect pathways are (solely) innervated by IT type axons. Although one study argues that the PT type axons provide the main input to the direct pathway (Lei et al. 2004), recent work (Ballion et al. 2008; Mathai and Smith 2011) indicates that the IT type axons are the most important input. The inhibitory double bouquet cells and chandelier cells, which have axons oriented perpendicular to the pial surface, were not modelled as their axons run alongside pyramidal axons, which typically have a larger diameter (Sloper and Powell 1979) and are, therefore, better excitable.

The inhibitory axonal population was represented by Basket cell axons, which were modelled as long axons running parallel to the pial surface at depths of 1950 μm and 850 μm from the pial surface, being halfway the Vth and the IIIth layer, respectively ((Nieuwenhuys 1994); Fig. 3, red and orange). These axons were placed in 91 xy-planes spaced 0.33 mm apart in z-direction: -15 to +15 mm from the middle in between the two electrode contacts. Thereby, 3D populations of 91 Basket cell axons in both the Vth and IIIth layer were obtained. The pyramidal axons (the PT and IT type axons) were placed such that the soma (which was not modelled) would lie at distances of 2125 μm, 1775 μm and 1125 μm from the pial surface. These depths correspond to the PT axon at 3/4th of layer V, and the IT axons at 1/4th of layer V and 3/4th of layer III, respectively. Furthermore, they were placed in the xy plane in three different ways (Fig. 3): (1) a vertical axon right beneath the stimulation electrode on the crown of the gyrus (blue); (2) a diagonal axon running through the lip (purple); and (3) a horizontal axon running through the sulcus bank (green) (Manola et al. 2007). They were also placed in z-direction from -15 to +15 mm, using 31 xy-planes spaced 1 mm apart, obtaining a population of 93 PT type axons in layer V, 93 IT type axons in both layer III and V. The pyramidal axons were represented by a main axon and an axon collateral (Nieuwenhuys 1994; Salvador et al. 2011) (Fig. 3). Two types of axon collaterals were used, both lying parallel to the pial surface but oriented

differently with respect to the medial-lateral and anterior-posterior axis (Fig. 3). Each pyramidal axon model was modelled using collateral type 1 or 2 and a 50% presence of both types was assumed. It was checked that the pyramidal axon model produced results consistent with several experimental studies (Hanajima et al. 2002; Lefaucheur et al. 2010; Janssen et al. 2012).

The diameters of the Basket cell axon models were retrieved from Feirabend (personal communication Feirabend, H.K.P.). They assessed the diameter of the myelinated fibre population, which they define as the thickness of the axon including the myelin sheets, in the human motor cortex. The axon diameter in our model is defined similarly. Only fibres with a diameter above 5 μm were considered by Feierabend et al., because thinner fibres are less interesting since they become increasingly difficult to activate. They distinguished diameters between differently oriented axons and between axons at different depths in the grey matter. As Basket cell axons are mainly located in layer III and V (Nieuwenhuys 1994), we used the axon diameters found at depths corresponding to the middle of both layers: The Basket cell axon has an average diameter of 5.4 μm in layer III and 5.7 μm in layer V.

The diameters of the pyramidal axons were derived from average diameters measured in human and the ratio between the axon diameters of different neuron types found in rat. The average diameter of perpendicularly oriented axons in the human motor cortex is 7.1 μm (personal communication Feirabend, H.K.P.). We differentiated different neuron types and neurons at different depths, by using ratios of soma sizes found in the rat motor cortex (Reiner et al. 2003), which were converted to axon diameters using the relation between axon and soma diameters (Sloper and Powell 1979). The following diameters were used: 10.6, 5.1 and 5.7 μm for PT type axons in layer V and IT type axons in layer III and V, respectively. The axon collaterals of these perpendicular axons ran parallel to the pial surface. The diameters of these collaterals were based on the diameter-ratio between parallel and perpendicular axon diameters in human 0.85:1 (personal communication Feirabend, H.K.P.). This gave collateral diameters of 9.0, 4.5 and 4.8 μm for the PT type axons in layer V and IT type axons in layer III and V, respectively.

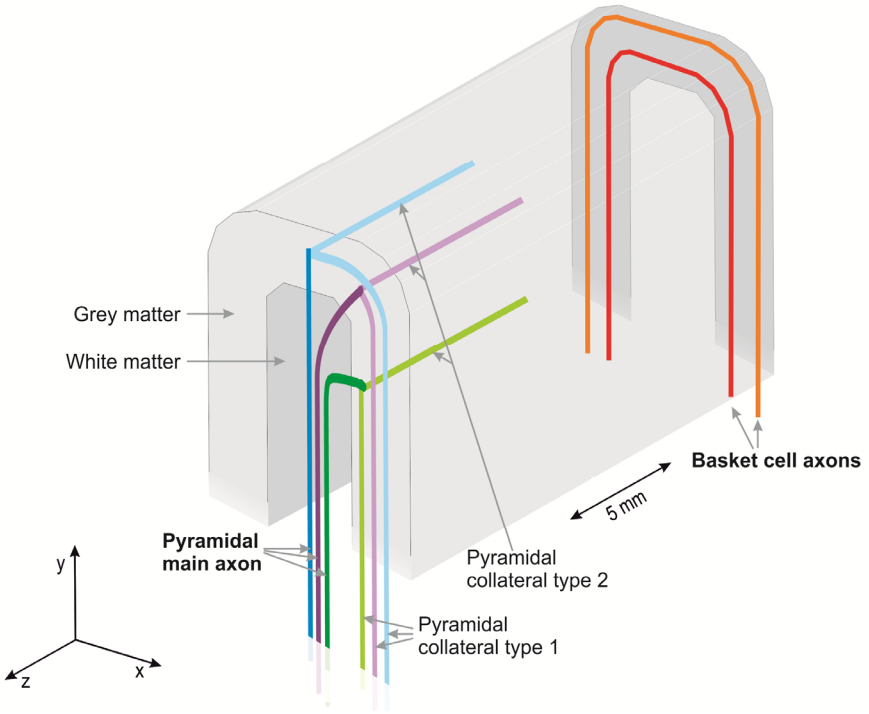

Figure 3. The motor cortex in which the Basket cell axon, PT and IT type pyramidal axon models are shown:
*Basket axons in layer III (orange) and layer V (red).
*Pyramidal axons (blue, purple and green). The pyramidal axons in one layer of one type are shown. In reality there is the PT type in layer V and IT type in layer III and V. The different colours represent three orientations. The pyramidal axons are modelled using a main axon and axon collaterals type 1 and 2. For illustrative purposes, the three pyramidal axons with collaterals are shown with a small distance in between the collaterals type 1, but in reality they overlie one another.
Only one xy-plane is shown for each axonal type, while multiple planes in *z*-direction were modelled.

Simulations

The simulations consisted of two parts: defining which axonal populations are activated during clinically effective MCS for PD; and proposing stimulation protocols to target these populations selectively. In both parts, the effect of the stimulation protocols was assessed by determining the activation threshold for each individual axon and subsequent computation of the activation fraction. The activation fraction is defined as the percentage of activated axons from the total

amount of axons we modelled in our 3D population. Assuming that within a volume of $8.2 \cdot 10^3$ mm^3 an equal number of each axon type exists, i.e. 91 Basket cell axons in both layer III and V, 93 IT type axons in both layer III and V, and 93 PT type axons. Results were obtained within clinically relevant stimulation amplitudes, which are up to 8 V (Meglio and Cioni 2009). Considering impedances of 750 and 1000 ohm during monopolar and bipolar stimulation respectively (Manola et al. 2005), this corresponds to 10.7 and 8 mA.

The first part of the simulations assess which neuronal populations are activated during clinically effective MCS treatment. This will be done by studying the effects of cortical stimulation on the earlier proposed axonal populations: the Basket cell, PT and IT type axons. The clinically effective stimulation protocols are epidural cathodal and bipolar stimulation (table 3). The effect of monopolar anodal stimulation has not been studied on humans as this is not possible due to the design of the present IPGs (Arle and Shils 2008).

In the second part, we looked for selective MCS protocols by varying the position and orientation of the strip (Fig. 4), the contact size and the distance between the contacts, the stimulation type, i.e. anodal/cathodal/bipolar, and the number of cathodes (table 3).

Table 3. MCS protocols.

Protocols	Position	Strip	D	I (mm)	Electrode configurations[b]
Clinical	Epidural	Parallel	4	10.2	- ; +-
Variations					
1	Epidural	Parallel	4	10.2	+
2	Subdural	Parallel	4	10.2	+
3	Epidural	Perpendicular	4	10.2	+
4	Epidural	Parallel	2; 6	10.2	+
5	Subdural	Parallel	4	10.2	-
6	Epidural	Perpendicular	4	10.2	-
7	Epidural	Parallel	2; 6	10.2	-
8	Epidural	Parallel	4	10.2	~ ; -o- ; ~ ; +o- ; +~
9	Epidural	Parallel	4	5.1; 15.3	+-

The first row shows clinically used MCS protocols (Canavero and Paolotti 2000; Drouot et al. 2004; Pagni et al. 2005; Cioni 2007; Arle et al. 2008; Arle and Shils 2008; Fasano et al. 2008; Cioni et al. 2009; Gutierrez et al. 2009; Meglio and Cioni 2009). The remaining rows show the variations on the clinical protocols, which are assessed to find selective stimulation protocols. Each variation is numbered. The change relatively to the clinical protocols is shaded.

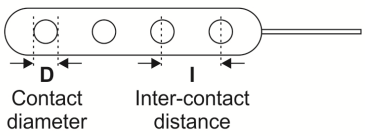

[a] Strip orientation relatively to the gyrus (Fig. 4).

[b] Electrode configurations: '+' is anode, '-' is cathode and 'o' is not active. When multiple cathodes were used, the current was divided between the contacts.

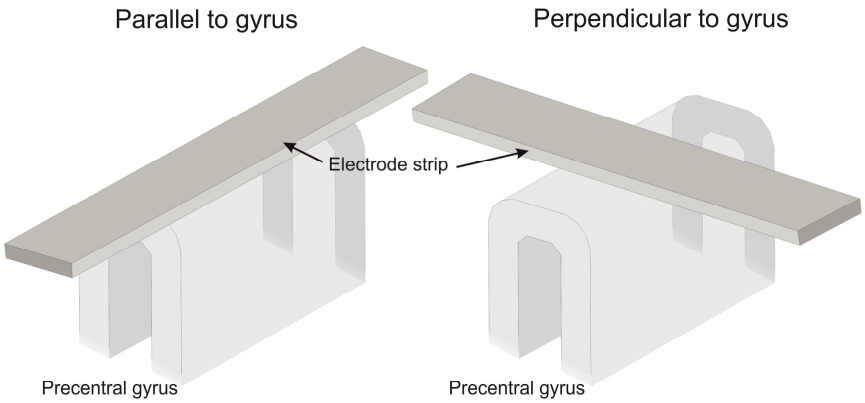

Figure 4. The orientation of the electrode strip relatively to the precentral gyrus. A strip orientation parallel and perpendicular to the gyrus were modelled.

4.3. Results

The axonal populations activated during clinically effective MCS for PD

The activation fractions during clinically effective stimulation protocols (table 3, 1st row) are shown in Fig. 5a and 5b. The activation fraction of the Basket cell axons was largest during cathodal stimulation, but also the PT type pyramidal axons were activated. The IT type pyramidal axons were activated at a threshold of 13.5 mA, which is beyond the clinical range of stimulation amplitudes used during MCS. During bipolar stimulation, all axon types were activated, but the activation fractions of Basket cell and PT type axons were larger than those of IT type axons. Furthermore, a larger fraction of the more superficially located Basket cells in layer III were activated than those in layer V in both stimulation protocols.

To get more insight into how the activation spreads in the cortex, the spreading of the Basket cell axon activation is depicted in Fig. 6. This distribution is slightly asymmetrical, because of the location of the reference electrode which influences the gradient of the potential field.

The activation of the axons was initiated at different nodes during different stimulation protocols. The following results were found for axons activated within the clinically used range of stimulation amplitudes. During anodal stimulation, excitation of the vertical pyramidal axons (Fig. 3, blue) started close to the boundary of the grey and white matter on the main axon. During cathodal stimulation, excitation of the vertical pyramidal axons (Fig. 3, blue) initiated at the axon collaterals close to the main axon, while the diagonal and horizontal

pyramidal axons (Fig. 3, purple and green) were activated first at nodes located in the bending part of the main axon. During cathodal stimulation, Basket cell axons (Fig. 3, orange and red) were activated first on the node in the horizontal part of the axon closest to the stimulation electrode. When considering bipolar stimulation, the locations of activation on the axons beneath the anode were similar to monopolar anodal stimulation, and beneath the cathode similar to monopolar cathodal stimulation.

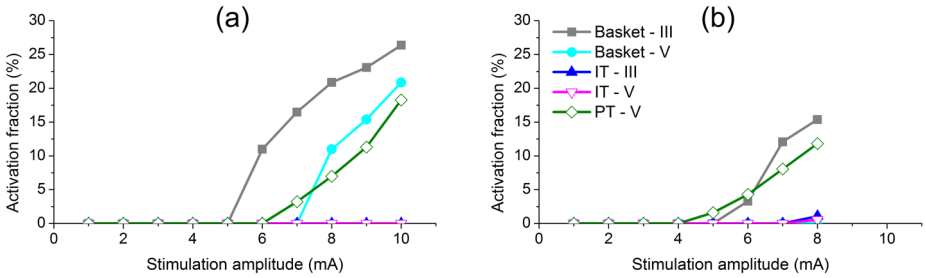

Figure 5. The activation fractions of different axonal populations that are believed to be involved in the mechanisms of MCS on PD. The clinically used stimulation protocols, epidural cathodal (a) and bipolar (b) stimulation, were modelled.

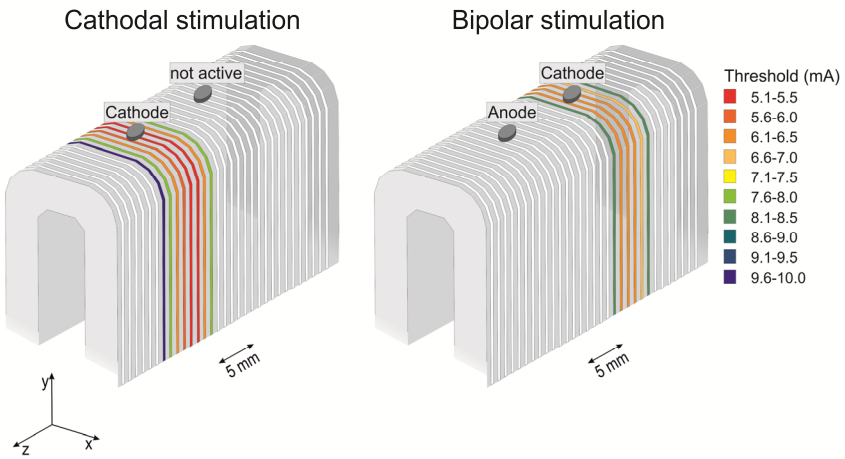

Figure 6. The spreading of the activation of the Basket cell axons in layer III during cathodal and bipolar epidural stimulation. Note that for illustrative reasons the Basket cell axons are depicted on the surface of the gyrus, while they are modelled at a depth corresponding to the middle of the third cortical layer.

Establishing more selective stimulation protocols

An extensive number of protocols was assessed in order to achieve more selective stimulation. The results of our model described above indicate that the Basket cell and PT type pyramidal axonal populations are excited in all clinically effective MCS protocols, while IT type pyramidal axons are not activated in all effective protocols. Therefore, we assume that the activation of IT type pyramidal axons is not involved in the clinical effect of MCS on PD and further assess selective stimulation of Basket cell axons and PT type pyramidal axons.

First, we assessed the two clinically applied protocols and varied the electrode configuration with an anode (table 3 – variation 1; Fig. 7). It is shown that cathodal stimulation most selectively activates Basket cell axons, while PT type axons are selectively targeted using anodal stimulation. Using these electrode configurations as a starting point, more selective stimulation protocols will be developed.

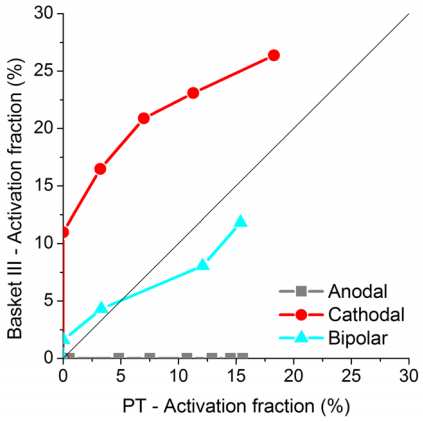

Figure 7. The two clinically applied stimulation protocols (table 3) and a variation in the electrode configuration, i.e. monopolar anodal stimulation (variation 1). Each point represents the activation fraction for a certain stimulation amplitude, which increases from 1 to 10 mA, in steps of 1 mA. Basket cell axons are most selectively activated during cathodal stimulation, while anodal stimulation selectively targets the PT type pyramidal axons.

Basket cell axons

The cathodal stimulation protocol most selectively stimulated Basket cell axons (Fig. 7). As IT type axons were not activated at all during this stimulation protocol (Fig. 5a), the selectivity of Basket cell axons against PT type axons was investigated further. Variations 5-9 (table 3) were assessed.

Selective stimulation of Basket cell axons can be improved by using multiple cathodes (variation 5; Fig. 8a). The optimal location and number of cathodes depended on the required Basket cell activation fraction. For higher fractions, multiple cathodes are preferable, while for lower fractions a single cathode or two separate cathodes offer the best selectivity. A second approach to stimulate the Basket cell axons more selectively was by using bipolar stimulation while placing the electrode strip perpendicular to the gyrus over the central sulcus with the cathode on top of the gyrus (variation 8). Compared to the cathodal stimulation protocol, the Basket cell axons were activated more selectively relatively to the PT type axons (Fig. 8b). Bipolar stimulation with the contacts placed closer to each other or further apart (variation 6) did not give a higher selective activation of the Basket cell axons. The electrode location (epidural/subdural; variation 7) and contact diameter (variation 9) had little influence on selectivity of Basket cell axons relatively to the PT population.

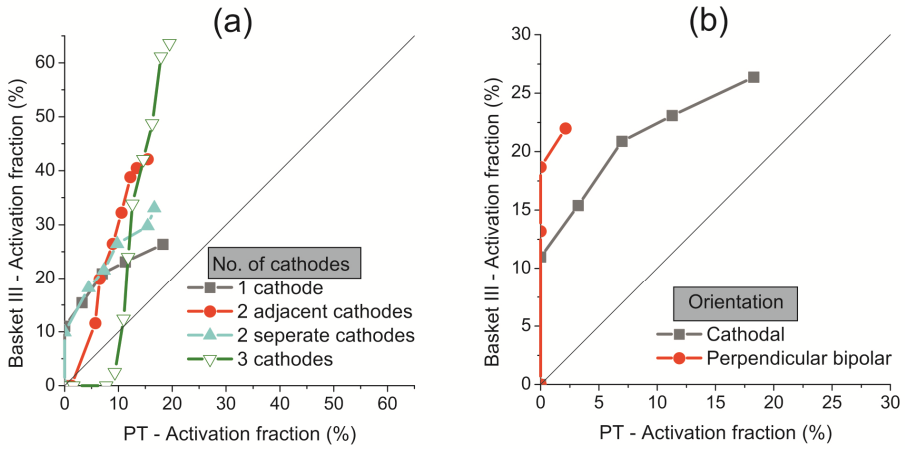

Figure 8. The following variations on the cathodal stimulation protocol provided more selective stimulation of the Basket cell axons relatively to the PT type pyramidal axons. Each point represents the activation fraction for a certain stimulation amplitude, which increases from 1 to 10 mA, in steps of 1 mA. (a) The activation fraction for a varying number of epidurally placed cathodes (variation 5). For Basket cell axon activation fractions up to ~20%, one cathode or two separate cathodes offered the highest selectivity. For larger activation fractions, two adjacent cathodes resulted in increased selectivity, and for fractions above 41% three cathodes was the best choice. (b) The perpendicular bipolar protocol with the cathode placed over the gyrus (variation 8) provided more selective stimulation of Basket cell axons than the cathodal stimulation protocol.

PT type pyramidal axons

Fig. 7 shows that anodal stimulation (variation 1) offers the highest selectivity for PT type pyramidal axons activation. As Basket cell axons are not activated at all within the clinically relevant stimulation amplitudes during anodal stimulation, the selectivity of PT type against IT type pyramidal axons is explored further. Variations 1-4 and 6 were assessed. Increased selectivity of PT type axon stimulation can be achieved by increasing the contact size (variation 4; Fig. 9a). Using subdural rather than epidural stimulation resulted in a lower selectivity towards PT type axons (variation 2; Fig. 9b). This selectivity was also decreased when using bipolar stimulation (variation 3) with the anode on top of the gyrus and the strip placed perpendicular to the gyrus over the sulcus and when using bipolar stimulation with the contacts spaced closer to each other or further away (variation 6).

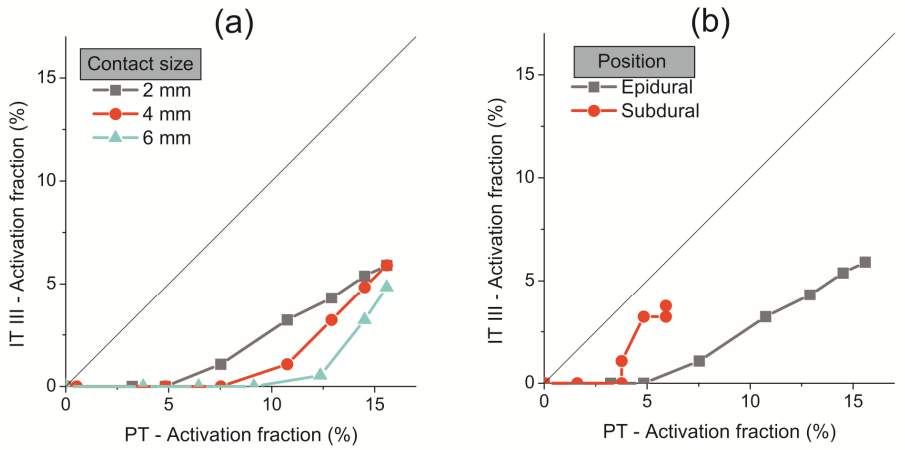

Figure 9. (a) The selectivity of the activation of PT type against IT type pyramidal axons during anodal stimulation increased with a larger contact size (variation 4). Each point represents the activation fraction for a certain stimulation amplitude, which increases from 1 to 10 mA, in steps of 1 mA. (b) PT type axons were activated more selectively durin epidural stimulation than during subdural stimulation. The activation fraction for increasing stimulation amplitudes from 0.1 to 1 mA, in steps of 0.1 mA, are shown.

4.4. Discussion

The axonal population responsible for clinically effective MCS on PD

We examined the activation of several axonal populations in order to identify the populations activated during clinically effective MCS treatment for PD. We found that IT type pyramidal axons were not activated during all clinically effective stimulation protocols, while both Basket cell axons and PT type pyramidal axons were activated. This suggests that it is unlikely that the activation of IT type axons is responsible for the clinical effect M CS has on PD. Our model predicts that either the activation of Basket cell axons or PT type pyramidal axon is involved in this clinical effect.

Activation of the Basket cell axons supports the theory that the inhibitory axonal population plays an important role in the clinical effect of MCS on PD (Hanajima et al. 2002; Cioni 2007; Arle et al. 2008; Meglio and Cioni 2009). However, since the pyramidal neurons that innervate the hyperdirect, direct and indirect pathways are inhibited by the Basket cells, theories suggesting the involvement of these pathways are also likely true (Pagni et al. 2005; Cioni 2007; Cioni et al. 2007; Meglio and Cioni 2009). These network properties are important as chronic MCS is performed by applying a continuous train of pulses instead of just a single pulse as in our model. The result of train stimulation is a cumulative sum of the facilitating and inhibitory effects, thus the effect of stimulation trains may depend on whether facilitation or inhibition dominates the response to single stimuli (Hanajima et al. 2002). The main hypothesis on the mechanisms of DBS concerns prevention of the transmission of the pathologic network activity generated in the cortico-basal-ganglia-thalamo-cortical loop (McIntyre and Hahn 2010). Likewise, the Basket cells have inhibitory properties and can thereby reduce the loop-gain in the motor cortex, which could prevent transmission of the pathological activity in these loops.

Activation of the PT type pyramidal axons agrees with theories suggesting modulation of the hyperdirect pathway to play a role in the mechanisms of MCS (Pagni et al. 2005), but as these axons innervate other pyramidal axons, excitation of the direct and indirect pathways could also explain the clinical effect (Cioni 2007; Cioni et al. 2007; Meglio and Cioni 2009).

Establishing more selective stimulation protocols

Since our model predicts that either the Basket cell axons or the PT type pyramidal axons are highly likely candidates for the clinical effect, activation of these axonal populations with a higher selectivity was assessed. Selective targeting

of the population involved in the clinical effect could improve the effect of the treatment.
Based on the modelling results, cathodal epidural stimulation, often used to treat PD, is the protocol that most selectively targets the Basket cell axons. The following protocols can increase this selectivity even further: the use of multiple cathodes either adjacent or with an inactive contact in between; applying bipolar stimulation rather than cathodal stimulation with the electrode strip placed perpendicular to the gyrus and the cathode overlying the gyrus. The contact size of the electrode contacts and the use of epidural rather than subdural stimulation did not influence selectivity towards Basket cell axons during cathodal stimulation.
According to our model, selective stimulation of PT type pyramidal axons can be achieved by anodal epidural stimulation using electrodes with large contact sizes. Selective stimulation of the PT type axons was reduced when using subdural stimulation and bipolar stimulation with the strip oriented parallel as well as perpendicular to the gyrus.
In the future, these new protocols should be tested experimentally with evaluation of the effect on motor symptoms using clinical rating scales (Fahn and Elton 1987) and objective movement measurements (Zwartjes et al. 2010). This could help to confine which axonal population, i.e. Basket cell axons or PT type pyramidal axons, should be activated in order to achieve clinically effective stimulation for the treatment of PD. The selective protocols could offer means to improve this treatment.

Comparison to previous modelling studies
Assessing the location at which the axon was excited, we found that during anodal stimulation excitation generally started at a node close to the grey and white matter boundary. This is in agreement with earlier modelling studies (Manola et al. 2007; Wongsarnpigoon and Grill 2012). Like Salvador et al. (Salvador et al. 2011), we found that during cathodal stimulation, the action potential was generated at the axon collateral in the vertical pyramidal axon (Fig. 3, blue). They indicated that with large diameter differences between the main and collateral axon, the action potential did not propagate from the collateral to the main axon. However when considering diameter differences consistent with our model, they did see propagation to the main axon, which is similar to our findings. In addition, they also found activation to be started on a node at the bend of the main axon in the diagonal and horizontal pyramidal axons (Fig. 3, purple and green). Furthermore, during cathodal stimulation the Basket cell axons were activated in the nodes closest to the electrode at the horizontal part of the main axon, which is similar to Manola's findings (Manola et al. 2007).

During bipolar stimulation, axons beneath the anode and cathode were activated at similar locations compared to monopolar stimulation. This is in agreement with the findings of Holsheimer et al. (Holsheimer et al. 2007), who argued that bipolar stimulation with the electrodes at least 10 mm apart is actually bifocal.
Our model shows that anodal stimulation favours activation of axons running perpendicular to the pial surface, i.e. pyramidal axons (Fig. 7), which is in agreement with a previous model study on MCS for pain (Manola et al. 2007). Cathodal stimulation selectively activates Basket cell axons, which run parallel to the pial. This is also in agreement with the study of Manola et al. (Manola et al. 2007). In contrast, our results also show activation of the vertical pyramidal axons (Fig. 3, blue), which were not activated in Manola's study. This is caused by the inclusion of axon collaterals in the pyramidal axon model.

Model limitations
In our model, we simulated single pulse stimulation. As the clinical application of MCS encompasses high frequency chronic stimulation, network properties are involved (Hanajima et al. 2002). The final effect of the stimulation depends on parameters such as the number of synaptic contacts and their strengths, as well as the axon density. These parameters are, except for certain axon density parameters (personal communication Feierabend. H.K.P.), not yet sufficiently available. Therefore, we looked at activation fractions of different axonal populations relatively to one another. Second, we used a fixed CSF-layer thickness, while the thickness depends on the brain location and is different per person. This will probably influence model outcomes (Manola et al. 2005) and it could therefore be included in patient specific models in the future. Third, the axon was modelled without a soma and dendrites, while both influence the axon boundary node. This may have introduced a small difference in the results, especially in the pyramidal axons which have somas close to the electrode contact. Fourth, although the diameters were for a large part based on human data, the ratios between the PT and IT type axon diameters were based on rat data, as no human data was available on this. Finally, the Basket cell axons were modelled running parallel to the pial surface in the xy-plane, while they also run in *z*-direction (Fig. 3). This likely has the largest influence on the results of bipolar stimulation parallel to the gyrus, which will probably excite Basket cell axons running in *z*-direction relatively more easily. This would provide better selective stimulation of Basket cell axons than anticipated in our current model, which is in favour of the hypothesis that these axon type is involved in clinically effective stimulation.

4.5. Conclusions

Our computational model predicts that the clinical effect of MCS in the treatment of PD is related to the activation of either the inhibitory Basket cell axonal population or the excitatory PT type pyramidal axons. Selective stimulation of the Basket cell axonal population can be achieved using cathodal, rather than anodal stimulation. When bipolar stimulation is applied, the electrode strip is preferably placed over the sulcus perpendicular to the gyrus. Furthermore, selective stimulation of the Basket cell axons can be increased by the use of multiple cathodes. PT type pyramidal axons can be selectively targeted using anodal stimulation with electrodes having large contact sizes. Epidural stimulation is advisable over subdural stimulation. To further confine which population is involved in the clinical effect of MCS, protocols selectively targeting one of both axonal populations can be tested for their effect on PD. Such selective stimulation protocols could also improve MCS for PD. In conclusion, this study provides more insight into the neuronal population involved in the clinical effect of chronic MCS on PD and proposes strategies to improve this therapy.

Appendix

The axon model (Schwarz et al. 1995) at 37◦C
Gating variables , with the gating coefficients α and β in s-1 and the membrane potential at the node, V_n, in V.

$$\alpha_m = \frac{7.1*10^6(V_n + 0.0184)}{1 - e^{\frac{-0.0184 - V_n}{0.0103}}}$$

$$\beta_m = \frac{3.3*10^5(-0.0227 - V_n)}{1 - e^{\frac{V_n + 0.0227}{0.0092}}}$$

$$\alpha_h = \frac{2.1*10^5(-0.111 - V_n)}{1 - e^{\frac{V_n - 0.111}{0.011}}}$$

$$\beta_h = \frac{1.4*10^4}{1 + e^{\frac{-0.0288 - V_n}{0.0134}}}$$

$$\alpha_n = \frac{5.2*10^4(V_n + 0.0932)}{1 - e^{\frac{-0.0932 - V_n}{0.0011}}}$$

$$\beta_n = \frac{9.2*10^4(-0.076 - V_n)}{1 - e^{\frac{V_n + 0.076}{0.0105}}}$$

$$\alpha_s = \frac{7.9*10^3(V_n + 0.0125)}{1 - e^{\frac{-0.0125 - V_n}{0.0236}}}$$

$$\beta_s = \frac{4.8*10^3(-0.0801 - V_n)}{1 - e^{\frac{V_n + 0.0801}{0.0218}}}$$

$$\frac{dm}{dt} = \alpha_m(1 - m) - \beta_m m$$

$$\frac{dh}{dt} = \alpha_h(1 - h) - \beta_h h$$

$$\frac{dn}{dt} = \alpha_n(1 - n) - \beta_n n$$

$$\frac{ds}{dt} = \alpha_s(1 - s) - \beta_s s$$

The ionic currents and leakage are in A/m^2

Sodium current

$$I_{Na} = m^3 * h * J$$

$$J = \frac{P_{Na} z^2 F^2 V_n}{RT} \frac{Na_i - Na_o e^{-\frac{zFV_n}{RT}}}{1 - e^{-\frac{zFV_n}{RT}}}$$

Fast potassium current

$$I_{Kf} = n^4 g_{Kf} (V_n - V_K)$$

Slow potassium current

$$I_{Ks} = s g_{Ks} (V_n - V_K)$$

Leakage current

$$I_L = g_L (V_n - V_L)$$

Sodium permeability, P_{Na}=7.04·10^{-5} m/s
Sodium ion valency, z=1
Faraday's constant, F=96485 C/mol
Gas constant, R=8.3144 J/K*mol
Temperature, T=310 K
Intracellular Na concentration, Na_i=18 mM
Extracellular Na concentration, Na_o=154 mM
Potassium equilibrium potential, V_k=-0.0887 V
Leakage equilibrium potential, V_L=-0.084 V
Fast K conductance, g_{Kf}=300 S/m^2
Slow K conductance, g_{Ks}=600 S/m^2
Leak conductance, g_L=400 S/m^2

References

Arle, J. E., D. Apetauerova, J. Zani, D. Vedran Deletis, D. L. Penney, D. Hoit, C. Gould and J. L. Shils (2008). "Motor cortex stimulation in patients with Parkinson disease: 12-month follow-up in 4 patients." J. Neurosurg. 109: 133-139.

Arle, J. E. and J. L. Shils (2008). "Motor Cortex Stimulation for Pain and Movement Disorders." Neurotherapeutics 5: 37-49.

Ballion, B., N. Mallet, E. Bézard, J. L. Lanciego and F. Gonon (2008). "Intratelencephalic corticostriatal neurons equally excite striatonigral and striatopallidal neurons

and their discharge activity is selectively reduced in experimental parkinsonism." Eur. J. Neurosci. 27(9): 2313-2321.

Baumann, S. B., D. R. Wozny, S. K. Kelly and F. M. Meno (1997). "The electrical conductivity of human cerebrospinal fluid at body temperature." IEEE Trans. Biomed. Eng. 44: 220-223.

Benabid, A. L. (2003). "Deep brain stimulation for Parkinson's disease." Curr. Opin. Neurobiol. 13: 696-706.

Butson, C. R. and C. C. McIntyre (2008). "Current steering to control the volume of tissue activated during deep brain stimulation." Brain Stimul. 1: 7-15.

Canavero, S. and R. Paolotti (2000). "Extradural motor cortex stimulation for advanced Parkinson's disease: Case report." Mov. Disord. 15(1): 169-171.

Cioni, B. (2007). "Motor cortex stimulation for Parkinson's disease." Acta Neurochir. S97(2): 233-238.

Cioni, B., A. Bentivoglio, C. De Simone, A. Fasano, C. Piano, D. Policicchio, V. Perotti and M. Meglio (2009). Invasive cortical stimulation for Parkinson's disease and movement disorders. New York, Nova Science Publishers, Inc.

Cioni, B., M. Meglio, V. Perotti, P. De Bonis and N. Montano (2007). "Neurophysiological aspect of chronic motor cortex stimulation." Clin. Neurophysiol. 37: 441-447.

Drouot, X., S. Oshino, B. Jarraya, L. Besret, H. Kishima, P. Remy, J. Dauguet, J. P. Lefaucheur, F. Dolle, F. Conde, M. Bottlaender, M. Peschanski, Y. Keravel, P. Hantraye and S. Palfi (2004). "Functional recovery in a primate model of parkinson's disease following motor cortex stimulation." Neuron 44: 769-778.

Fahn, S. and R. L. Elton (1987). Unified Parkinson's Disease Rating Scale development Committee: Unified Parkinson's Disease Rating Scale. Recent developments in Parkinson's disease. S. Fahn, C. D. Marsden and D. Calne. New York, Macmillan**:** 153-164.

Fasano, A., C. Piano, C. De Simone, B. Cioni, D. Di Giuda, M. Zinno, A. Daniele, M. Meglio, A. Giordano and A. Bentivoglio (2008). "High frequency extradural motor cortex stimulation transiently improves axial symptoms in a patient with Parkinson's disease." Mov. Disord. 23(13): 1916-1919.

Foster, K. R., J. M. Bidinger and D. O. Carpenter (1976). "The electrical resistivity of cytoplasm." Biophys. J. 16: 991-1001.

Frankemolle, A. M. M., J. Wu and A. M. Noecker (2010). "Reversing cognitive-motor impairments in Parkinson's disease patients using a computational modelling approach to deep brain stimulation programming." Brain 133: 746-761.

Gabriel, S., R. W. Lau and C. Gabriel (1996). "The dielectric properties of biological tissues: III. Parametric models for the dielectric spectrum of tissues." Phys. Med. Biol. 41(11): 2271-2293.

Giuffrida, R., G. Li Volsi, G. Maugeri and V. Percivalle (1985). "Influences of pyramidal tract on the subthalamic nucleus in the subthalamic nucleus of the cat." Neurosci. Lett. 54: 231-235.

Grant, P. F. and M. M. Lowery (2009). "Electric field distribution in a finite-volume head model of deep brain stimulation." Med. Eng. Phys. 31: 1095-1103.

Gutierrez, J. C., F. J. Seijo, M. A. Alcarez Vega, F. Fernandez Gonzalez, B. Lozano Aragoneses and M. Blazquez (2009). "Therapeutic extradural cortical stimulation for Parkinson's diseease: Report of six cases and review of the literature." Clin. Neurol. Neurosurg. 111: 703-707.

Hanajima, R., P. Ashby, A. E. Lang and A. M. Lozano (2002). "Effects of acute stimulation through contacts placed on the motor cortex for chronic stimulation." Clin. Neurophysiol. 113: 635-641.

Holsheimer, J., J. Nguyen, J. P. Lefaucheur and L. Manola (2007). "Cathodal, anodal or bifocal stimulation of the motor cortex in the management of chronic pain?" Acta Neurochir. S97(2): 57-66.

Huxley, A. F. and R. Stämpfli (1949). "Evidence for saltatory conduction in peripheral myelinated nerve fibers." J. of Physiol. 108: 315-339.

Janssen, M. L. F., D. G. M. Zwartjes, Y. Temel, V. Van Kranen-Mastenbroek, A. Duits, L. J. Bour, P. H. Veltink, T. Heida and V. Visser-Vandewalle (2012). "Subthalamic neuronal responses to cortical stimulation." Mov. Disord. 27(3): 435-438.

Lefaucheur, J. P., J. Holsheimer, C. Goujon, Y. Keravel and J. Nguyen (2010). "Descending volleys generated by efficacious epidural motor cortex stimulation in patients with chronic neuropathic pain." Exp. Neurol. 223: 609-614.

Lei, W., Y. Jiao, N. Del Mar and A. Reiner (2004). "Evidence for Differential Cortical Input to Direct Pathway versus Indirect Pathway Striatal Projection Neurons in Rats " J. Neurosci. 24(38): 8289-8299.

Manola, L. and J. Holsheimer (2007). "Motor cortex stimulation: role of computer modelling." Acta Neurochir. S97(2): 497-503.

Manola, L., J. Holsheimer, P. H. Veltink and J. R. Buitenweg (2007). "Anodal vs cathodal stimulation of motor cortex: A modeling study." Clin. Neurophysiol. 118: 464-474.

Manola, L., B. H. Roelofsen, J. Holsheimer, E. Marani and J. A. Geelen (2005). "Modelling motor cortex stimulation for chronic pain control: Electrical potential field, activating functions and responses of simple nerve fibre models." Med. Biol. Eng. Comput. 43: 335-343.

Mathai, A. and S. Smith (2011). "The corticostriatal and corticosubthalamic pathways: two entries, one target. So what?" Front. Syst. Neurosci. 5(64).

McIntyre, C. C. and P. J. Hahn (2010). "Network perspectives on the mechanisms of deep brain stimulation." Neurobiol. Dis. 38: 329-337.

McIntyre, C. C., S. Mori, D. L. Sherman, N. V. Thakor and J. L. Vitek (2004). "Electric field and stimulating influence generated by deep brain stimulation of the subthalamic nucleus." Clin. Neurophysiol. 115: 589-595.

McNeal, D. R. (1976). "Analysis of a Model for Excitation of Myelinated Nerve." IEEE Trans. Biomed. Eng. BME-23(4): 329-337.

Meglio, M. and B. Cioni (2009). Motor cortex stimulation for Parkinson's disease. Textbook of stereotactic and functional neurosurgery. A. M. Lozano, P. Gildenberg and R. Tasker. Berlin Heidelberg, Springer. 7**:** 1679-1690.

Nieuwenhuys, R. (1994). "The neocortex An overview of its evolutionary development, structural organization and synaptology." Anatomy and embryology 190: 307-337.

Nishibayashi, H., M. Ogura, K. Kakishita, S. Tanaka, Y. Tachibana, A. Nambu, H. Kita and T. Itakura (2011). "Cortically Evoked Responses of Human Pallidal Neurons Recorded During Stereotactic Surgery." Mov. Disord. 26(3): 469-476.

Nowak, L. G. and J. Bullier (1998a). "Axons, but not cell bodies, are activated by electrical stimulation in cortical gray matter. I. Evidence from chronaxie measurements." Exp. Brain Res. 118(4): 477-488.

Nowak, L. G. and J. Bullier (1998b). "Axons, but not cell bodies, are activated by electrical stimulation in cortical gray matter. II. Evidence from selective inactivation of cell bodies and axon initial segments." Exp Brain Res 118(4): 489-500.

Pagni, C. A., M. G. Altibrandi, A. Bentivoglio, G. Caruso, B. Cioni, C. Fiorella, A. Insola, A. Lavano, R. Maina, P. Mazzone, C. D. Signorelli, C. Sturiale, F. Valzania, S. Zeme and F. Zenga (2005). "Extradural Motor Cortex Stimulation (EMCS) for Parkinson's disease. History and first results by the study group of the Italian neurosurgical society." Acta Neurochir. S93: 113-119.

Plonsey, R. and D. B. Heppner (1967). "Considerations of quasi-stationarity in electrophysiological systems." Bulletin of Mathematical Biophysics 29(4): 657-664.

Ranck, J. B. and S. L. BeMent (1965). "The specific impedance of the dorsal columns of the cat: An anisotropic medium." Exp. Neurol. 11: 451-463.

Reiner, A., Y. Jiao, N. Del Mar, A. V. Laverghettam and W. Lei (2003). "Differential morphology of pyramidal tract-type and intratelencephalically projecting-type corticostriatal neurons and their intrastriatal terminals in rat." J. Comp. Neurol. 457: 420-440.

Richardson, A. G., C. C. McIntyre and W. M. Grill (2000). "Modeling the effects of electric fields on nerve fibres: Influence of the myelin sheath " Med. Biol. Eng. Comput. 38(4): 438-446.

Salvador, R., S. Silva, P. J. Basser and P. C. Miranda (2011). "Determining which mechanisms lead to activation in the motor cortex: A modeling study of transcranial magnetic stimulation using realistic stimulus waveforms and sulcal geometry." Clin. Neurophysiol. 122(4): 748-758.

Scheufler, O., N. M. Kania, C. M. Heinrichs and K. Exner (2003). "Hyperplasia of the subcutaneous adipose tissue is the primary histopathologic abnormality in lipedematous scalp." Am. J. Dermatopathol. 25(3): 248-252.

Schwarz, J. R., G. Reid and H. Bostock (1995). "Action potentials and membrane currents in the human node of Ranvier." Pflugers Arch. 430: 283-292.

Silva, S., P. J. Basser and P. C. Miranda (2008). "Elucidating the mechanisms and loci of neuronal excitation of transcranial magnetic stimulation using a finite element model of cortical sulcus." Clin. Neurophysiol. 119: 2405-2413.

Sloper, J. J. and T. P. S. Powell (1979). "A study of the axon intial segment and proximal axon of neurons in the primate motor and somatic sensory cortices."

Philisophical transactions of the royal society of London. Series B, Biological sciences 285(1006): 173-197.

Snyder, W. S. (1975). International Commission of Radiological Protection. Report of the task group on reference man. Londen, Oxford Pergamon Press.

Sotiropoulos, S. N. and P. N. Steinmetz (2007). "Assessing the direct effects of deep brain stimulation using embedded axon models." J. Neural Eng. 4: 107-119.

Struijk, J. J., J. Holsheimer, G. Barolat, J. He and H. B. K. Boom (1993). "Paresthesia thresholds in spinal cord stimulation: A comparison of theoretical results with clinical data." IEEE Trans. Neural Syst. Rehabil. Eng. 1(2): 101-108.

Takada, M., H. Tokuno, A. Nambu and M. Inase (1998). "Corticostriatal projections from the somatic motor areas of the frontal cortex in the macaque monkey: segregation versus overlap of input zones from the primary motor cortex, the supplementary motor area, and the premotor cortex." Exp. Brain Res. 120: 114-128.

Tsubokawa, T., Y. Katayama, T. Yamamoto, T. Hirayama and S. Koyama (1991). "Treatment of thalamic pain by chronic motor cortex stimulation." PACE-Pacing Clin. Electrophysiol. 14(1): 131-134.

Wesselink, W. A., J. Holsheimer and H. B. K. Boom (1999). "A model of the electrical behaviour of myelinated sensory nerve fibres based on human data." Med. Biol. Eng. Comput. 37: 228-235.

Wongsarnpigoon, A. and W. M. Grill (2008). "Computational modeling of epidural cortical stimulation." J. Neural Eng. 5: 443-454.

Wongsarnpigoon, A. and W. M. Grill (2012). "Computer-based model of epidural motor cortex stimulation: Effects of electrode position and geometry on activation of cortical neurons." Clin. Neurophysiol. 123: 160-172.

Zwartjes, D. G. M., T. Heida, J. P. van Vugt, J. A. Geelen and P. H. Veltink (2010). "Ambulatory monitoring of activities and motor symptoms in Parkinson's disease." IEEE Trans. Biomed. Eng. 57(11): 2778-2786.

Chapter 5

Current source density analysis of cortically evoked potentials in the rat subthalamic nucleus

Daphne G.M. Zwartjes
Marcus L.F. Janssen
Kees J. van Dijk
Yasin Temel
Veerle Visser-Vandewalle
Peter H. Veltink
Abdelhamid Benazzouz
Tjitske Heida

Abstract

The subthalamic nucleus (STN) is the main target for deep brain stimulation (DBS) in Parkinson's disease. As the STN has been shown to contain multiple functional areas, the sensorimotor part of the nucleus should be targeted to guarantee the optimal motor benefit. Thus, we propose locating the motor region by measuring the subthalamic response to motor cortex (MC) stimulation (MCS). To interpret the response, we assess an approach enabling computation of the sources and sinks of the neuronal input in the STN. This approach involves the inverse current source density (iCSD) method to estimate the CSD from cortically evoked local field potentials in the STN. We assess this new approach by studying the cortically evoked potentials in a three dimensional grid in anesthetized rats. Cortical stimulation evokes two excitatory periods in the STN, which are interrupted by a brief inhibition. These events are followed by a long inhibitory period. CSD analysis of our experiments resulted in clear and well discriminable sources and sinks of the neuronal input activity in the STN. The analysis showed that the sink corresponding to the direct input from the MC was located medial to the source of the globus pallidus input. Furthermore, the inputs of the paths evoking the long inhibitory period after MCS and cingulate gyrus stimulation are located in the same STN area. Finally, our results indicate that the long inhibitory period after MCS results from an inhibitory input from the globus pallidus, which might have been induced by cortical disfacilitation affecting the indirect pathway.

5.1. Introduction

Deep brain stimulation of the subthalamic nucleus (STN-DBS) has emerged as an effective surgical

The subthalamic nucleus (STN) is one of the entry ports of trough which cortical information enters the basal ganglia output nuclei (Nambu et al. 2002). Cortical signals are conveyed to the STN by the monosynaptic cortico-subthalamic, also known as the ' hyperdirect' pathway, and the multisynaptic, indirect pathway. The indirect pathway first passes through the striatum and globus pallidus (GP) before entering the STN.

In primates and humans, it has been shown that the STN is involved in motor, limbic and associative behaviors (Temel et al. 2005). The dorso-lateral subthalamic region is linked to motor function and the ventro-medial region to limbic and associative processes. The rat STN is segregated to a lesser extent (Kolomiets et al. 2001; Janssen et al. 2010). Tracing studies have shown that the lateral two thirds of the rodent STN mainly receive input from motor and pre-motor cortices. The medial third mainly receives input from the cingulate (CG), prelimbic and agranular insular cortices (for review see(Janssen et al. 2010). In addition, electrophysiological studies (Magill et al. 2004) have shown that rostral areas of the STN respond differently to stimulation of the frontal cortex than caudal areas. In response to motor cortex stimulation (MCS), STN neurons show a distinctive pattern of increased and decreased spike activity. The periods of increased spike activity are related to the excitation of the monosynaptic cortico-subthalamic pathway (N1, Fig. 1) (Kitai and Deniau 1981; Fujimoto and Kita 1993; Maurice et al. 1998; Nambu et al. 2000; Kolomiets et al. 2001; Magill et al. 2004) and disinhibition via the indirect pathway (N2, Fig. 1) (Maurice et al. 1998; Nambu et al. 2000; Magill et al. 2004). These events are interrupted by an inhibitory period, which is believed to result from the STN-GP-STN connection (P1, Fig. 1) (Fujimoto and Kita 1993; Maurice et al. 1998; Nambu et al. 2000; Magill et al. 2004). After the last excitation, a long-latency, long-duration inhibitory period follows (P2, Fig. 1). The source of this inhibition is unknown. Some neurons show the entire pattern of increased and decreased spiking rate, while others only show a part of this typical pattern (Magill et al. 2004).

In the last decades, deep brain stimulation (DBS) of the STN has shown to be an effective treatment for motor symptoms in MPTP monkeys (Benazzouz et al. 1993) and in patients with Parkinson's disease (PD) (Krack et al. 2003; Deuschl et al. 2006; Weaver et al. 2009). One of the major hurdles is the occurrence of cognitive and limbic alterations in some of the STN DBS treated patients (Temel et al. 2006; Witt et al. 2008). We hypothesized that the occurrence of psychiatric side effects of STN DBS can be reduced by selectively targeting the STN motor

area (Janssen et al. 2012; Zwartjes et al. 2013). To selectively target the motor area, we propose to identify the STN motor region by measuring the subthalamic neuronal responses to MCS (Janssen et al. 2012; Zwartjes et al. 2013). This cortically evoked subthalamic response signal contains information about the optimal location for the DBS electrode, but it has yet to be determined how this information can be extracted from the response signal most optimally. The response signal consists of two components, namely the unit activity and the local field potential (LFP). The unit activity reflects the action potentials generated by the neurons, while the LFPs represent the postsynaptic activity (Buzsaki 2004). In other words, the unit activity is a measure of the output of a single neuron and the LFP represents the input of a larger neuronal population. By computing the current source density (CSD) from the LFPs, one can study the sinks and sources of the neuronal input (Pettersen et al. 2006; Łęski et al. 2007). The CSD approach offers interesting opportunities to interpret the subthalamic response signal: the sources and sinks of the neuronal input could be used to determine the placement of the electrode during human DBS surgery. Before this approach can be applied in human, certain aspects of the CSD method should be assessed in more detail: are there clear sources and sinks present in the STN, which correspond to inputs from different brain structures?; How are these sources and sinks of different brain structures located relatively to each other?

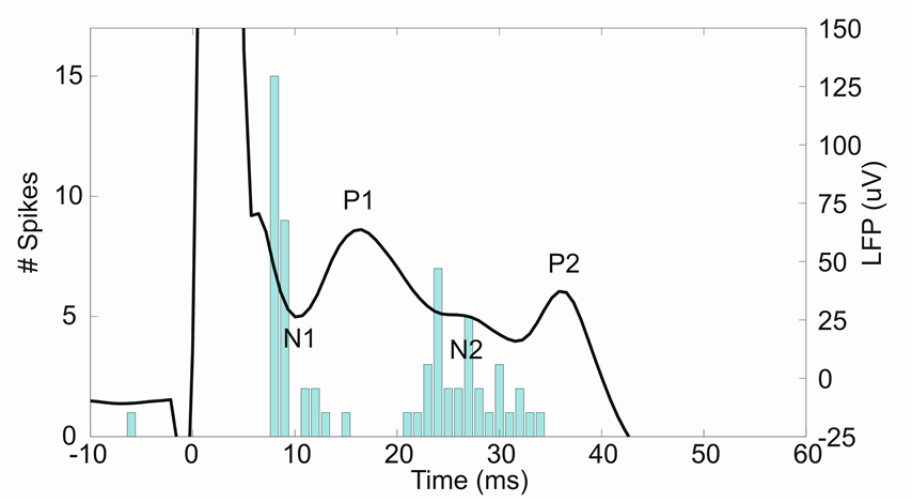

Figure 1. The evoked LFP and peristimulus time histogram (PSTH) of the unit activity in the STN after 600 μA MCS. At 0 ms the stimulus is given. The negative deflections of the LFP, N1 and N2, are accompanied by an increased spiking rate as seen in the PSTH. In contrast, the positive deflections, P1 and P2, occurred concurrently with a decreased spiking rate in the PSTH.

Current electrophysiological studies on cortically evoked subthalamic responses have mainly focused on unit activity (Fujimoto and Kita 1993; Maurice et al. 1998; Kolomiets et al. 2001; Magill et al. 2004) only one study has also assessed the LFPs but not the CSD (Magill et al. 2004). In this study, we applied an approach to estimate the CSD from cortically evoked subthalamic LFPs measured in a 3D grid, which allowed us to assess the neuronal input activity into the rat STN. We distinguished cortical inputs from the MC and CG. Secondly, we assessed the cortico-subthalamic pathways, i.e. both the monosynaptic (hyperdirect) and multisynaptic (indirect) pathways, and the STN-GP-STN connections. Additionally, we elaborated on the source of the long-latency inhibitory period, P2, after MCS. Finally, we discussed the future prospects of this approach for locating the optimal target during STN DBS surgery in PD patients.

5.2. Methods

Experimental design

The experiments described in this paper were conducted on seven male Sprague Dawley rats (IFFA Credo), weighing 250-400 g. Experiments were carried out according to the European Economic Community (86-6091 EEC) and the French National Committee (décret 87/848, Ministère de l'Agriculture et de la Forêt) guidelines for the care and use of laboratory animals and were approved by the Ethical Committee of Centre National de la Recherche Scientifique, Région Aquitaine-Limousin. In each rat, measurements were performed in the right hemisphere. The rats were anesthetized with urethane hydrochloride (1.2 g/kg, i.p. injections, Sigma-Alrich, France) and fixed in a stereotactic frame (Horsley Clarke apparatus, Unimécanique, Epinay sur Seine, France). Body temperature was monitored with a rectal probe and maintained at 37 ^{o}C with a homeothermic warming blanket (model 50-7061, Harvard Apparatus, Les Ulis, France). Burr holes in the skull were made above the stimulation and recording sites. A saline solution was applied on all exposed cortical areas to prevent dehydration. The microelectrode probe with 16 contacts was used to perform the electrophsyiological recordings (A1x16–10mm–100–703–A16 , Neuronexus, Ann Arbor, USA). Each contact on the probe has a contact area of 703 μm^2, which are spaced 100 µm from each other. The probe was lowered into the brain towards the STN using a microdrive (Microcontroler ESP 300, Newport, Evry, France). Stereotactic coordinates in mm relative to Bregma were: AP −3.8, ML ±2.5, DV −8.0 (Paxinos and Watson 1998). When the electrode was in place, the stimulation session started. Recordings of both the unit activity at a sample rate

of 22321 Hz and the LFPs at a sample rate of 1395 Hz were performed concurrently with cortical stimulation using the AlphaLab SnR system (AlphaOmega, Jeruzalem, Israel). Stimulation was performed ipsilateral to the recording site with two concentric bipolar electrodes in the MC and CG (Tan et al. 2010). Electrical stimuli were generated with an isolated stimulator (DS3, Digitimer Ltd., Hertfordshire, UK) triggered by the AlphaLab SnR (AlphaOmega, Jeruzalem, Israel). After the first stimulation session, the recording probe was retrieved and inserted again at the same depth, but shifted 200 µm in medial-lateral or anterior-posterior direction. This was repeated to obtain a total of 20 trajectories, five in medio-lateral direction and four in anterio-posterior direction. As the probe consisted of 16 electrode contacts, a 3D measurement grid of 4x5x16 (anterior-posterior x medial-lateral x dorsal-ventral) was achieved (Fig. 3 and 4). Traces of the electrodes along the trajectories have been verified anatomically under the microscope (Fig. 2). Only data from rats in which the traces had been within the STN were analyzed. Precise coordinates of the electrode trajectories were unfortunately not retrievable.

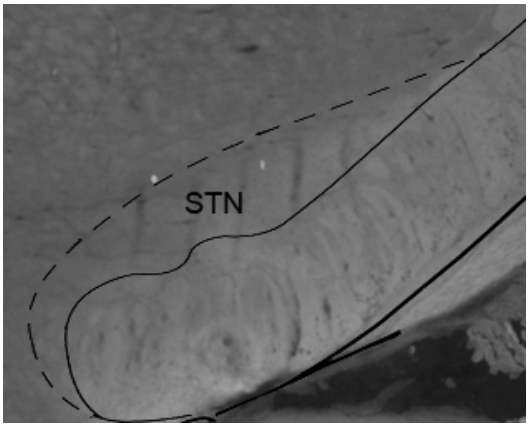

Figure 2. A selection of a microscope image of a coronal brain slice (Anterior-posterior -3.8 mm relative to Bregma). In the brain slice, the electrode trajectories are visible within the STN.

Stimulation protocol

During each session, stimulation was performed at two different cortical areas, the MC and CG. Before starting stimulation, a baseline recording of 2 minutes was made. During MCS, 99 stimuli with an amplitude of 300 µA and 99 stimuli with an amplitude of 600 µA were given. Another 99 stimuli with an amplitude of 600 µA were given during cingulate gyrus stimulation (CGS). The stimuli had a pulse width of 0.3 ms and the stimulation frequency was 1.1 Hz.

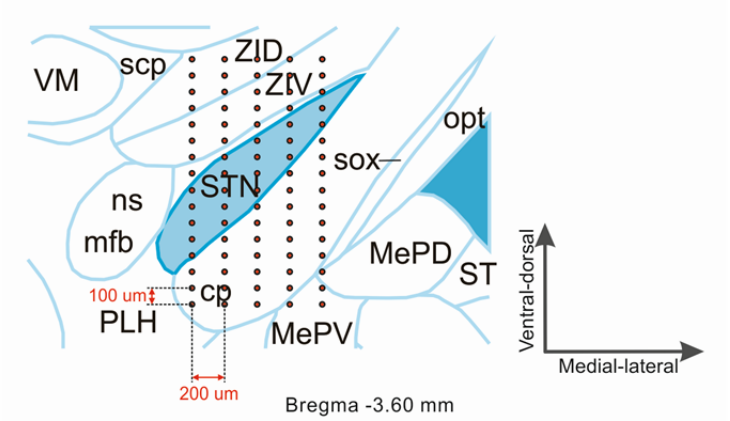

Figure 3. A slice of the 3D measurement grid in the anterior-posterior plane (bregma -3.60 mm)(Paxinos and Watson 1998), a 5x16 grid (medial-lateral x dorsal-ventral). Each row of 16 points in the dorsal-ventral direction corresponds with one trajectory of the electrode.

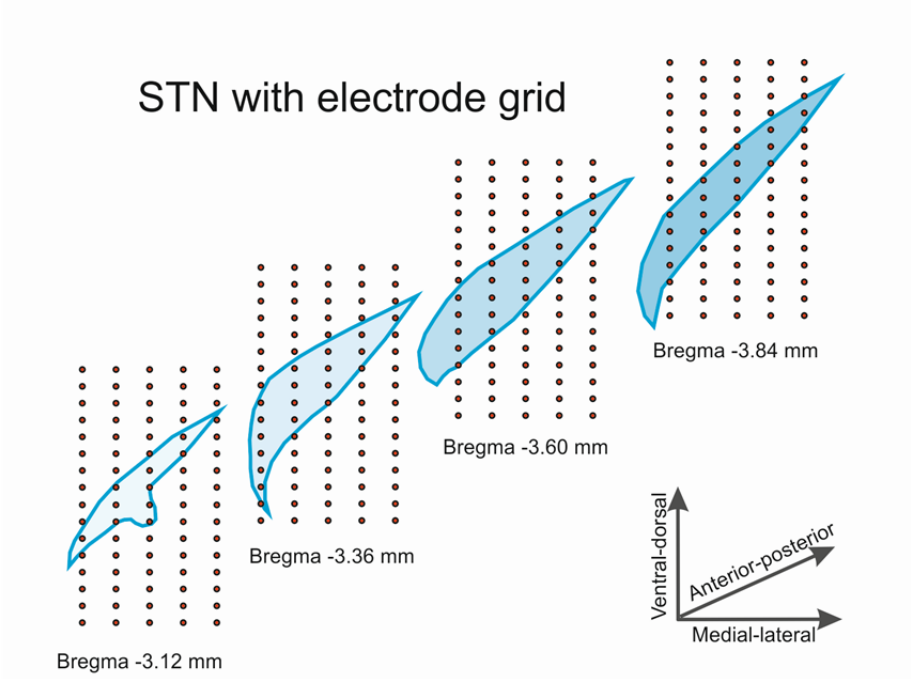

Figure 4. The 3D electrode grid inside different STN slices in the anterior-posterior direction (bregma -3.1 to -3.8 mm)(Paxinos and Watson 1998). In total, this gives a 4x5x16 grid (anterior-posterior x medial-lateral x dorsal-ventral). Note that the four illustrated slices are 0.24 mm apart, in reality the measurements were performed 0.2 mm apart.

Data analysis

First, the signals at each grid point were checked. If the power between 2 and 200 Hz of the signal during baseline recording exceeded 10 times the average power of all baseline recordings in that particular rat, the measurements at that grid point were rejected. In that case, the average LFP responses of the surrounding grid points were used during CSD analysis. Second, the signals were divided into epochs of 45 ms before stimulation until 750 ms after stimulation. Each epoch was filtered using a second order high-pass non-causal Butterworth filter with a cut-off frequency of 2 Hz. All epochs were checked for artifacts, when one was present the epoch was rejected. An artifact was detected if the absolute signal in the epoch exceeded 400 μA (note that the signal during the stimulation artifact, from 0 ms to +7 ms relatively to the trigger, was excluded from this criterion). The remaining epochs of the 99 stimuli were averaged per grid point per stimulation type. Subsequently, this average LFP response was smoothed over time using a third order Savitzky–Golay filter with a window size of 9 samples (Savitzky and Golay 1964). The advantage of using this filter over a moving average filter is that it better preserves features such as relative maxima and minima and peak width. Third, to overcome erroneous outcomes due to different physical properties of the contacts, we performed signal normalization. For this purpose, we calculated the RMS value of the LFPs after removing the part of the signal in which the stimulation artifact was present, from 0 ms until +7 ms relatively to the trigger. For each rat and stimulation setting, the RMS value of the LFPs belonging to one contact were averaged and normalized by setting the contact with the highest RMS value to one. Subsequently, the normalized RMS values of all rats and stimulation settings were averaged per contact. This value was divided by the average RMS value of all contacts, which provided a measure of the relative RMS value of that particular contact in relation the remaining contacts. Prior to computation of the CSD, the LFPs of each contact were normalized by dividing them with this relative RMS value. Finally, these normalized LFP responses were spatially filtered in dorsal-ventral direction using a third order Savitzky–Golay filter with a window size of 5 samples.

For each rat, we studied the mean LFP response of each grid point to verify whether a neuronal response was present and visible. In case we saw an LFP response, it was verified whether the response was of true neuronal nature by comparing it to the peristimulus time histogram (PSTH) of the simultaneously measured spike signal. The procedure for construction of the PSTHs is described in (Janssen et al. 2012). Only the rats in which we saw the typical pattern in the

LFP response and corresponding PSTH as earlier described by Magill et al. (Magill et al. 2004), were used for further analysis.
We studied the LFPs by analyzing the CSD, which enables us to study the occurrence, spatial distribution and extend of the current sources and sinks of the neuronal activity. The general approach to compute the CSD is to use the static approximation of the Maxwell's equations (Mitzdorf 1985) (equation 1).

$$\nabla \cdot (\sigma \nabla LFP) = -CSD \tag{1}$$

With LFP the local field potential [V], CSD the current source density [A/m^3] and σ the electrical conductivity tensor [Sm^{-1}]. In this approach, the extracellular medium is assumed to act as an ohmic volume conductor in the relevant frequency range. One of the main drawbacks of this method is the exclusion of the boundary points. Our 3D grid is 4x5x16, giving a total of 320 grid points of which 236 are boundary points. For this reason, we used a different method to solve the CSD, i.e. the inverse Current Source Density (iCSD) method. The iCSD method has been described for one dimensional recordings by Pettersen et al. (Pettersen et al. 2006) and has been generalized to three-dimensional recordings by Łęski et al. (Łęski et al. 2007). The iCSD method is based on linear inversion of the electrostatic forward solution. In the iCSD method, the CSD is assumed to have a certain known distribution class. This distribution class should be parameterized with as many parameters as the number of recorded signals. By using the electrostatic forward solution one can find a linear relation *F* between the CSD distribution and the LFP generated by the CSD on the electrode locations (equation 2). The linear relation can be used to solve the inverse problem by using the inverse of *F* to calculate the CSD distribution from the recorded LFP signals (equation 3).

$$\overrightarrow{LFP} = \boldsymbol{F} \cdot \overrightarrow{CSD} \tag{2}$$
$$\overrightarrow{LFP} = \boldsymbol{F^{-1}} \cdot \overrightarrow{CSD} \tag{3}$$

With $\overrightarrow{LFP}$ the LFP vector ($\overrightarrow{LFP}\ in\ \boldsymbol{R^{320}}$), $\overrightarrow{CSD}$ the CSD vector ($\overrightarrow{CSD}\ in\ \boldsymbol{R^{320}}$)) and F the iCSD transformation matrix. The LFP vector consists of 320 cortically evoked LFPs corresponding to the number of grid points. To describe the CSD distribution we used the natural spline iCSD in which the CSD values within the grid are obtained using natural spline interpolation (Łęski et al. 2007). As this approach assumes all sources to be within the measurement grid, an additional boundary condition was introduced (Łęski et al. 2007). This boundary condition extends the CSD distribution with one layer beyond the original grid, with the grid points in the outer layer having the same value as the nearest CSD value.

The current sources and sinks of the neuronal activity were analyzed at the points in time at which we saw the peaks of N1, P1 and P2 of the subthalamic LFP response to cortical stimulation. To determine whether these sources and sinks were of significant amplitude, we used the CSD of 45 ms preceding stimulation and determined the threshold as the mean of this signal +/- 6 times the standard deviation. This strict threshold was chosen to rule out any significant activity due to the noise component of the signal. When sources and sinks were above or below this threshold, they were considered significant. The locations of the sources and sinks were compared to each other by determining the highest amplitude of the absolute CSD and defining this as the center of the source/sink. In the coronal sections where the centers of the sources and sinks were located, the average center location of the source P1 and sink N1 relatively to the source P2 were computed. A paired one-tailed t-test with a significance level of 0.05 was used to check whether the centers of the sources and sinks were situated significantly different along the dorsoventral and mediolateral axis. Furthermore, the sizes of the sources and sinks were determined by computing the distance from the center location to the medial, lateral, ventral and dorsal border of the source/sink in each rat and averaging these values over all rats.

5.3. Results

First, we checked which rats showed an LFP response after MCS similar to the response described by Magill *et al.*(Magill et al. 2004). Additionally, we confirmed that this LFP response coincided with the PSTHs of the unit responses (see Fig. 1). This was the case in four out of the seven rats.

For each rat, the CSD was analyzed. The CSD was evaluated at the points in time at which N1, P1 and P2 occur in the evoked LFP (Fig. 1). A negative peak in the LFP coincides with an increased spiking rate: the neuron receives an excitatory input, which increases the potential in the intracellular medium and reduces the potential in the extracellular medium causing a negative deflection in the LFP. This negative peak in the LFP gives a sink in the CSD, which is visualized by a blue area (Fig. 5). Vice versa, a decreased spiking rate causes a positive peak in the LFP giving a source in the CSD, which is represented by a red area.

We first focus on the results obtained during 600 μA MCS and representative examples of the CSDs are shown in Fig. 5. Furthermore in each rat for each source and sink, the center location as well as the sizes of the sources and sink in four directions (medial, lateral, dorsal and ventral) were computed (Fig. 6). During 600 μA MCS, the sink corresponding to N1 was always seen medial to the source P1 and P2, and the location of both the P1 and P2 source along the mediolateral axis differed significantly from the location of N1 along this axis. In

each rat, the sources P1 and P2 were approximately located at the same coordinates, and thus no significant differences were found both along the mediolateral and dorsoventral axis. Furthermore, no significant differences along the dorsoventral axis between P1, P2 and N1 were found.
During 300 μA MCS, the same results were seen in three out of four rats, but sinks and sources became weaker and covered a smaller area (Fig. 5 and 6). The sources P1 and P2 reduced in size more dramatically than the sink N1. In the fourth rat, the STN did not respond to the lower amplitude MCS.
During 600 μA CGS in each rat, the source of P2 was located in the same area as the source of P2 after MCS, although it was generally somewhat weaker of amplitude and covering a smaller area (Fig. 5). The sink of N1 during CGS was differently located in each rat, but it was always located in an area different to the sink of N1 following MCS. A source during P1 was not visible during CGS.

5.4. Discussion

In this study, for the first time we have performed CSD analysis of cortically evoked LFP responses in the rat STN. To estimate the CSD from the LFP response, the iCSD method of Łęski *et al.* (Łęski et al. 2007) was applied. The CSD method allowed us to assess the sources and sinks of the neuronal input activity in the rat STN.

Validity of the results
It was, first, verified whether the LFPs were of neuronal nature. In four rats, we found that the LFP responses were similar to previously described results (Magill et al. 2004) and also corresponded to simultaneously measured PSTHs of unit responses. In the remaining three rats without LFP response, misplacement of either the stimulation or the recording electrode could have occurred. The placing of the recording electrode was checked and confirmed, so misplacement of the recording electrode was not the case. Wearing and tearing of the recording electrode due to blood clotting and cleaning probably caused a decreased impedance of the electrode which resulted in a decreased signal to noise ratio.

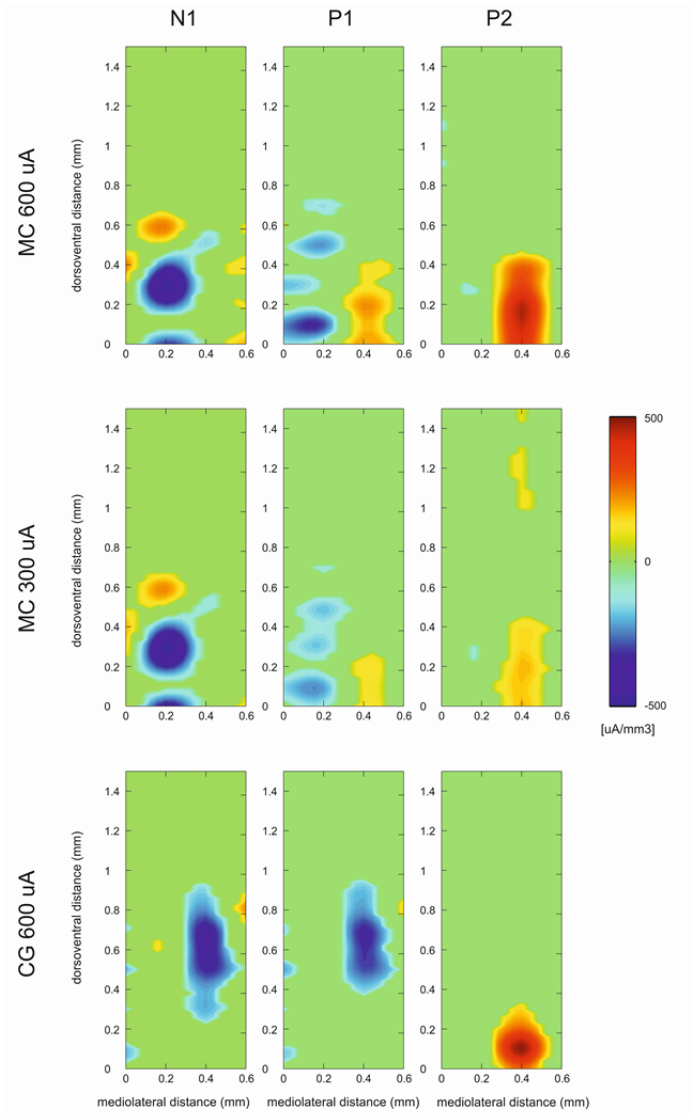

Figure 5. Representative examples of CSDs are shown. The relative anatomical positions of the sources and sinks of the neuronal input in the STN as estimated by the CSDs of the cortically evoked subthalamic LFPs. This is a typical example of one rat. The top, middle and bottom rows contain data obtained during respectively 600 and 300 µA MCS and 600 µA CGS. From left to right, the columns give the CSD at the timing of N1, P1 and P2 respectively. At N1 a sink (blue) is visible, at P1 and P2 a source (red) is visible. The x-axis gives the distance from the most medial recording (0 mm) to the most lateral recording (0.6 mm). The y-axis gives the distance from the most ventral recording (0 mm) to the most dorsal recording (1.5 mm).

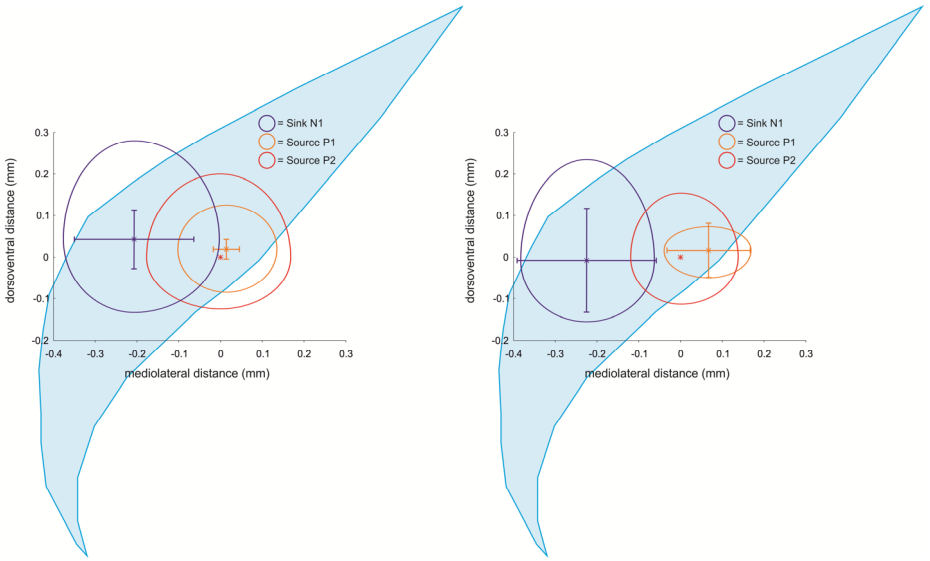

Figure 6. The center locations of the source of P1 and the sink of N1 relatively to the source of P2 during 600 μA (left) and 300 μA (right) MCS. The relative center locations are averaged over all rats and the standard deviations are included. The average size of the sources and sink in four directions (medial, lateral, dorsal and ventral) are also shown. The location along the mediolateral axis of N1 differs significantly from both P1 and P2. A contour of the STN (Paxinos and Watson 1998) bregma -3.60 mm is included in the background. As the exact parameters of the electrode positions relative to the STN were not available, the placing of the STN is for illustrative purposes only.

To perform the iCSD method, the responses in the 3D grid have to be measured simultaneously. Our measurements were performed in multiple trials, but by averaging the responses of 99 trials; by making sure that the stimulation electrode was not moved during the experiments; and by performing RMS normalization to diminish effects resulting from debris, we can assume that the responses were similar to what would have been measured if all the points in the 3D grid were measured simultaneously.

Different locations of the MC and GP input into the STN

The results during high amplitude MCS were consistent for all analyzed rats. The sources for P1 and P2 were approximately located at similar coordinates. The sink of N1 was always located medial to these sources. It has been argued that N1 is the result of the monosynaptic cortico-subthalamic input (Kitai and Deniau 1981; Fujimoto and Kita 1993; Maurice et al. 1998; Nambu et al. 2000; Kolomiets et al. 2001; Magill et al. 2004). Next, P1 is the results of the STN-GP-STN connection (Fujimoto and Kita 1993; Maurice et al. 1998; Nambu et al.

2000; Magill et al. 2004). Thus the source of P1 is caused by input activity from the GP. More specifically, this input comes from the lateral GP, which projects to the lateral STN (Parent and Hazrati 1995; Marani et al. 2008). These results indicate that the source of the afferent projections from the MC and GP is segregated. In rodents, it has been shown that inputs from the GP invade the entire extent of the STN (Parent and Hazrati 1995). The lateral two-thirds of the STN receive input from neurons in the lateral portion of the GP, whereas the medial third of the STN receives input from neurons in the medial part of the GP. To the best of our knowledge, we are the first to report on the different relative locations of the MC and GP inputs within the STN.

The source of the long-latency inhibitory period P2

The source of the long-latency, long-duration inhibitory period, P2, is unknown. We found that P2 is located in the same area as P1. As P1 is caused by an inhibitory input from the (lateral) GP, we expect that P2 is also caused by an inhibitory input from the GP.

Several hypotheses of the P2 source can be suggested. First, we propose that P2 is due to a disfacilitation of the cortex (Fujimoto and Kita 1993; Nambu et al. 2002). Our results are in line with this hypothesis, as disfacilitation of the cortex reduces the excitatory input from the cortex to the striatum (Fig. 7), which decreased the inhibition of GP resulting in a strong inhibition of the STN. This is in line with our findings suggesting that P2 could be generated by an inhibitory input from the GP. Furthermore, our results indicate that the disfacilitation occurs in the cortical neuronal population involved in the indirect, rather than the monosynaptic cortico-subthalamic pathway. The neuronal population involved in the indirect pathway are thought to be the intratelencephalic neurons (Ballion et al. 2008; Mathai and Smith 2011). The second hypothesis is based on the fact that accumulation of calcium and calcium-dependent potassium currents during the activation N2 lead to a prolonged after hyperpolarization of STN cell bodies (Bevan and Wilson 1999; Magill et al. 2006). Hyperpolarization would lead to an increased potential of the extracellular medium, which we do see. However, we see a short elevation in the LFP of about 5 to 10 ms, which indicates dendritic input activity. A prolonged hyperpolarization, as suggested by this theory, would give a prolonged change in extracellular potential, which would have to last as long as the inhibitory period being about 170 ms (Magill et al. 2006). The third hypothesis we found was that P2 may be generated by a silent plateau potential (Kass and Mintz 2006). This hypothesis suggests that after the short inhibition causing P1, the disinhibition by the indirect pathway causes a burst at the onset (N2) and a subsequent silencing during the plateau potential (P2). This theory is not in concordance with our results, as it does not explain the

source we found at P2: The theory does not predict an input at the timing of P2; and the plateau is a depolarization, which implies a decreased potential in the extracellular medium, while we found an increased potential.

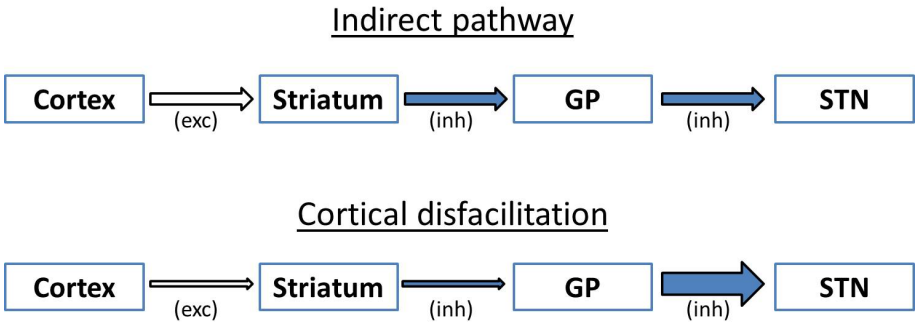

Figure 7. The top diagram shows the normal situation of the cortico-STN indirect pathway. The bottom diagram shows the effect of cortical disfacilitation on the STN. The decreased cortical excitation of the striatum causes a reduced inhibition of the GP, which gives a stronger inhibition of the STN from the GP.

When comparing the results obtained with 300 μA to those obtained with 600 μA MCS, it is evident that both the area and the amplitude of the source of P2 are reduced more drastically than the sink of N1. This could be explained by the fact that P2 occured after multiple synaptic stations and thus required temporal-spatial summation to be effective. In contrast, N1 is caused by the monosynaptic corticosubthalamic pathway. This agrees with the previous notion that P2 could be caused by cortical disfacilitation affecting the indirect pathway. Furthermore, these results could be explained by a different neuronal mechanism at the origin of N1 and P2, which is also in agreement with this hypothesis. A last reason could be that different cortical fibers have to be activated for N1 and P2. Again, this agrees with P2 being caused by cortical disfacilitation affecting the indirect pathway: the monosynaptic cortico-subthalamic pathway (N1) originates from pyramidal tract neurons (Giuffrida et al. 1985), while the indirect pathway is thought to originate from intratelecenphalic neurons (Ballion et al. 2008; Mathai and Smith 2011). A previous modeling study (Zwartjes et al. 2012) showed that both neuronal populations get activated differently by various stimulation protocols.
In summary, our results indicate that P2 is caused by a disfacilitation of the cortical neuronal population, which provides the input of the indirect pathway.

Similar location of the long-latency MC and CG input in the STN
Previous studies indicated that the anterior CG projects to the medial third of the STN, whereas the MC projects to the lateral two thirds of the rat STN

(Janssen et al. 2010). The results concerning the long-latency inhibitory period, P2, were similar in all rats. The source of P2 during CGS was located at a similar position as the source of P2 during MCS. This indicates that the pathways from the CG and MC to the STN, which are involved in the late responses, use the same input fibres in the STN or are transmitted through different fibers, which provide input in the same subthalamic area. Magill et al. (Magill et al. 2006) also observed that the circuit involved in the long-latency response, P2, is less strictly organized than the short latency response, N1. This finding is not surprising when we would consider P2 to arise from general disfacilitation in the cortex, as argued in the previous paragraph. As the whole cortex is inactive and thus the striatum is not activated during this period, it does not matter where the initial stimulus on the cortex was given.

Future prospects

MCS and simultaneous measurements of the subthalamic response has been performed in PD patients in order to locate the motor area of the STN (Janssen et al. 2012; Zwartjes et al. 2013). The method presented in this paper was able to distinguish the different sources and sinks of the neuronal input in the STN. Martens *et al.* (Martens et al. 2011) presented a new DBS electrode design, which is capable of high resolution stimulation and recording in different directions. This new electrode design enables the CSD approach. The sources and sinks resulting from the CSD approach could be used to optimize the target location for the DBS electrode. In that regard, it has to be determined which location relative to these sources and sinks provides the optimal clinical benefit for the patient. In future, this new approach enables a more precise localization of the STN motor area and could improve surgical outcomes of DBS for PD.

5.5. Conclusions

In this study, we used CSD analysis in the rat to determine the sources and sinks of neuronal input in the STN after cortical stimulation. The CSD method resulted in clear and distinguishable sources and sinks of the neuronal input activity in the STN. We showed that the inputs from the MC and GP are located in different STN areas. Furthermore, the inputs of the long latency responses following cortical stimulation were found at similar locations within the STN when comparing the MC to the CG. Finally, our results indicate that the long-latency, long-duration inhibitory period following MCS is caused by cortical disfacilitation affecting the indirect pathway.

References

Ballion, B., N. Mallet, E. Bézard, J. L. Lanciego and F. Gonon (2008). "Intratelencephalic corticostriatal neurons equally excite striatonigral and striatopallidal neurons and their discharge activity is selectively reduced in experimental parkinsonism." Eur. J. Neurosci. 27(9): 2313-2321.

Benazzouz, A., C. Gross, J. Feger, T. Boraud and B. Bioulac (1993). "Reversal of rigidity and improvement in motor performance by subthalamic high-frequency stimulation in MPTP-treated monkeys." Eur J Neurosci 5(4): 382-389.

Bevan, M. D. and C. J. Wilson (1999). "Mechanisms Underlying Spontaneous Oscillation and Rhythmic Firing in Rat Subthalamic Neurons." J Neurosci 19(17): 7617-7628.

Buzsaki, G. (2004). "Large-scale recording of neuronal ensembles." Nat. Neurosci. 7(5): 446-451.

Deuschl, G., C. Schade-Brittinger, P. Krack, J. Volkmann, H. Schafer, K. Botzel, C. Daniels, A. Deutschlander, U. Dillmann, W. Eisner, D. Gruber, W. Hamel, J. Herzog, R. Hilker, S. Klebe, M. Kloss, J. Koy, M. Krause, A. Kupsch, D. Lorenz, S. Lorenzl, H. M. Mehdorn, J. R. Moringlane, W. Oertel, M. O. Pinsker, H. Reichmann, A. Reuss, G. H. Schneider, A. Schnitzler, U. Steude, V. Sturm, L. Timmermann, V. Tronnier, T. Trottenberg, L. Wojtecki, E. Wolf, W. Poewe and J. Voges (2006). "A randomized trial of deep-brain stimulation for Parkinson's disease." N. Engl. J. Med. 355: 896-908.

Fujimoto, K. and H. Kita (1993). "Response characteristics of subthalamic neurons to the stimulation of the sensorimotor cortex in the rat." Brain Res. 609: 185-192.

Giuffrida, R., G. Li Volsi, G. Maugeri and V. Percivalle (1985). "Influences of pyramidal tract on the subthalamic nucleus in the subthalamic nucleus of the cat." Neurosci. Lett. 54: 231-235.

Janssen, M., V. Visser-Vandewalle and Y. Temel (2010). "Cortico-subthalamic projections in the rat." J Exp Clin Med 27(1): 4-12.

Janssen, M. L. F., V. Visser-Vandewalle and Y. Temel (2010). "Cortico-subthalamic projections in the rat." J Exp Clin Med 27(1): 4-10.

Janssen, M. L. F., D. G. M. Zwartjes, Y. Temel, V. Van Kranen-Mastenbroek, A. Duits, L. J. Bour, P. H. Veltink, T. Heida and V. Visser-Vandewalle (2012). "Subthalamic neuronal responses to cortical stimulation." Mov. Disord. 27(3): 435-438.

Kass, J. I. and I. M. Mintz (2006). "Silent plateau potentials, rhythmic bursts, and pacemaker firing: Three patterns of activity that coexist in quadristable subthalamic neurons." Proc Natl Acad Sci USA 103(1): 183-188.

Kitai, S. T. and J. M. Deniau (1981). "Cortical inputs to the subthalamus: intracellular analysis." Brain Res. 214(2): 411-415.

Kolomiets, B. P., J. M. Deniau, P. Mailly, A. Menetrey, J. Glowinski and A. Thierry (2001). "Segregation and Convergence of Information Flow through the Cortico-Subthalamic Pathways " J. Neurosci. 21(15): 5764-5772.

Kolomiets, B. P., J. M. Deniau, P. Mailly, A. Menetrey, J. Glowinski and A. M. Thierry (2001). "Segregation and convergence of information flow through the cortico-subthalamic pathways." J Neurosci 21(15): 5764-5772.

Krack, P., A. Batir, N. Van Blercom, S. Chabardes, V. Fraix, C. Ardouin, A. Koudsie, P. D. Limousin, A. Benazzouz, J. F. LeBas, A. L. Benabid and P. Pollak (2003). "Five-year follow-up of bilateral stimulation of the subthalamic nucleus in advanced Parkinson's disease." N Engl J Med 349(20): 1925-1934.

Łęski, S., D. K. Wojcik, J. Tereszczuk, D. A. Swiejkowski, E. Kublik and A. Wrobel (2007). "Inverse current-source density method in 3D: reconstruction fidelity, boundary effects, and influence of distance sources." Neuroinformatics 5(4): 207-222.

Magill, P. J., A. Sharott, M. D. Bevan, P. Brown and J. P. Bolam (2004). "Synchronous unit activity and local field potentials evoked in the subthalamic nucleus by cortical stimulation." J. Neurophysiol. 92: 700-714.

Magill, P. J., A. Sharott, J. P. Bolam and P. Brown (2006). "Delayed synchronization of activity in cortex and subthalamic nucleus following cortical stimulation in the rat." J. Physiol. 574: 929-946.

Marani, E., T. Heida, E. A. J. F. Lakke and K. G. Usunoff (2008). The subthalamic nucleus. Part I: Development, Cytology, Topography and Connections. Berlin, Springer-Verlag.

Martens, H. C., E. Toader, M. M. J. Decre, D. J. Anderson, R. Vetter, D. R. Kipke, K. B. Baker, M. D. Johnson and J. L. Vitek (2011). "Spatial steering of deep brain stimulation volumes using a novel lead design." Clin. Neurophysiol. 122(3): 558-566.

Mathai, A. and S. Smith (2011). "The corticostriatal and corticosubthalamic pathways: two entries, one target. So what?" Front. Syst. Neurosci. 5(64).

Maurice, N., J. M. Deniau, J. Glowinski and A. Thierry (1998). "Relationships between the prefrontal cortex and the basal ganglia in the rat Physiology of the corticosubthalamic circuits." J. Neurosci. 18(22): 9539-9546.

Mitzdorf, U. (1985). "Current Source-Density method and application in cat cerebral cortex Investigation of evoked potentials and EEG phenomena." Physiol. Rev. 65(1): 37-100.

Nambu, A., H. Tokuno, I. Hamada, H. Kita, M. Imanishi, T. Akazawa, Y. Ikeuchi and N. Hasegawa (2000). "Excitatory cortical inputs to pallidal neurons via the subthalamic nucleus in the monkey." J. Neurophysiol. 84: 289-300.

Nambu, A., H. Tokuno and M. Takada (2002). "Functional significance of the cortico-subthalamo-pallidal 'hyperdirect' pathway." Neurosci. Res. 43: 111-117.

Parent, A. and L. Hazrati (1995). "Functional anatomy of the basal ganglia. II. The place of the subthalamic nucleus and external pallidum in basal ganglia circuitry." Brain Res. Rev. 20: 128-154.

Paxinos, G. and C. Watson (1998). The rat brain in stereotaxic coordinates. New York, Academic Press.

Pettersen, K. H., A. Devor, I. Ulbert, A. M. Dale and G. T. Einevoll (2006). "Current-source density estimation based on inversion of electrostatic forward solution:

Effects of finite extent of neuronal activity and conductivity discontinuities." J. Neurosci. Methods 154: 116-133.

Savitzky, A. and M. J. Golay (1964). "Smoothing and differentiation of data by simplified least squares procedures." Anal Chem 36(8): 1627-1639.

Tan, S. K. H., R. Vlamings, L. Lim, T. Sesia, M. L. F. Janssen, W. M. Steinbusch, V. Visser-Vandewalle and Y. Temel (2010). "Experimental deep brain stimulation in animal models." Neurosurgery 67(4): 1073-1080.

Temel, Y., A. Blokland, W. M. Steinbusch and V. Visser-Vandewalle (2005). "The functional role of the subthalamic nucleus in cognitive and limbic circuits." Prog. Neurobiol. 76: 393-413.

Temel, Y., A. Kessels, S. Tan, A. Topdag, P. Boon and V. Visser-Vandewalle (2006). "Behavioural changes after bilateral subthalamic stimulation in advanced Parkinson disease: A systematic review." Parkinsonism & Related Disorders 12(5): 265-272.

Weaver, F. M., K. Follett, M. Stern, K. Hur, C. Harris, W. J. Marks, J. Rothlind, O. Sagher, D. Reda, C. S. Moy, R. Pahwa, K. Burchiel, P. Hogarth, E. C. Lai, J. E. Duda, K. Holloway, A. Samii, S. Horn, J. M. Bronstein, G. Stoner, J. Heemskerk and G. D. Huang (2009). "Bilateral deep brain stimulation vs best medical therapy for patients with advanced Parkinson disease: a randomized controlled trial." JAMA 301: 63-73.

Witt, K., C. Daniels, J. Reiff, P. Krack, J. Volkmann, M. O. Pinsker, M. Krause, V. Tronnier, M. Kloss, A. Schnitzler, L. Wojtecki, K. Botzel, A. Danek, R. Hilker, V. Sturm, A. Kupsch, E. Karner and G. Deuschl (2008). "Neurophysiological and psychiatric changes after deep brain stimulation for Parkinson's disease: a randomised, multicentre study." Lancet Neurol. 7: 605-614.

Zwartjes, D. G. M., T. Heida, H. K. P. Feirabend, M. L. F. Janssen, V. Visser-Vandewalle, H. C. F. Martens and P. H. Veltink (2012). "Motor cortex stimulation for Parkinson's disease: a modelling study " J Neural Eng 9(5): 056005.

Zwartjes, D. G. M., M. L. F. Janssen, T. Heida, V. Van Kranen-Mastenbroek, L. J. Bour, Y. Temel, V. Visser-Vandewalle and P. H. Veltink (2013). "Cortically evoked potentials in the human subthalamic nucleus." Neurosci. Lett. 539: 27-31.

Chapter 6

Different spatial distribution of neural beta and gamma activity of the subthalamic nucleus in Parkinson's disease

Daphne G.M. Zwartjes
Tjitske Heida
Evita C. Wiegers
Rens Verhagen
Rob M.A. de Bie
Maria F. Contarino
Pepijn van den Munckhof
Peter R. Schuurman
Peter H. Veltink
Hubert C.F. Martens
Lo J. Bour

Abstract

Objective
We evaluated the spatial distribution of beta and gamma local field potential (LFP) activity in the subthalamic nucleus (STN) and assessed its potential use to locate the STN and STN sub-areas during deep brain stimulation (DBS) surgery.

Methods
Unit activity and LFPs were measured simultaneously in 25 patients with Parkinson's disease (PD) undergoing DBS surgery. After initial processing, data on 44 STNs were available. The beta and gamma oscillations were assessed in the sensorimotor and non-sensorimotor STN and areas outside of the STN. A novel approach to map the measurement points on an STN atlas was used for an accurate and detailed spatial representation.

Results
We found a pronounced increase in LFP power within the gamma band throughout the entire STN. LFPs in the beta frequency band had a significantly higher power in the sensorimotor STN compared to the non-sensorimotor STN. We also demonstrated a temporal coupling between the spike and LFP signal in the beta and gamma frequency band.

Conclusions
In PD, gamma oscillations are increased throughout the entire STN, while beta oscillations are elevated only within the sensorimotor STN.

Significance
LFP gamma oscillations may provide a useful tool for locating the borders of the STN, and LFP beta oscillations could be used to locate the dorsolateral sensorimotor area within the STN.

6.1. Introduction

Deep brain stimulation of the subthalamic nucleus (STN-DBS) has emerged as an effective surgical treatment for Parkinson's disease (PD) (Deuschl et al. 2006; Benabid et al. 2009; Weaver et al. 2009; Odekerken et al. 2012). The underlying mechanisms explaining why DBS is effective are not yet fully understood, but a leading hypothesis is that DBS suppresses pathological synchronized oscillations in the basal ganglia (Brown and Eusebio 2008; Eusebio et al. 2012). DBS of the STN may be accompanied by side effects on cognition, behavior, and mood (Temel et al. 2006; Witt et al. 2008). Side effects could be avoided by stimulating selectively the dorsolateral STN area (Janssen et al. 2012; Zwartjes et al. 2013), which is associated with sensorimotor function (Parent and Hazrati 1995; Hamani et al. 2004; Temel et al. 2005). In this regard, the challenging task is to locate the borders of the sensorimotor area inside the STN.

Previous studies in PD have shown that neural beta frequency band activity measured by micro electrode recordings (MER) and local field potentials (LFP) in the sensorimotor STN has an increased power compared to different STN regions and areas outside the STN (Kühn et al. 2005; Chen et al. 2006; Weinberger et al. 2006; Trottenberg et al. 2007; Contarino et al. 2012; Lourens et al. 2012). Elevated beta activity is considered to be related to antikinetic motor activity (Brown 2003) and therefore seems to be associated with bradykinesia and rigidity in PD (Kühn et al. 2006; Eusebio et al. 2012). Brown et al. (Brown 2007; Jenkinson and Brown 2011) suggest that beta oscillations promote tonic activity at the expense of voluntary movement and that beta oscillations are modulated by dopamine. Indeed, dopaminergic therapy induces a shift of the neural activity power from the beta to the gamma frequency band (Cassidy et al. 2002; Williams et al. 2002; Alegre et al. 2005; Fogelson et al. 2005; Androulidakis et al. 2007) and it is thought that these subthalamic gamma oscillations are physiological rather than pathological (Brown 2003; Androulidakis et al. 2007; Jenkinson et al. 2012).

The gamma frequency synchronization of neurons in the basal ganglia is a relatively less explored phenomenon, but it has recently been proposed that the function of the gamma oscillations lies in the determination of response vigor and not in the determination of exact kinematic parameters (Jenkinson et al. 2012). In a study by Trottenberg et al. (Trottenberg et al. 2006), gamma activity was found to be increased in the zona incerta and the dorsal STN.

In this study, we investigated the spatial distribution of MER and LFP neural activity in both the beta and gamma frequency bands inside and around the human STN in a large study population. We used a novel tool for mapping of MER points on an atlas of the STN (Lourens et al. 2012). This tool enabled us to

acquire a more accurate and detailed spatial representation of the MER locations inside and outside the STN and subsequently to compare LFP measurements with MER in different functional STN areas.
More knowledge about the spatial distribution of LFP oscillations, in the future, might be of help to consider whether LFPs instead of MER could be used to determine the optimal area for stimulation during DBS surgery.

6.2. Methods

Patients
Twenty-five patients with idiopathic PD (age 60±10 years) who underwent DBS surgery were measured. Twenty-three patients underwent bilateral STN-DBS and two patients had unilateral STN-surgery (table 1). The selected patients - despite optimal drug treatment - suffered from severe response fluctuations, dyskinesias, painful dystonia and/or bradykinesia. Exclusion criteria were an age below 18 years, a Hoehn and Yahr stage of five at the best moment of the day, a MATTIS dementia rating scale score of 120 or below, psychosis, and any other contra-indication for stereotactic surgery.

Table 1. Clinical characteristics of the PD patients included in this study

Number of patients	25
Gender (women/men)	6/19
Age (years)	60±10
Disease duration (years)	13±7
Total UPDRS* III off	41±10
Number of sides	48
Number of electrodes	3±1

*UPDRS = unified Parkinson's disease rating scale

Surgical procedure
The procedure for DBS was a one-stage bilateral or unilateral stereotactic approach. Frame-based 3D T1-weighted MRI reconstructions were used for target calculations and path-planning. The standard STN coordinates were 12 mm lateral to the midplane of the third ventricle, 2 mm posterior to the midcommissural point (MCP), and 4 mm below the intercommissural line (ICL). Direct visualization of the STN on T2-weighted MRI was used to make individual adjustments. One to five steel cannulas and microelectrodes (FHC, Inc., Bowdoin, ME, USA) arranged in a cross shaped array with an inter-electrode distance of 2 mm were inserted through a 12-mm diameter precoronal burr hole. The following criteria for the paths of the central channel were used: anterior angulation to ICL of 70–75°, lateral angulation from midline 20–30°, entry on

top of a gyrus, avoiding sulci, cortical surface veins and the lateral ventricles. Intraoperative microelectrode recording (MER) was performed using Medtronic microelectrodes 291 (Medtronic, Minneapolis, MN, USA; 10 µm exposure) to determine the borders of the STN with the Leadpoint system (Medtronic, Minneapolis, MN, USA). Test macro-stimulation was performed at equidistant sites (2 mm) inside the STN with clinical evaluation performed by a neurologist experienced in movement disorders (Bour et al. 2010). The site with the best therapeutic window was chosen for the implantation of the permanent DBS electrode (model 3389, Medtronic, Minneapolis, MN, USA) with four platinum–iridium cylindrical surfaces (1.3 mm diameter and 1.5 mm length, with an inter-contact separation of 0.5 mm). Patients were awake during the surgical procedure and sedatives were not used. Surgery and MER were performed following overnight withdrawal of anti-parkinsonian medication. To verify electrode position, patients underwent intra-operative fluoroscopy and postoperative computed tomography (CT), which was co-registered with the pre-operative stereotactic MRI.

Recording protocol

MERs were performed with the Leadpoint system in 0.5 mm steps, at each depth immediately followed by recording of both local field potentials (LFPs) and single/multi-unit activity using the REFA amplifier (TMSi, Oldenzaal, the Netherlands) on each side. The REFA signals were sampled at 20 kHz. After the first ten patients, the REFA amplifiers were modified to further reduce high frequency noise. This modification caused a reduction of the total noise band up till 5 kHz, but did not have a significant effect on the beta and gamma frequency bands of the rectified MER signals and the LFPs. The data from the entire patient group was combined. The REFA recordings were referenced against the 1 mm exposed surface of the inner cannula located 10 mm above the tip of the micro-electrode. The number of micro-electrodes was determined by the neurosurgeon, mainly based on the quality of the pre-operative imaging (details are included in table 1). The recordings started from either 8 or 6 mm before the pre-operatively determined MRI-based target point until substantia nigra activity was recognizable in at least one channel or activity significantly decreased in all channels indicating the lower border of the STN. In addition to the usual MER to determine STN borders during DBS surgery, MER/LFP recordings of 10 (11 patients) or 15 (14 patients) seconds per depth were made for the purpose of this study. This short measurement time was chosen as it was assumed that this time window provided a sufficient representation of the STN activity, while keeping the additional surgery time as short as possible.

The study protocol was approved by the local medical ethical committee and all subjects gave written informed consent.

Mapping strategy

Recordings were made inside and outside the STN. In order to compare measurements outside the STN, measurements within the sensorimotor area and measurements within the non-sensorimotor area of the STN, we used a novel approach to map the micro electrode recording sites on an atlas of the STN, which was first described by Luján et al. (Luján et al. 2009) and optimized by Lourens et al. (Lourens et al. 2012). This 3-dimenstional mapping method uses the classification of the MER sites to be in- or outside the STN by the neurophysiologist during surgery. A 3D brain atlas is used in which the STN is represented as a three-dimensional polygon surface (Butson et al. 2007; Miocinovic et al. 2007). A cost function was used to find the optimal position and rotation of the STN atlas relative to the MER sites. The cost function depended on the minimum Euclidean distance between MER sites that are erroneously plotted in- or outside the STN and the surface of the atlas STN. The cost function was minimized using a simulated annealing optimization algorithm in which the initial position of the STN atlas was defined by the anterior commissure (AC) and posterior commissure (PC) coordinates obtained from preoperative MRI. Additionally, the initial STN atlas was rotated in such a way that the AC-PC line was aligned with the y-axis of the stereotactic coordinate system. The optimization algorithm was performed 50 times and the realization with the minimal cost function value was chosen. If more than one minimal value was found, the solution with the smallest transformation from the initial position and rotation of the STN was chosen. A more extensive description of this mapping procedure and the specific settings used during the procedure can be found in (Lourens et al. 2012).

As indicated, we wanted to distinguish different functional areas. For this purpose, we divided the STN atlas into three different functional areas. All MER sites superior to the dorsal border of the STN were marked as outside the STN. Based on the work of Hamani, et al. and Benarroch et al. (Hamani et al. 2004; Benarroch 2008), we estimated the sensorimotor area of the STN to be in the lateral part of the dorsal 2/3rd of the STN, and non-sensorimotor STN was estimate to be the 1/3rd ventral part and the 1/10th medial tip of the STN. MER sites were labeled based on their location in these different functional subthalamic areas (Fig. 1).

Spectral Analysis

The raw signals contained artifacts, due to movement of the wires, talking of the patient, electrode properties, and other sources, which interfered with the

analysis. A very strict and extensive procedure to identify and remove trials with artifacts was adopted. For each recording, artifacts were identified and only artifact-free periods of 8 or more consecutive seconds were used for further analysis. Two criteria for artifact detection were used: 1. the power spectral density (PSD) of each one-second data-window was calculated for all 10- or 15-second recordings. Subsequently, the power in the 3-45 and 55-95 Hz band of each one-second data-window was computed. The power of both frequency bands was not allowed to exceed three times the averaged power of these frequency bands of the entire 10- or 15-second recording and it was also not allowed to exceed three times the averaged power of these frequency bands of all the recordings made in the same trajectory. 2. Artifacts in the spike signal were detected by first estimating the noise-level using the spike signal's envelope (Dolan et al. 2009). The maximum value of the rectified spike signal was not allowed to exceed this value multiplied by a factor of 20.

In this study, we focused on the beta and gamma frequencies. For both frequency ranges, we defined a low and a high frequency band to perform analysis on: the low beta frequency band 12-20 Hz, the high beta frequency band 20-30 Hz, the low gamma frequency band 30-48 Hz and the high gamma frequency band 60-80 Hz. The frequencies around 50 Hz, which contain noise from the mains electricity, were left out of the analysis. The high gamma frequency band was defined from 60 to 80 Hz based on a previous study demonstrating oscillatory neural activity in the STN in this particular frequency band (Alonso-Frech et al. 2006). In each frequency band, two features were extracted from the data, the PSD of the LFP signal and the coherence between the envelope of the spike train (MER) and LFP signal. The LFP signal was filtered by a 2^{nd} order non-causal band pass filter between 1-90 Hz. The PSD of this signal was calculated using a Hanning window per second and 50% overlap. The PSD was calculated over 2^{16} samples, which were obtained by zero padding. The LFP power was calculated for each recording in a trajectory of one micro-electrode. Subsequently, these values were normalized by locating the maximum value in that trajectory and dividing each value of the trajectory by this maximum value. This last step corrected for the differences in LFP power due to differences in impedance of each electrode and/or channel interface. In each STN, the averages of the LFP power of all trajectories were calculated per area-category ('outside STN', 'sensorimotor STN', and 'non-sensorimotor STN'). The values per STN were used in a two-tailed paired student t-test to compare the differences per area-category. A significance level $p<0.05$ was used. The average and standard deviation were also computed per area-category.

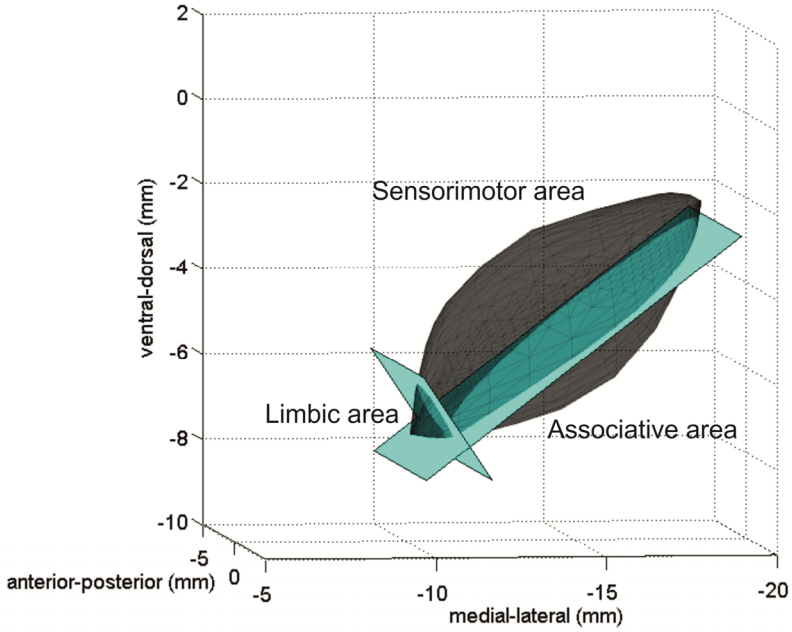

Figure 1. The STN is represented by a polygon surface in the 3D brain atlas. The STN is subdivided into functional areas using the blue cross-sections. We define the lateral part of the upper 2/3rd area as the sensorimotor area, the lower 1/3rd area as the associative area and the 1/10th medial tip is the limbic area. Numerics on the axes are relative to the midcommissural point.

Coherence Analysis

As a second feature, the coherence between the MER and LFP signal was calculated following the assumption that increased coherence between MER and LFP signals could confirm that the spectral information extracted from the LFP signal was indeed coming from the micro-tip of the recording electrode. It was not certain that the LFP signal was recorded from the micro-tip, because the tip was referenced to the exposed surface of the macro-tip located 10 mm above the micro-tip. The resulting LFP signal, which is a bipolar derivation of both signals, could be from the reference macro-tip as well as from the micro-tip. Since we wanted to link the LFP information to the location of the micro tip relatively to the STN, it was essential to check whether this LFP information indeed came from the micro tip. If an increase of coherence is observed between the envelope of the spike signal, coming from the micro-tip, and the bipolar recording of the LFP signal, this will indicate that this LFP frequency component is coming from the micro-tip located inside the STN. This coherence feature was calculated in

the following way. First, the spike signal was obtained by filtering the raw signal between 350-3500 Hz using a 2nd order non-causal Butterworth filter. Second, to obtain the envelop of the spike signal, the instantaneous amplitude of this signal, which is the amplitude of the complex Hilbert transform, was determined. Third, the LFP signal was obtained similar to how it was computed previously. Subsequently, the coherence between the LFP signal and the instantaneous amplitude of the spike signal was computed using Welch's power spectral density method with a 50% overlap Hanning window per second. The 95% confidence limit was computed using an extension of Koopman's method (Koopmans 1995; Gallet and Julien 2010) (equation 1) with $\gamma^2_{th}(\alpha)$ the coherence threshold in which α denotes the significance level; $\widetilde{K}$ replaces K in Koopman's equation and is defined by $2\widetilde{K} = 2K/c_w(D)$ in which K is the degrees of freedom and $c_w(D)$ is determined by the number of samples per window, the number of samples overlap and the window type used in the coherence analysis. For a more detailed explanation see Gallet and Julien (Gallet and Julien 2010). In each STN for each area-category, the percentage of trials in which the 99% confidence limit was exceeded was calculated. These values were compared per area-category using a two-tailed paired student t-test with a significance level of 1%.

$$\gamma^2_{th} = 1 - \alpha^{1/(\widetilde{K}-1)} \quad (1)$$

6.3. Results

The MER sites were mapped onto the STN. Fig. 2 shows an example of this mapping. Certain recordings contained too many artifacts and therefore had to be rejected entirely: in these recordings, no artifact-free period(s) of 8 or more consecutive seconds was (were) present. In some patients, this led to an area-category without recordings. As a paired t-test was used, the remaining recordings in that particular STN of that patient were not used. After artifact removal from a total of 48 STNs, 44 STNs of 24 patients remained.

From the remaining data, the average power in the low and high beta and gamma band was calculated per area-category. A typical example of normalized LFP power in one trajectory is shown in Fig. 3 and the averaged normalized LFP power across all STNs per (functional) area is shown in Fig. 4. Fig. 4 shows that the power in the high beta band typically increased when entering the sensorimotor area of the STN, but the power in the high beta band inside the sensorimotor STN was not significantly higher than this power outside the STN. As the electrodes moved into the non-sensorimotor area of the STN, the power in the high beta band decreased significantly ($p<0.01$). The elevation of high beta

power in the sensorimotor area was however not visible in each individual STN. When studying individual STNs, we saw that 73% of the STNs had a higher high beta power in the sensorimotor area compared to the non-sensorimotor area. Differences of power inside the low beta band were very small compared to differences in the high beta band and accordingly no significant differences were found. Considering the high gamma band in the individual case, there was an immediate increase in power when entering the STN, which was maintained throughout the entire STN (Fig. 3). The same was seen when averaging the results across all subjects and trajectories. The increase of high gamma power was significant when comparing the sensorimotor area to the outside area and when comparing the non-sensorimotor area to the outside area. No differences were found when comparing the sensorimotor to the non-sensorimotor area (Fig. 4). When assessing the results of each individual STN, 100% of the STNs had a higher average LFP high gamma power fraction in the sensorimotor STN compared to the outside STN. The average LFP high gamma power fraction was also elevated in the non-sensorimotor areas compared to the outside STN in 90% of the STNs. Similar results were found when assessing the low gamma band power, but differences were smaller and values found in the non-sensorimotor did not differ significantly from values measured outside the STN.

The percentage of significant coherence between the envelope of the spike signal and the LFP signal was computed per area-category (Fig. 5). In all frequency bands, a significantly higher percentage of significant coherences are seen within both the sensorimotor area and non-sensorimotor area of the STN, except for the low beta frequency band, which had a significantly different percentage of significant coherences only when comparing the sensorimotor STN to the area outside the STN. Furthermore, the percentage of significant coherences found in the sensorimotor area was significantly higher than in the non-sensorimotor STN when considering neural activity in the high beta frequency band. These results indicate: 1. the differences of the LFP power shown in Fig. 4 can be attributed to LFPs measured at the micro tip. 2. There is a temporal coupling between the LFPs, serving as an input for STN neurons, and MER, representing the output of the STN neurons, in both the beta and gamma frequency range.

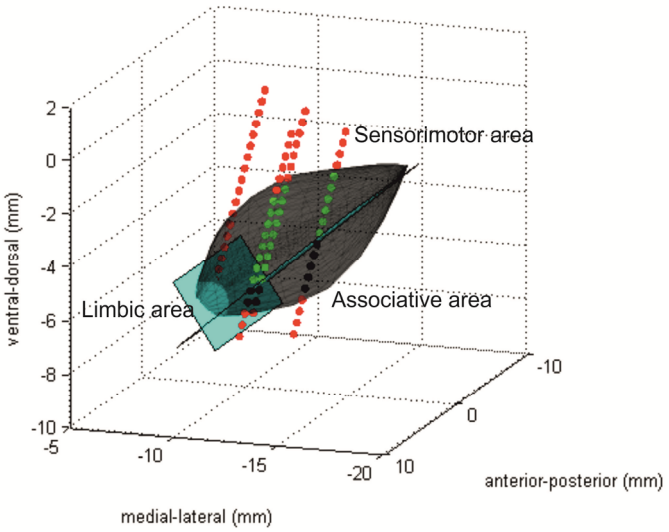

Figure 2. Mapping of the MER sites onto an atlas of the STN. Red dots indicate recordings outside the STN. Green dots represent recordings inside the STN sensorimotor area and black dots represent recordings inside non-sensorimotor areas of the STN.

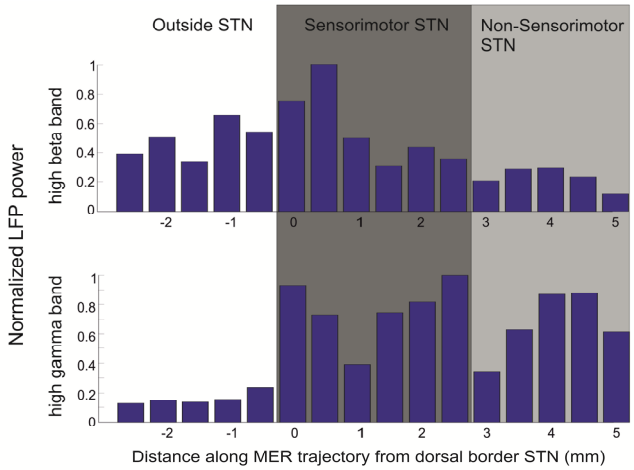

Figure 3. A typical example of the normalized LFP power in the high beta and the high gamma band along the trajectory of a single central micro-electrode. A prominent increase in the gamma LFP power is visible upon entering the sensorimotor area of the STN and a slight increase in the beta LFP power is present at that instance. The increase in gamma LFP power remains visible in the non-sensorimotor area of the STN. In contrast, the LFP beta power decreases as the electrode moves from the sensorimotor area to the non-sensorimotor area.

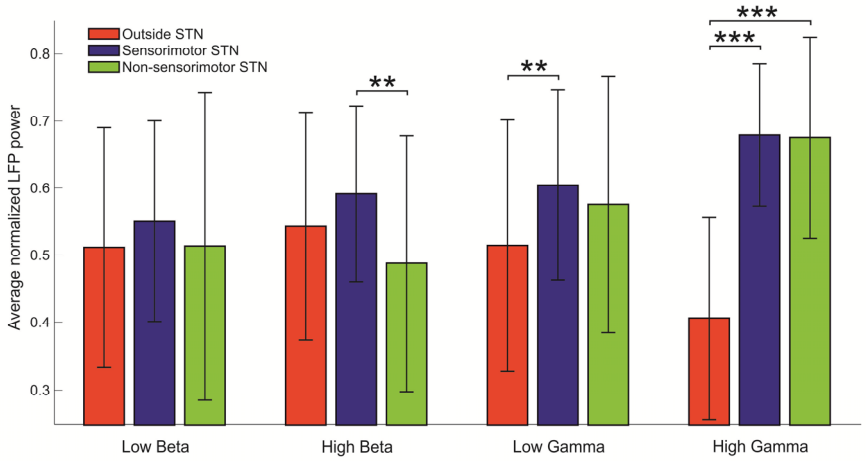

Figure 4. The average (n=44) fractions of the LFP power in the low and high beta and gamma frequency bands for the sensorimotor en non-sensorimotor STN and the region outside the STN. Asterisks indicate significant (* $p<0.05$; ** $p<0.01$; *** $p<0.001$) changes. A significant decrease in high beta LFP power is visible when comparing non-sensorimotor parts of the STN to the sensorimotor STN. The average high beta power in the sensorimotor STN is also higher than the high beta power outside the STN, but this is not statistically significant. Results in the low beta frequency range did show the same tendencies as the high beta range, but differences were small and not statistically significant. In the low and high gamma band, the sensorimotor STN had a significantly higher LFP power than the areas outside the STN. In the high gamma band, the LFP power was also significantly higher when comparing non-sensorimotor parts of the STN to areas outside the STN.

6.4. Discussion

In this study, we have shown that neural activity inside the STN has an increased power in the LFP gamma frequency band compared to neural activity outside the STN. This elevated power in the gamma band is seen in 100% of the investigated sensorimotor STN areas and in 90% of the investigated non-sensorimotor STN areas compared to outside the STN. In the gamma band, no differences were observed when comparing different functional regions inside the STN. However, significant differences between the sensorimotor and non-sensorimotor areas were observed in the high beta frequency band. Seventy-three percent of the STNs displayed a higher power in the high beta frequency band inside the sensorimotor subthalamic area compared to the non-sensorimotor subthalamic areas. In addition, our coherence analysis indicated a temporal coupling between the envelope of the MER signal and the LFP signal inside the STN.

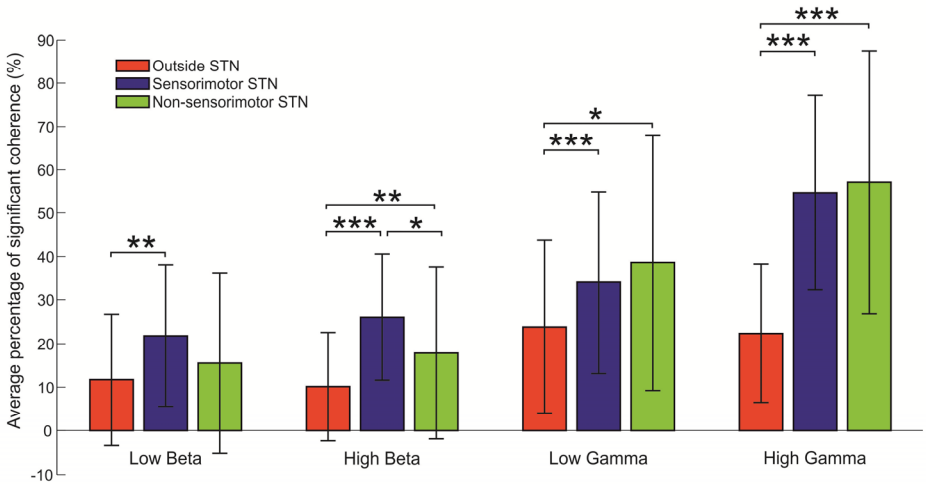

Figure 5. The average (n=44) percentage of trials showing significant coherence in the low and high beta and gamma frequency band for the sensorimotor and non-sensorimotor part of the STN and the region outside the STN. The coherence between the LFP signal and the envelope of the MER signal was calculated. Asterisks indicate significant (* $p<0.05$; ** $p<0.01$; *** $p<0.001$) changes. For all frequency bands, in both the sensorimotor STN and the non-sensorimotor parts of the STN a significantly higher percentage of significant coherences was found than outside the STN. Except for the low beta frequency band, which lacked a statistically significant difference between the non-sensorimotor parts of the STN and areas outside of the STN ($p>005$). Furthermore, a significantly higher percentage of significant coherences was found in the sensorimotor area as compared to the non-sensorimotor areas in the high beta frequency band.

Mapping strategy

In this study, we used a novel three-dimensional mapping strategy from Lourens et al. (Lourens et al. 2012) to determine the locations of the measurement points with respect to different areas within the STN. Up till now, studies performing similar analyses as the current paper usually compare measurements in the first several millimeters after hitting the dorsal STN to measurements made more ventral along the trajectory (Kühn et al. 2005; Chen et al. 2006; Trottenberg et al. 2006; Weinberger et al. 2006). This approach does not take into account the fact that the microelectrodes enter the STN at different locations and under a certain angle, which could result in certain trajectories covering a larger distance within the sensorimotor area than others.

The use of brain atlases is associated with certain limitations. The geometry of the STN varies per person, so the general brain atlas used in the mapping strategy could introduce errors. The approach partly deals with this by allowing the atlas

STN to scale, translate and rotate while searching for the most optimal solution. Boundary conditions on these transformation parameters also influence the results and introduce errors. Nonetheless, Luján et al. (Luján et al. 2009) showed that the performance of a 3-dimensional mapping strategy was as well as experienced human experts, but without the variability between experts.
The main limitations, however, are introduced by the definition of the functional areas within the STN. First of all, the borders of the functional areas within the STN are not known exactly. Second, these areas might slightly differ per patient and could also be influenced by a loss of functional segregation observed in PD (Pessiglione et al. 2005). Nevertheless, we believe that the estimate of the functional areas within the STN used in this study should provide a more accurate representation than simply subdividing the STN based on the first several recordings when entering the dorsal border of the STN.

Neural beta activity
Like previous researchers (Kühn et al. 2005; Chen et al. 2006; Weinberger et al. 2006; Trottenberg et al. 2007), we found an increase in beta LFP power in the sensorimotor area compared to non-sensorimotor areas. We found that this increase in beta power was mainly present in the upper part of the frequency range, i.e. 20-30 Hz. Contarino et al. (Contarino et al. 2012) assessed single/multi-unit activity and found that the power in the entire beta frequency band was higher in the dorsal than in the ventral STN with the low beta LFPs displaying an even slightly larger difference in power between the dorsal and ventral STN than the high beta LFPs. It is a point of concern that the we found the elevation in high beta power only in 73% of the investigated STNs. Chen et al. (Chen et al. 2006) found 100% of the STNs displaying this elevation in neural beta activity. Reasons for this discrepancy can be that Chen et al. used measurements performed with macro electrodes instead of the micro-tips we used. Furthermore, we should note that although we found a higher beta power in the sensorimotor STN area compared to areas outside the STN, this difference was not significant as would be expected (Kühn et al. 2005; Chen et al. 2006; Weinberger et al. 2006; Trottenberg et al. 2007). The lack of significance could be explained by our measurement setup: we referenced the micro-tip to the 1 mm exposed surface of the inner cannula. The measurements might thus have been influenced by recordings made on this 1 mm exposed surface. The coherence analysis indicated that the results can be attributed to measurements made on the micro-tip, but the signals might have been slightly polluted by measurements coming from the 1 mm exposed surface. Only when the high beta LFP activity is always elevated in this dorsal region of the STN, this feature could become useful for identifying the sensorimotor STN.

Neural gamma activity

Our results concerning the LFP gamma power are not in correspondence with the study of Trottenberg et al. (Trottenberg et al. 2006), who found the subthalamic gamma activity to be increased in the zona incerta and the dorsal STN. In addition, they found that just eight out of 15 STNs displayed peaks in the LFP gamma power. Certain methodological differences between this study and our study were present: the mapping strategy of the MER points on the STN atlas; the size of the subject group (15 STNs against 44 STNs in our study); and the definition of the gamma frequency band (40-100 Hz compared to 30-48 and 60-80 Hz in our study). The latter difference, however, is not a likely explanation for the discrepancy, as we found fairly similar results in the low and high gamma frequency band. The remaining differences might partly explain the different findings of our studies. Previous research on unit activity (Contarino et al. 2012) found an equal distribution of gamma oscillations within the STN, which is in concordance with our findings in the LFPs. Another study by Cagnan et al (Cagnan et al. 2011) found relatively low correlations of elevated beta and gamma activity in the unit activities with STN borders. Our research indicates that gamma activity within the LFPs could be a useful feature to distinguish the STN from its surroundings. However, it remains to be investigated how accurate each measurement point within the STN can be distinguished from all measurement points outside of the STN, as we only investigated average values of the measurements points within one area-category of an STN.

The remarkable finding in our data is that the power in the LFP gamma band is increased across the entire STN and not just in the sensorimotor area as opposed to previous findings (Trottenberg et al. 2006). It has been argued that gamma oscillations are prokinetic, physiological and involved in accurate execution of motor programs (Brown 2003). Therefore, they would be expected to be present in the sensorimotor area of STN, which agrees with our findings. The fact that we also found elevated LFP gamma power in the non-sensorimotor areas of the STN could be due to the loss of functional segregation in the cortico-basal ganglia circuits in PD (Pessiglione et al. 2005), which causes the STN motor function not to be restricted to a particular STN area. This, however, is not a likely explanation as we did see segregated beta oscillations within the STN. The presence of gamma oscillations in the entire STN could also indicate their involvement in other functional processes. In literature, it is argued that gamma-band activity in the primary somatosensory cortex is enhanced and prolonged by spatial-selective tactile attention (Bauer et al. 2006). Furthermore, it has been argued that gamma oscillations are involved in the determination of response vigor (Jenkinson et al. 2012), which needs not necessarily be just restricted to

motor tasks. It is also known that the STN is involved in the processing of verbal fluency tasks, resulting in an increase of gamma frequency power during such tasks (Anzak et al. 2011). The frontal and temporal lobe areas are involved in verbal fluency tasks (Baldo et al. 2006). In addition, it is known that cortical gamma oscillations play an important role in attention and memory (Kaiser and Lutzenberger 2005). These data suggest a more widespread involvement of gamma oscillations in multiple functions and thus suggests that the gamma oscillations do not have to be just restricted to the sensorimotor area of the STN.

Coherence between the single/multi-unit activity and LFPs

The coherence analysis suggests that LFPs measured in the beta and gamma frequency band truly came from measurements made at the tip of the micro-electrode. They also indicate a temporal relation in the beta and gamma frequency band between the spike and the LFP signal inside the entire STN. The spike signal reflects the action potentials generated by the neurons, while LFPs represent postsynaptic activity of a larger neuronal population (Buzsaki 2004). The spike signal is, thus, considered as the output, while LFPs serve as the input of the neural activity. Therefore, a temporal coupling between both signals would be expected in case of synchronized neural activity in that particular frequency band. Our results indicate that LFPs in the gamma and high beta frequency band result in bursts of neural spiking activity at the same frequencies. These results are in concordance with Trottenberg et al. (Trottenberg et al. 2006), who found discharges of neurons in the upper STN to be locked to gamma oscillations in the LFP. An important note is that the coherence analysis might not be the most optimal measure for the input-output relation considering the linear character of this measure.

Implications for the future

In future, the spatial distribution of LFP oscillations in the STN could be used to locate the optimal site for stimulation during DBS surgery. Recently, a novel electrode design incorporating a multitude of small contact points, which are able to stimulate in different directions around the electrode, has been introduced (Martens et al. 2011). When applying this electrode to measure LFPs, an accurate determination of the optimal stimulation site could be possible. Our results favor this possibility, but it should be noted that we used measurements of micro electrodes, instead of the larger contacts of the electrode described by Martens et al. (Martens et al. 2011), which may display less localized activity. Nonetheless, our results indicate that in future we might be able to rely on LFP recordings for the determination of the optimal stimulation site.

6.5. Conclusions

In conclusion, our results provide new information on the spatial distribution of gamma oscillations in the STN, confirm previous findings about the spatial distribution of beta oscillations in the STN but also show that this spatial distribution is most strongly present in the upper sub-band of the beta band (20-30 Hz). In the STN, an increased power in the LFP gamma band is visible compared to outside the STN. This increase in gamma power is present in 100% of the STNs and could therefore provide a good measure for locating the borders of the STN during DBS surgery based on LFP signals. In this regard, gamma oscillations certainly provide a better means for locating the STN than beta oscillations. In contrast to the LFP gamma power, the LFP power in the high beta frequency band was elevated within the sensorimotor STN compared to the non-sensorimotor areas. Therefore, LFP beta oscillations could be used for discriminating between different subthalamic functional areas.

References

Alegre, M., F. Alonso-Frech, M. C. Rodriguez, J. Guridi, I. Zamarbide, M. Valencia, M. Manrique, J. A. Obeso and J. Artieda (2005). "Movement-related changes in oscillatory activity in the human subthalamic nucleus: ipsilateral vs. contralateral movements." Eur. J. Neurosci. 22: 2315-2324.

Alonso-Frech, F., I. Zamarbide, M. Alegre, M. C. Rodriguez-Oroz, J. Guridi, M. Manrique, M. Valencia, J. Artieda and J. A. Obeso (2006). "Slow oscillatory activity and levodopa-induced dyskinesias in Parkinson's disease." Brain 129: 1748-1757.

Androulidakis, A. G., A. A. Kühn, C. C. Chen, P. Blomstedt, F. Kempf, A. Kupsch, G. H. Schneider, L. Doyle, P. Dowsey-Limousin, M. I. Hariz and P. Brown (2007). "Dopaminergic therapy promotes lateralized motor activity in the subthalamic area in Parkinson's disease." Brain 130: 457-468.

Anzak, A., L. Gaynor, M. Beigi, P. Limousin, M. Hariz, Z. Ludvic, T. Foltynie, P. Brown and M. Jahanshahi (2011). "A gamma band specific role of the subthalamic nucleus in switching during verbal fluency tasks in Parkinson's disease." Exp Neurol 232: 136-142.

Baldo, J. V., S. Schwarz, D. Wilkins and N. F. Dronkers (2006). " Role of frontal versus temporal cortex in verbal fluency as revealed by voxel-based lesion symptom mapping." J. int. neuropsychol. soc. 12(6): 896-900.

Bauer, M., R. Oostenveld, M. Peeters and P. Fries (2006). "Tactile spatial attention enhances gamma-band activity in somatosensory cortex and reduces low-frequency activity in parieto-occipital areas." J. Neurosci. 26(2): 490-501.

Benabid, A. L., S. Chabardes, J. Mitrofanis and P. Pollak (2009). "Deep brain stimulation of the subthalamic nucleus for the treatment of Parkinson's disease." Lancet Neurol. 8: 67-81.

Benarroch, E. E. (2008). "Subthalamic nucleus and its connections Anatomic substrate for the network effects of deep brain stimulation." Neurology 70(21): 1991-1995.

Bour, L. J., M. F. Contarino, E. M. J. Froncke, R. M. A. de Bie, P. van den Munckhof, J. D. Speelman and P. R. Schuurman (2010). "Long-term experience with intraoperative microrecording during DBS neurosurgery in STN and GPi." Acta Neurochir. 152(12): 2069-2077.

Brown, P. (2003). "Oscillatory nature of human basal ganglia activity: relationship to the pathophysiology of Parkinson's disease." Mov. Disord. 18: 357-363.

Brown, P. (2007). "Abnormal oscillatory synchronisation in the motor system leads to impaired movement." Curr. Opin. Neurobiol. 17: 656-664.

Brown, P. and A. Eusebio (2008). "Paradoxes of functional neurosurgery: clues from basal ganglia recordings." Mov. Disord. 23(1): 12-20.

Butson, C. R., S. E. Cooper, J. M. Henderson and C. C. McIntyre (2007). "Patient-specific analysis of the volume of tissue activated during deep brain stimulation." Neurimage 34(2): 661-670.

Buzsaki, G. (2004). "Large-scale recording of neuronal ensembles." Nat. Neurosci. 7(5): 446-451.

Cagnan, H., K. Dolan, X. He, M. F. Contarino, P. R. Schuurman, P. van den Munckhof, W. J. Wadman, L. Bour and H. C. F. Martens (2011). "Automatic subthalamic nucleus detection from microelectrode recordings based on noise level and neuronal activity." J Neural Eng 8: 046006.

Cassidy, M., P. Mazzone, A. Oliviero, A. Insola, P. Tonali, V. Di Lazzaro and P. Brown (2002). "Movement-related changes in synchronization in the human basal ganglia." Brain 125: 1235-1246.

Chen, C. C., A. Pogosyan, L. U. Zrinzo, S. Tisch, P. Limousin, K. Ashkan, T. Yousry, M. I. Hariz and P. Brown (2006). "Intra-operative recordings of local field potentials can help localize the subthalamic nucleus in Parkinson's disease surgery." Exp. Neurol. 198: 214-221.

Contarino, M. F., L. J. Bour, M. Bot, P. van den Munckhof, J. D. Speelman, P. R. Schuurman and R. M. de Bie (2012). "Tremor-specific neuronal oscillation pattern in dorsal subthalamic nucleus of parkinsonian patients." Brain Stimul. 5: 305-314.

Deuschl, G., C. Schade-Brittinger, P. Krack, J. Volkmann, H. Schafer, K. Botzel, C. Daniels, A. Deutschlander, U. Dillmann, W. Eisner, D. Gruber, W. Hamel, J. Herzog, R. Hilker, S. Klebe, M. Kloss, J. Koy, M. Krause, A. Kupsch, D. Lorenz, S. Lorenzl, H. M. Mehdorn, J. R. Moringlane, W. Oertel, M. O. Pinsker, H. Reichmann, A. Reuss, G. H. Schneider, A. Schnitzler, U. Steude, V. Sturm, L. Timmermann, V. Tronnier, T. Trottenberg, L. Wojtecki, E. Wolf, W. Poewe and J. Voges (2006). "A randomized trial of deep-brain stimulation for Parkinson's disease." N. Engl. J. Med. 355: 896-908.

Dolan, K., H. C. Martens, P. R. Schuurman and L. J. Bour (2009). "Automatic noise-level detection for extra-cellular micro-electrode recordings." Medical and Biological Engineering and Computing 47: 791-800.

Eusebio, A., H. Cagnan and P. Brown (2012). "Does suppression of oscillatory synchronisation mediate some of the therapeutic effects of DBS in patients with Parkinson's disease?" Front. Integr. Neurosci. 6(47): 1-9.

Fogelson, N., A. Pogosyan, A. A. Kühn, A. Kupsch, G. van Bruggen, H. Speelman, M. Tijssen, A. Quartarone, A. Insola, P. Mazzone, V. Di Lazzaro, P. Limousin and P. Brown (2005). "Reciprocal interactions between oscillatory activities of different frequencies in the subthalamic region of patients with Parkinson's disease." Eur. J. Neurosci. 22: 257-266.

Gallet, C. and C. Julien (2010). "The significance threshold for coherence when using the Welch's periodogram method: Effect of overlapping segments." Biomedical Signal Processing Control.

Hamani, C., J. A. Saint-Cyr, J. Fraser, M. Kaplitt and A. M. Lozano (2004). "The subthalamic nucleus in the context of movement disorders." Brain 127(1): 4-10.

Janssen, M. L. F., D. G. M. Zwartjes, Y. Temel, V. Van Kranen-Mastenbroek, A. Duits, L. J. Bour, P. H. Veltink, T. Heida and V. Visser-Vandewalle (2012). "Subthalamic neuronal responses to cortical stimulation." Mov. Disord. 27(3): 435-438.

Jenkinson, N. and P. Brown (2011). "New insights into the relationship between dopamine, beta oscillations and motor function." Trends Neurosci. 34(12): 611-618.

Jenkinson, N., A. A. Kühn and P. Brown (2012). "Gamma oscillations in the human basal ganglia." Exp Neurol.

Kaiser, J. and W. Lutzenberger (2005). "Human gamma-band activity: a window to cognitive processing." Neuroreport 16: 207-211.

Koopmans, L. (1995). The Spectral Analysis of Time series. San Diego, Academic Press, Inc.

Kühn, A. A., A. Kupsch, G. H. Schneider and P. Brown (2006). "Reduction in subthalamic 8–35 Hz oscillatory activity correlates with clinical improvement in Parkinson's disease." Eur. J. Neurosci. 23: 1956-1960.

Kühn, A. A., T. Trottenberg, A. Kivi, A. Kupsch, G. H. Schneider and P. Brown (2005). "The relationship between local field potential and neuronal discharge in the subthalamic nucleus of patients with Parkinson's disease " Exp Neurol 194: 212-220.

Lourens, M. A. J., H. G. E. Meijer, M. F. Contarino, P. van den Munckhof, P. R. Schuurman, S. A. van Gils and L. J. Bour (2012). "Functional neuronal activity and connectivity within the subthalamic nucleus in Parkinson's disease." Clin. Neurophysiol.: In Press.

Luján, J. L., A. M. Noecker, C. R. Butson, S. E. Cooper, B. L. Walter, J. L. Vitek and C. C. McIntyre (2009). "Automated 3-Dimensional Brain Atlas Fitting to Microelectrode Recordings from Deep Brain Stimulation Surgeries." Stereotact Funct Neurosurg 87(4): 229-240.

Martens, H. C., E. Toader, M. M. J. Decre, D. J. Anderson, R. Vetter, D. R. Kipke, K. B. Baker, M. D. Johnson and J. L. Vitek (2011). "Spatial steering of deep brain stimulation volumes using a novel lead design." Clin. Neurophysiol. 122(3): 558-566.

Miocinovic, S., A. M. Noecker, C. B. Maks, C. R. Butson and C. C. McIntyre (2007). "Cicerone: stereotactic neurophysiological recording and deep brain stimulation electrode placement software system." Acta Neurochir. Suppl. 97(2): 561-567.

Odekerken, V., T. van Laar, M. Staal, A. Mosch, C. Hoffmann, P. Nijssen, G. Beute, J. van Vugt, M. Lenders, M. F. Contarino, M. Mink, L. Bour, P. van den Munckhof, B. Schmand, R. de Haan, P. Schuurman and R. de Bie (2012). "Subthalamic nucleus versus globus pallidus bilateral deep brain stimulation for advanced Parkinson's disease (NSTAPS study): a randomised controlled trial." Lancet Neurol.

Parent, A. and L. Hazrati (1995). "Functional anatomy of the basal ganglia. II. The place of the subthalamic nucleus and external pallidum in basal ganglia circuitry." Brain Res. Rev. 20: 128-154.

Pessiglione, M., D. Guehl, A. Rolland, C. François, E. C. Hirsch, J. Féger and L. Tremblay (2005). "Thalamic neuronal activity in dopamine-depleted primates: evidence for a loss of functional segregation within basal ganglia circuits." J Neurosci 25(6): 1523-1531.

Temel, Y., A. Blokland, W. M. Steinbusch and V. Visser-Vandewalle (2005). "The functional role of the subthalamic nucleus in cognitive and limbic circuits." Prog. Neurobiol. 76: 393-413.

Temel, Y., A. Kessels, S. Tan, A. Topdag, P. Boon and V. Visser-Vandewalle (2006). "Behavioural changes after bilateral subthalamic stimulation in advanced Parkinson disease: A systematic review." Parkinsonism & Related Disorders 12(5): 265-272.

Trottenberg, T., N. Fogelson, A. A. Kühn, A. Kivi, A. Kupsch, G. H. Schneider and P. Brown (2006). "Subthalamic gamma activity in patients with Parkinson's disease." Exp Neurol 200: 56-65.

Trottenberg, T., A. Kupsch, G. H. Schneider, P. Brown and A. A. Kühn (2007). "Frequency-dependent distribution of local field activity within the subthalamic nucleus in Parkinson's disease " Exp Neurol 205(1): 287-291.

Weaver, F. M., K. Follett, M. Stern, K. Hur, C. Harris, W. J. Marks, J. Rothlind, O. Sagher, D. Reda, C. S. Moy, R. Pahwa, K. Burchiel, P. Hogarth, E. C. Lai, J. E. Duda, K. Holloway, A. Samii, S. Horn, J. M. Bronstein, G. Stoner, J. Heemskerk and G. D. Huang (2009). "Bilateral deep brain stimulation vs best medical therapy for patients with advanced Parkinson disease: a randomized controlled trial." JAMA 301: 63-73.

Weinberger, H., N. Mahant, W. D. Hutchison, L. A.M., E. Moro, M. Hodaie, A. E. Lang and J. O. Dostrovsky (2006). "Beta oscillatory activity in the subthalamic nucleus and its relation to dopeminergic response in Parkinson's disease " J Neurophysiol 96: 3248-3256.

Williams, D., M. Tijssen, G. van Bruggen, A. Bosch, A. Insola, V. Di Lazzaro, P. Mazzone, A. Oliviero, A. Quartarone, H. Speelman and P. Brown (2002). "Dopamine-dependent changes in the functional connectivity between basal ganglia and cerebral cortex in humans." Brain 125: 1558-1569.

Witt, K., C. Daniels, J. Reiff, P. Krack, J. Volkmann, M. O. Pinsker, M. Krause, V. Tronnier, M. Kloss, A. Schnitzler, L. Wojtecki, K. Botzel, A. Danek, R. Hilker, V. Sturm, A. Kupsch, E. Karner and G. Deuschl (2008). "Neurophysiological and psychiatric changes after deep brain stimulation for Parkinson's disease: a randomised, multicentre study." Lancet Neurol. 7: 605-614.

Zwartjes, D. G. M., M. L. F. Janssen, T. Heida, V. Van Kranen-Mastenbroek, L. J. Bour, Y. Temel, V. Visser-Vandewalle and P. H. Veltink (2013). "Cortically evoked potentials in the human subthalamic nucleus." Neurosci. Lett. 539: 27-31.

Chapter 7

Ambulatory monitoring of activities and motor symptoms in Parkinson's disease

Daphne G.M. Zwartjes
Tjitske Heida
Jeroen P.P. van Vugt
Jan A.G. Geelen
Peter H. Veltink

IEEE Trans Biomed Eng, 2010, 57(11): 2778-2786

Abstract

Ambulatory monitoring of motor symptoms in Parkinson's disease (PD) can improve our therapeutic strategies, especially in patients with motor fluctuations. Previously published monitors usually assess only one or a few basic aspects of the cardinal motor symptoms in a laboratory setting. We developed a novel ambulatory monitoring system that provides a complete motor assessment by simultaneously analyzing current motor activity of the patient (e.g. sitting, walking) and the severity of many aspects related to tremor, bradykinesia, and hypokinesia.

The monitor consists of a set of four inertial sensors. Validity of our monitor was established in seven healthy controls and six PD patients treated with deep brain stimulation (DBS) of the subthalamic nucleus. Patients were tested at three different levels of DBS treatment. Subjects were monitored while performing different tasks, including motor tests of the Unified Parkinson's Disease Rating Scale (UPDRS). Output of the monitor was compared to simultaneously recorded videos.

The monitor proved very accurate in discriminating between several motor activities. Monitor output correlated well with blinded UPDRS ratings during different DBS levels. The combined analysis of motor activity and symptom severity by our PD monitor brings true ambulatory monitoring of a wide variety of motor symptoms one step closer.

7.1. Introduction

Parkinson's disease (PD) motor symptoms mainly consist of progressive bradykinesia, tremor, hypokinesia, rigidity, and impaired postural control. The patients are usually treated with drugs, but some are additionally treated with deep brain stimulation (DBS). To optimize therapies, it is essential to know how much the symptoms are suppressed by treatment. Currently, the specialist assesses the effect on the symptoms by taking the history and by performing clinical examinations (e.g. the Unified Parkinson's Disease Rating Scale - UPDRS). These procedures cover only a short episode of the patient's condition, in spite of the fact that symptoms often fluctuate significantly within and between days. Patients sometimes keep diaries to record motor fluctuations, but these are subjective and influenced by subject inaccuracies. Clinical observation of fluctuations by medical staff is time consuming and not always representative since the clinical environment is unfamiliar and sometimes rather stressful to the patient. In addition, the demand on healthcare is growing rapidly, i.e. the number of PD patients worldwide is predicted to increase from 10 million in 2000 to 40 million patients in 2020 (Morris 2000). For these reasons, an objective monitor performing both long-term and ambulatory measurements of symptom severity is needed.

Ambulatory monitoring of Parkinson's disease, studying tremor, bradykinesia, and hypokinesia with kinematic sensors has been widely studied over the last decades (Dunnewold et al. 1997; Hoff et al. 2001; Salarian 2006; Someren et al. 2006). However, these studies usually only consider a few basic aspects of the complex symptomatology. When assessing tremor, rest and kinetic tremor should be treated as separate phenomena (Fahn and Elton 1987; Kraus et al. 2006). Nevertheless, in previous studies they are usually quantified as a single symptom. In addition, only rest tremor in the arm is commonly evaluated, even though tremor in the leg and upper body can also be significant in PD (Fahn and Elton 1987). Bradykinesia and hypokinesia are generally assessed by looking at arm activity. These symptoms, however, also impair walking, and cause decreased step length and velocity, increased variation in step length, and reduced arm swing. Another major problem in PD patients is standing up from a sitting position. Thus far, only Salarian (Salarian 2006) has attempted to use additional measures retrieved during posture transitions.

The PD monitor, presented in this paper, is able to perform both long-term and ambulatory measurements to assess patients objectively. Whereas previous monitors only assess a few aspects of motor symptoms, our PD monitor performs a detailed analysis of multiple symptoms and provides a complete assessment of tremor, bradykinesia, and hypokinesia. On top of that, the use of an activity

classifier (AC) within a PD monitor is proposed to differentiate between lying, sitting, standing, standing up, and walking. This enables the complete analysis of motor symptoms and the possibility for direct implementation into an ambulatory environment. The AC is essential for these applications: For instance, to compute step length, the activity 'walking' should be classified first. In addition, when an activity without arm movement is detected, rest tremor in the arm can be evaluated, but when arm movement is detected, kinetic tremor can be evaluated.

The AC has hardly been studied in combination with PD monitors, even though it is essential for a complete ambulatory assessment. Salarian et al. (Salarian 2006) incorporated an AC into a PD monitoring system, but used it only for the determination of on and off periods. In addition, Dunnewold et al. (Dunnewold et al. 1998) used an AC, but they only considered static activities and they assessed just a few basic aspects of PD motor symptoms. In contrast, the AC itself has been a subject of research for a long time (Bouten et al. 1994; Veltink et al. 1996; Dunnewold et al. 1998; Najafi et al. 2003; Zhang et al. 2003; Bao and Intille 2004; Mackey et al. 2006). Methods have been proposed for the discrimination of static from dynamic activities using the alternating current component of an acceleration signal (Bouten et al. 1994; Veltink et al. 1996). Within the static activities, posture detection can be performed by assessing the direct current component of the acceleration signal (Veltink et al. 1996; Dunnewold et al. 1998). Considering dynamic activities, it has been proposed that detection of walking is possible by analyzing signal morphology (Veltink et al. 1996), peak detection (Najafi et al. 2003) or the frequency domain entropy (Bao and Intille 2004).

In this paper, we studied a new ambulatory monitoring system that combines several algorithms to classify current motor activity and symptom severity simultaneously. This combined detection of motor activity and symptom severity yields a monitor that is truly ambulatory, in a way that it provides easily interpretable data even when used in the patient's home environment. A preliminary version of this work has been reported (de Klerk et al. 2008).

7.2. Methods

Experimental setup

Six PD patients (age 54-68) treated with DBS in the subthalamic nucleus took part in the experiments We chose to use patients with DBS in order to test whether our PD monitor was responsive to instantaneous changes in symptom severity within subjects. Patients were included when they had good clinical results with DBS and responded within 5 minutes to changes in stimulator

settings. Furthermore, they had to be able to fully cooperate with the experiments, show no major symptom fluctuations due to medication, and not suffer from dementia or dyskinesias. As a control group, seven healthy subjects (age 53-61) were also included. The study protocol was approved by the local medical ethical committee and all subjects gave written informed consent after a thorough written and oral explanation of the experimental setup.

The patients were measured under three conditions. Condition 1 ("on"): Stimulator at the optimal settings (as determined previously by the treating physician). Condition 2 ("intermediate"): Stimulator at a stimulation amplitude of 80% of the optimal setting. Condition 3 ("off"): Stimulator off. The measurements started 15 to 30 minutes after the adjustment of the DBS. The healthy control group was measured in one condition, their healthy state. During each condition, the subject was asked to perform certain daily tasks and UPDRS motor tests in a randomly predefined order. Each task was repeated two times, except for the tasks related to standing up. These tasks were each repeated three times. The daily tasks included: sitting quietly for 30 seconds; sitting while rapidly tapping three predefined spots forming a triangular shape on a table using the most affected arm for 20 seconds; transition from sitting to standing (UPDRS motor score item 27); transition from sitting to standing and walking (the timed-up-and-go test); walking for 30 seconds (UPDRS item 29); standing still for 30 seconds; standing while picking up, drinking, and returning a cup of water; standing while moving a bottle of water from one spot to another; lying down on a bed for 30 seconds. In addition, the following UPDRS-III motor tests were assessed: rest tremor of the arm and leg (UPDRS item 20); postural tremor of the arm (UPDRS item 21) and kinetic tremor while touching the nose and researcher's index finger alternately using the most affected arm; rapid pronating and supinating movements for 20 seconds (UPDRS item 25); foot tapping for 20 seconds (UPDRS item 26).

During all these tasks, motor activity was measured using four MT9 inertial sensors (3D accelerometers and 3D gyroscopes, Xsens Technologies BV, Enschede the Netherlands). The sensors were placed on the trunk and wrist, thigh, and foot of the most affected side of patients and the dominant side of the control group (Fig. 1). A 50 Hz sample frequency was used. The Xbus master, worn around the waist, sent the data from the sensors to a laptop via Bluetooth. The activities of the subject were videotaped. The video recording was of a satisfactory quality, i.e. resolution of 720x576 pixels and a rate of 25 frames/second (Schoffer et al. 2005). Using this video, actual activities were visually determined as a gold standard to which the PD monitor's AC output was compared. The physician, who was blind to stimulator settings, also used this recording to score a subset of the UPDRS (Fahn and Elton 1987) during each of

the three conditions. Louis et al. (Louis et al. 2002) showed that videotaped UPDRS motor examination is a sufficiently accurate alternative to in field studies.

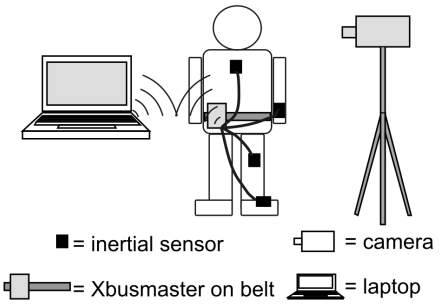

Figure 1. Schematic representation of the experimental setup. The subject wore four inertial sensors placed on the wrist, thigh, and foot of the most affected site and on the sternum. The sensors were wired to the 'Xbus master', which provided power, collected and sent data to the laptop via Bluetooth. The patient was also videotaped.

Data analysis

Our PD monitor used a three-step approach. First, the raw signal was preprocessed. Second, the AC evaluated the current motor activity of the patient for each measured second (e.g. sitting still, sitting while moving the arm, standing etc.). Third, the motor symptom monitor (MSM) determined the severity of the motor symptoms, i.e. tremor, bradykinesia, and hypokinesia. Fig. 2 shows the general structure of the PD monitor. The next three paragraphs describe each step of the PD monitor's approach.

Preprocessing algorithm

The raw signal was expressed in sensor coordinates (s_s). As information in the body coordinate system was needed, the signal had to be converted from sensor to body coordinates (s_b). This was done using a rotation matrix (R_{bs}) (1), as previously proposed by Luinge et al. (Luinge et al. 2007). Briefly, the calibration procedure of the sternum sensor was as follows. First, the subject stood upright. During this, the body z-axis was equal to the gravity vector and could be expressed in the sensor coordinate system. Second, the trunk was bended forward around the hip-axis being the body y-axis, by which this axis could be expressed in the sensor coordinate system. The body y- and z-axis were cross-multiplied to obtain the x-axis. The bending task was repeated three times. The thigh and foot sensor were calibrated starting in a sitting posture. Subsequently, they were lifted while turning around the hip-axis (thigh) and knee-axis (foot).

Finally, the arm was laid horizontally on a table and lifted while turning around the elbow-axis.

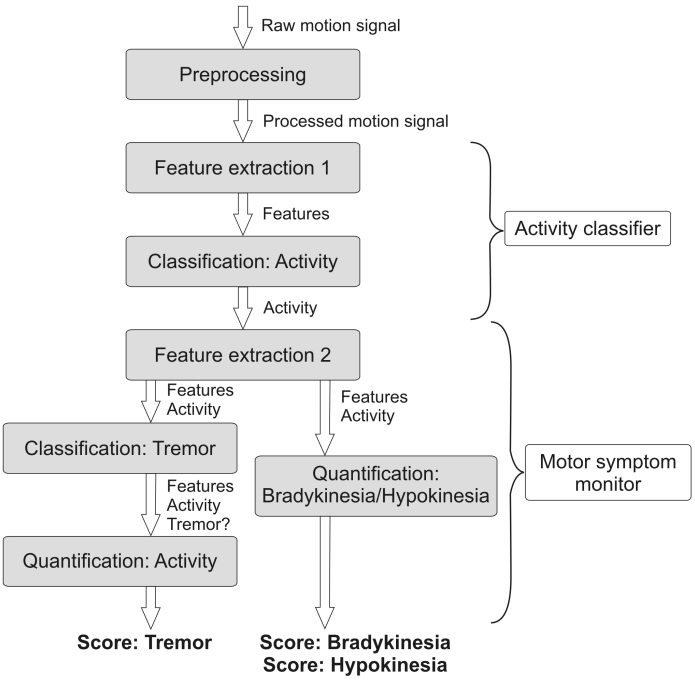

Figure 2. The general structure of the PD monitor. Body motion is measured by the inertial sensors and the raw motion signal is preprocessed. The AC first extracts features, which are used by the classifier to determine the activities (Fig. 3). After the AC, the information is split into two data streams of the MSM, one for tremor and one for bradykinesia and hypokinesia. Dependent on the activity, certain features are extracted and tremor detection is performed. When tremor is present, the tremor severity is determined (Fig. 4). In the second data stream, bradykinesia and hypokinesia severity are determined (Fig. 5).

$$\vec{s} = R_{bs}\vec{s}_s \tag{1}$$

After this, the contents of the raw sensor signal were analyzed, namely acceleration (a), gravity (g), offset (o), and noise (n) (2).

$$\vec{s}_b = \vec{a}_b - \vec{g}_b + o_b + n_b \tag{2}$$

To obtain the acceleration signal, all other signal components were removed. First, a second-order low-pass Butterworth filter with a cut-off frequency of 23 Hz (H_{lpf1}) reduced high frequency noise (3).

$$\vec{s}_b = H_{lpf1}(\vec{s}_b) \approx \vec{a}_b - \vec{g}_b + o_b \tag{3}$$

Assuming that there were no fast orientation changes of the sensor and thus no fast changes in the direction of gravity, gravity and offset were estimated by low-pass filtering the signal. For this purpose, a second-order low-pass Butterworth filter having a cut-off frequency of 0.25 Hz (H_{lpf2}) was used. Subtracting this low-pass filtered signal from the original signal, which had already been compensated for high frequency noise, provided the acceleration (4).

$$\vec{s}_{b,2} = \vec{s}_{b,1} - H_{lpf2}\left(\vec{s}_{b,1}\right) \approx \vec{a}_b \tag{4}$$

The acceleration signal (a_b) was essential for further analysis. Furthermore, the low-pass filtered signal ($H_{lpf2}(s_{b,1})$) was useful for the estimation of body inclination. The inclination is defined as the angle of the body axes relatively to the global vertical. As the direction of gravity equals the vertical axis in the global space, the orientation of the body relative to the global vertical is known when the gravity vector in the body system is known. Luinge et al. (Luinge and Veltink 2004) showed that, although a better method exists, the low-pass filtered signal still gives a good estimate of the inclination. The average error of sensors placed on the trunk and pelvis was 3 degrees with reference to an optical tracking system, with an increasing error with movement speed. Especially during slow movements, which are often present in PD, this method is useful. As calibrated signals were obtained from the Xsens software, the offset was negligible and so the low pass filtered signal was a good estimate of the inclination.

Activity Classifier

The AC uses the concept of a decision tree (Fig. 3). The following features were used on the particular nodes. Node 1 used the integrals of the absolute value of the accelerometer output (IAA, (5), (Bouten et al. 1994)) to detect whether the person was performing a static or dynamic activity.

$$IAA = \frac{1}{t}\left(\int_0^t |a_x|dt + \int_0^t |a_y|dt + \int_0^t |a_z|dt\right) \tag{5}$$

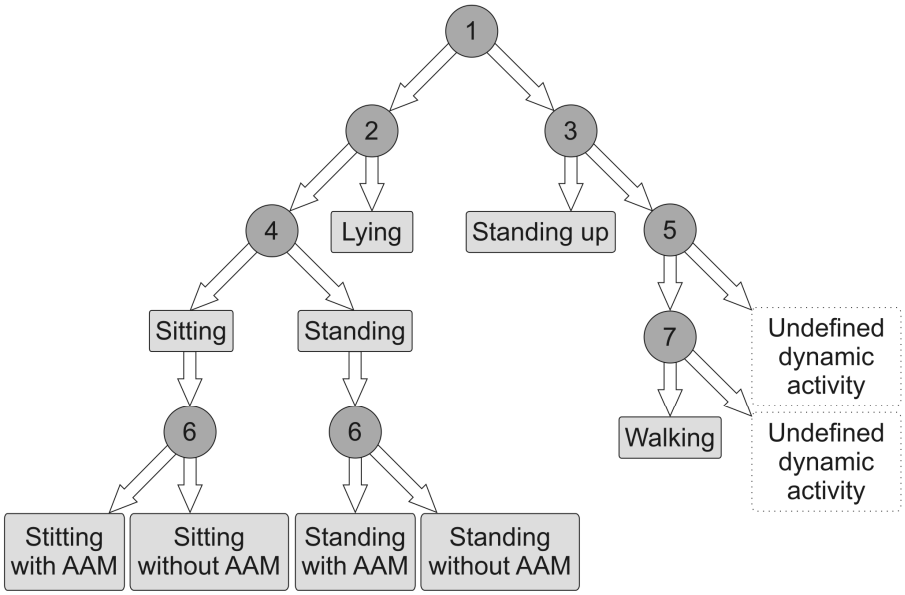

Figure 3. Schematic overview of the decision tree for the classification of activities. The differentiation made in the binary decision nodes (BDN):
BDN 1: Discrimination of static from dynamic activities
BDN 2: Discrimination of an upright from a lying posture
BDN 3: Discrimination of 'sit to stand' from other possible motions
BDN 4: Discrimination of sitting from standing
BDN 5: Discrimination of dynamic activities in a standing posture from all other dynamic activities
BDN 6: Discrimination of postures with and without AAM
BDN 7: Discrimination of walking from all other 'active standing' activities

The acceleration (a) of the thigh sensor was used in (5). As this feature sometimes missed slow movements (i.e. <0.25 Hz), which are especially present in PD patients, a second feature was introduced in this node. This feature identified the change in thigh inclination per second (t = 1 s), i.e. the difference in value of the inclination signal between one second and the next. When the difference was above a threshold, a dynamic activity was also recognized.
Node 2 was used to differentiate an upright trunk position from a horizontal one. This was accomplished by using the trunk sensor, assessing the inclination of the trunk (Veltink et al. 1996). The same principle was applied on node 4 using the thigh sensor, which distinguishes standing from sitting by assessing the thigh inclination. In node 6, active arm movement (AAM) was detected by determining the IAA of the acceleration measured in the wrist sensor.

The other branch of the tree considered the dynamic activities. Node 3 detected standing up, which was defined when the following sequence of events was recognized. First, the subject's thigh had to be orientated horizontally in global space. Subsequently, an inclination change had to be present. For this purpose, a feature representing the change of inclination in the thigh over one second was used. During the inclination change, the orientation of the thigh had to be changed to a vertical one. A vertical orientation was defined using the same parameters as node 4. Finally, nodes 5 and 7 differentiated walking from other dynamic activities. Node 5 checked whether the orientations of the thigh and trunk were upright. Node 7 applied a method for walking detection based on, but not similar to, a method proposed by Najafi et al. (Najafi et al. 2003). First, a peak detection algorithm was applied on the acceleration signal measured on the foot, which was filtered below 5 Hz using a second-order Butterworth filter. Only sufficiently high peaks, thus peaks above a certain threshold (determined during the algorithm's training procedure), were detected. Successive peaks with intervals of 0.25-2.25 s defined potential steps. Two successive potential steps defined walking.

Motor Symptom Monitor – Tremor

Two types of tremor were evaluated, namely rest and kinetic tremor. Arm rest tremor was only determined when the arm was not moving, thus when the activities sitting or standing without AAM were identified by the AC (Fig. 4). In contrast, arm kinetic tremor was only evaluated when sitting and standing with AAM were classified. Furthermore, thigh and trunk rest tremor were quantified during the entire sitting and standing time, i.e. sitting and standing with or without AAM (as the thigh and trunk were not moving during these activities).

For rest tremor evaluation, the acceleration was first filtered between 3.5 and 9 Hz (Deuschl et al. 2000) and subsequently windowed using a Blackman window. The window had a length of 3 seconds and it was shifted over the data each second. Subsequently, the frequency spectrum of each window was computed using FFT. In the spectrum, the dominant frequency was determined. When the power of this frequency was sufficiently high, tremor was identified. During the training of the algorithm, the threshold for tremor detection was determined per activity, i.e. sitting and standing without AAM, separately. Tremors detected in isolated windows were rejected. After this, the RMS values (intensity) of the signal in all directions within the positively labelled windows were computed, as well as the percentage of time during which tremor was present. The intensity (i) and the duration (d) of tremor together quantified tremor severity (TS) (6).

$$TS = i\sqrt{d} \tag{6}$$

TS was computed for all axes of the 3D acceleration. The TS values of each axis separately, of each possible combination of two axes, and the three axes combined were computed. The combined axes were calculated using Pythagoras. This gave a total of seven different combinations of which the one that best quantified tremor was determined per body part. This was done by evaluating the correlation between this parameter and the UPDRS 20 score determined by the physician.

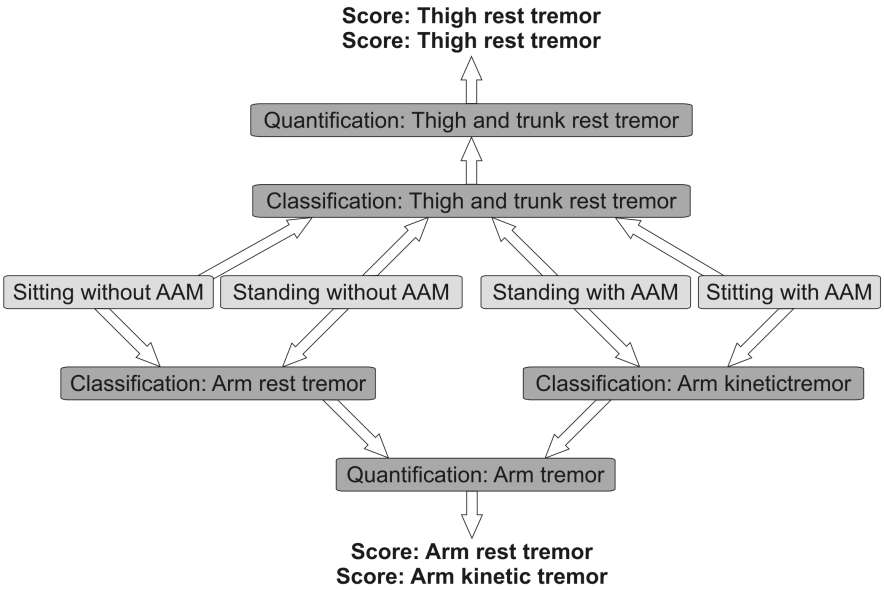

Figure 4. Schematic overview of the detection and quantification of tremor. The middle boxes in light grey show the current activity. Dependent on the activity, different types of tremors are analyzed, resulting in scores for the different types of tremor.

A different method was used to evaluate kinetic tremor, because this type of tremor occurs during limb movement. This movement interferes with the previous tremor detection approach. First, a second-order Butterworth filter filtered the acceleration signal between 3.5 and 12 Hz (Deuschl et al. 2000). Subsequently, the signal was windowed using 3-second Blackman windows, and slid over the data each second. For each window, the periodogram was computed. From the periodogram, a first and second-order moment were calculated. Before the moments could be calculated, the total energy (E_x) of the signal had to be calculated using the Fourier transformed signal (X(f)) (7). The frequency (f) is normalized by the sample frequency.

$$E_x = \int_0^{0.5} |X(f)|^2 df \quad (7)$$

The total energy was subsequently used to normalize the moments. The first-order moment (f_{m1}) determined the mean frequency (Rangayyan 2002) (8).

$$f_{m1} = \frac{f_s}{E_x} \int_0^{0.5} f|X(f)|^2 df \quad (8)$$

In this equation, f_s represents the sample frequency. The second-order moment (f_{m2}) represents the variance in frequency, which provides a measure of spectral spread (standard deviation of the mean). This parameter is an indication of the bandwidth of the signal about the mean frequency. Equation (9) shows the computation of this parameter (Rangayyan 2002).

$$f_{m2} = \frac{f_s}{E_x} \int_0^{0.5} (f - f_{m1})^2 |X(f)|^2 df \quad (9)$$

The variance of the frequency was used to define whether the power was concentrated in a small frequency band around the mean frequency, which is the case for PD patients (Findley et al. 1981). Kinetic tremor was detected when the value of the variance was beneath a certain threshold. The severity of the kinetic tremor was quantified by computing the percentage of time that kinetic tremor was observed. The amplitude was not used as a measure, because ordinary movement too heavily influenced this parameter. The variance of frequency (9), which is used to compute the percentage of time with kinetic tremor, is also influenced by ordinary movement, i.e. this parameter is increased by about 50% when ordinary movement is present in comparison to periods without movement. However, the average variance of frequency during periods of movement with tremor, i.e. 0.073±0.027, still differs significantly from the value during periods of movement without tremor, i.e. 0.090±0.031 ($P<0.01$).

Motor Symptom Monitor – Bradykinesia

Since bradykinesia manifests in many ways, several aspects of this phenomenon were assessed (Fig. 5). The average value of acceleration represents the slowness of the movements. To obtain a meaningful parameter related to bradykinesia (and not hypokinesia) the average arm acceleration was only computed during periods with AAM. Because bradykinesia affects walking, parameters related to step length and step velocity were extracted during this activity. It has previously been demonstrated that the walking velocity decreases with a reducing step length (Morris 2000). Another feature of bradykinesia is the difficulty experienced

during standing up (Salarian 2006). Therefore, the duration of standing up and a range of movement parameters were extracted during this activity (Fig. 5).

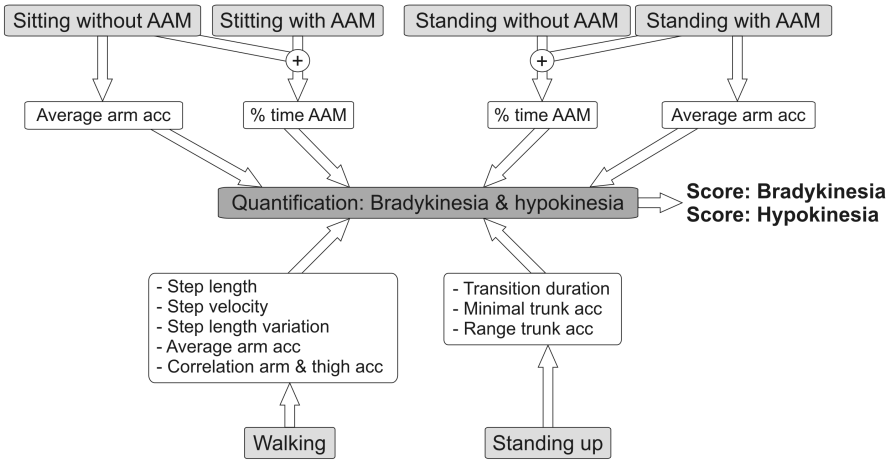

Figure 5. Schematic overview of the quantification of bradykinesia and hypokinesia. The upper and lower boxes in light grey show the current activity. The white boxes represent the features that are extracted during these activities. Bradykinesia and hypokinesia are characterized using multiple parameters. The wide variety of parameters assessed provide a detailed analysis of bradykinesia and hypokinesia. acc=acceleration; corr=correlation

Step velocity and length were computed using an accelerometer and gyroscope placed on the foot. The validated algorithm proposed by Sabatini et al. (Sabatini et al. 2005) was applied for this purpose. Step length and velocity were normalized according to leg length. The length of the inside leg was measured manually using a ruler. Parameters related to standing up were extracted from the low-pass filtered trunk accelerometer signal using a second-order Butterworth filter with a cut-off frequency of 0.65 Hz (Salarian 2006). This provided information about the inclination change in the upper body. From this signal, the transition duration was obtained by calculating the time between the two subsequent negative peaks (Salarian 2006). The minimal trunk acceleration was defined by the peak with the highest negative value. Finally, the difference between the value of this same negative peak and the highest positive peak defined the range of trunk acceleration.

Finally, the average acceleration due to arm movement was computed during standing and/or sitting with AAM. This parameter was calculated by combining the 3D acceleration using Pythagoras and subsequently taking the RMS value. Previous to this, the acceleration was low-pass filtered below 3 Hz with a fourth

order Butterworth filter, to remove movement due to tremor (Deuschl et al. 2000).

Motor Symptom Monitor – Hypokinesia

Hypokinesia is characterized by the poverty of movement. This can be studied by assessing how much a patient moves his arms, which was defined by the time during which the arm was moving as a percentage of the entire sitting and/or standing time (Fig. 5). The arm movement was studied after movement due to tremor was filtered off using the same procedure as applied in the bradykinesia evaluation. Hypokinesia also presents as diminished arm swing during walking (Morris 2000). In healthy people, the arm moves forward as the thigh moves backward and vice versa, which provides a high correlation between both in healthy people. However, when arm swing becomes random and there is a changing phase between arm and thigh swing, correlation decreases. As arm swing occurs slowly, it can be assessed by studying the acceleration signals below 1 Hz. Therefore, the correlation between the low-pass filtered (<1 Hz) acceleration signals of the arm and thigh were computed during walking. Furthermore, the amplitude of the arm swing diminishes in PD. For this reason, the average acceleration due to arm movement during walking was assessed.

Training the algorithm

Training was performed to define the threshold values to be applied in the algorithm. These thresholds were needed for activity and tremor detection. During the training procedure, the activities determined by the algorithm while using different threshold levels, were compared to the activities defined by manual labelling of the video data. Manual labelling of the video data was performed per second during which both the current activity and the presence of tremor were determined.

The training was achieved using the leave-one-subject-out approach (Russel and Norvig 1995). This method keeps training and test data strictly separated. The training set was created out of all subjects except one. This 'excluded' subject was used as the test set and was thus used to evaluate the performance of the PD monitor. This was repeated five times. During each time, the training set was composed of another combination of five subjects and the test set was composed of the 'excluded' subject. The results of subjects were combined to obtain the overall evaluation of the PD monitor.

Statistical analysis
To assess the performance of the AC and tremor detection, the accuracy, the ability to correctly classify each window, was computed. Equation (10) shows the formulae used for the computation of accuracy, TP=true positives; TN=true negatives; FP=false positives; FN=false negatives.

$$accuracy(\%) = \frac{TP+TN}{TP+TN+FP+FN} \cdot 100 \quad (10)$$

Furthermore, the PD monitor's ability to accurately score symptoms was assessed by comparing its output scores for the symptoms to the UPDRS scores given by the physician after analysing the video data. This relation was quantified by the between-subject Spearman rank correlation. Finally, the use of the PD monitor to optimize treatment was assessed by analysing its ability to discriminate different settings of the stimulator. This was assessed by a repeated measures ANOVA test and a subsequent Tukey test.

7.3. Results

Preprocessing
The inclination estimate was compared to the one of the Xsens software. They report a root mean square error of 3 degrees, while using the accelerometer, gyroscope, and magnetometer. We used the accelerometer only, to reduce the amount of sensors for future ambulatory use. Our estimation differed by 1.9 degrees from the Xsens estimate.

Activity Classifier
The manually (video recordings) and automatically labelled activities were compared. Fig. 6 gives an example of one PD patient's trial. Table I gives the results of a test of the AC's ability to classify activities in PD patients. The AC achieved an overall accuracy of 98.9%.
Data of a healthy population were also used for training and evaluation of the AC. This gave slightly better results, namely an overall accuracy of 99.3%. Especially, the activities walking and AAM during standing were detected better in healthy subjects.

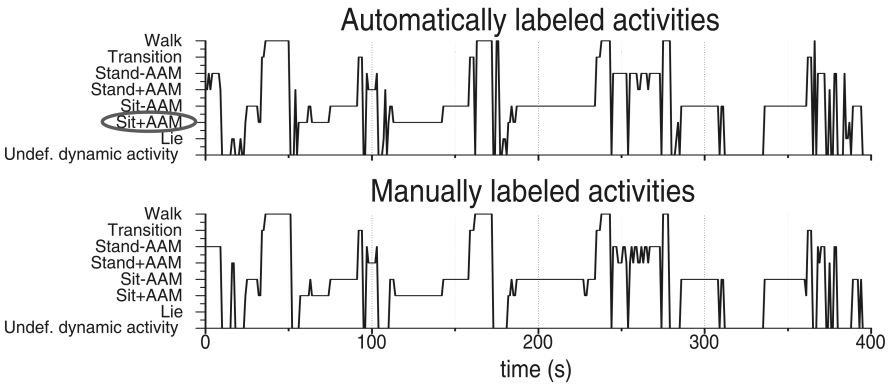

Figure 6. The results of the AC. The figure shows manually and automatically labeled activities for one person during a 400 second during trial. The upper graph presents the activities labeled by the AC. The lower graph shows the automatically labeled data using the video recordings. The manually labeled data act as a control for the automatic labeling of the AC. The activities determined by the AC show great similarity to the manually labeled data. During the encircled activity, sitting with AAM, the feature 'average arm acceleration' was computed (Fig. 7).

Table 1. The evaluation of the AC – accuracy (%)

Activity	PD patients	Healthy control
Lie	99.6	100.0
Sit	99.3	99.7
Sit + AAM	98.9	99.4
Sit – AAM	98.7	99.3
Stand	99.1	99.9
Stand +	98.6	99.7
Stand –	98.9	99.5
Standing	99.7	99.3
Walk	97.2	97.8
All	**98.9**	**99.3**

The evaluation of the AC for PD patients and healthy controls. The activities detected by the AC were compared to the activities manually labeled using the video data. The accuracy were determined per activity and over all activities.

Motor Symptom Monitor – Tremor

Rest tremor detection was performed with an accuracy of 84.5% during sitting and 94.1% during standing in the arm, while it was 79.1% during sitting and 90.1% during standing in the thigh. Kinetic tremor in the arm detection had an accuracy of 78.7% during sitting and 81.7% during standing.

The ability of the MSM to quantify the various forms of tremor was assessed by comparing the output of the algorithm to the physician's UPDRS scores. For rest tremor in the arm, the best correlation between the PD monitor's output and the UPDRS scores was achieved when using acceleration data in the axial and radial direction while sitting, namely a correlation of 0.84 ($P < 0.01$). A correlation analysis on rest tremor in the thigh was not performed, because too little variation in UPDRS scores given by the physician was present for a proper analysis. The correlation of the trunk rest tremor was also not computed, because it was not scored by the physician as it is not a standard UPDRS item. Quantification of kinetic tremor was assessed and proved to be more difficult, so a correlation of 0.67 ($P < 0.01$) to UPDRS item 21 was achieved during sitting. Furthermore, the severities of rest tremors, which were observed within one individual, were often different within the arm, thigh, and trunk. The same observation was made for rest and kinetic tremors, which also differed within individuals.

The ability of the MSM to discriminate between different settings of the stimulator was assessed by performing a repeated measures ANOVA test and subsequent Tukey test. Arm, thigh, and trunk rest tremor differed significantly between all conditions ($P < 0.05$, $P = 0.01$, and $P < 0.01$ respectively). Furthermore, the post-hoc Tukey test revealed significant differences between "on" and "off" (arm: $P < 0.05$, thigh $P < 0.05$, trunk $P < 0.01$) and between "intermediate" and "off" (arm: not significant, thigh: $P < 0.05$, trunk $P < 0.05$). In contrast to rest tremor, no significant differences were found between severity levels of kinetic tremor during different stimulation settings. However, the trends were as expected. This means that kinetic tremor increased as the treatment level was reduced. An evaluation of the UPDRS test's ability to discriminate the conditions showed no significant differences (UPDRS item 20 arm: $P = 0.58$, thigh: $P = 0.70$, UPDRS item 21: $P = 0.77$).

Motor Symptom Monitor – Bradykinesia & hypokinesia

The correlation between the output scores of the PD monitor for bradykinesia and hypokinesia and the UPDRS scores are summarized in Table II. As the parameters cannot directly be translated into single UPDRS items, we chose to compare them to item 31, which represents overall bradykinesia and hypokinesia. The table shows that most of the bradykinesia related parameters had a

significant correlation with the UPDRS score. However, the achieved correlations were lower than those obtained for rest tremor. None of the hypokinesia related parameters were significantly correlated with the UPDRS item 31. However, the hypokinesia parameter 'percentage of time during which the arm was active while standing and sitting' just failed to reach significance (P = 0.053).

Bradykinesia and hypokinesia scores of the PD monitor did not differ significantly between the "off", "intermediate" and "on" states, although trends were as expected (i.e. less bradykinesia and hypokinesia in the "on" state). Fig. 7 shows an example of the bradykinesia score 'average arm movement during sitting' averaged over all subjects per condition. This figure shows that bradykinesia worsens as the treatment level is reduced. Note that this trend is visible when averaging over all subjects, but individual patients may not always follow this trend. For example, one patient suffered from more severe bradykinesia during condition "intermediate" than during condition "off". The UPDRS item 31 scores did not show significant differences between conditions either (P = 0.23).

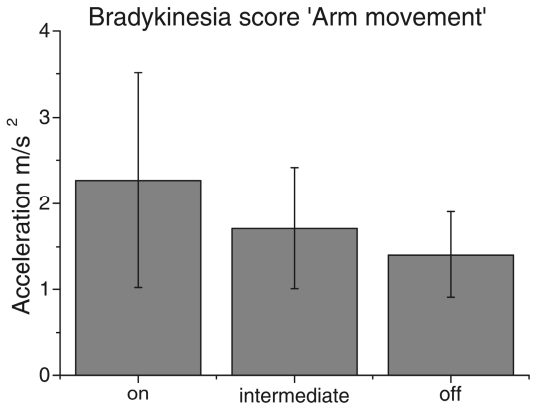

Figure 7. The bradykinesia score 'average arm acceleration', which is determined during the activity sit with AAM (see encircled activity Fig. 6), is compared per condition. The score is averaged over all subjects per condition, the mean and the standard deviation of the mean are shown. A trend of a decrease in the average acceleration, representing worsening of bradykinesia, is shown as the treatment level is reduced.

Table 2. The evaluation of the MSM – coherence

Activity	MSM-Parameter	Bradykinesia/ Hypokinesia	Healthy control
Standing up	Duration	B	0.70 (P<0.01)
	Minimal acceleration	B	-0.68 (P<0.01)
	Range of acceleration	B	-0.64 (P<0.01)
Walking	Average arm movement	H	-0.19 (P=0.47)
	Correlation thigh vs. arm	H	-0.43 (P=0.08)
	Step length	B	-0.70 (P<0.01)
	Step length variation	B	-0.03 (P<0.9)
	Step velocity	B	-0.71 (P<0.01)
With AAM	Sit average arm movement	B	-0.69 (P<0.01)
	Stand average arm movement	B	-0.72 (P<0.01)
	Sit and stand average arm	B	-0.57 (P=0.02)
With & without AAM	Sit % of movement time	H	-0.35 (P=0.17)
	Stand % of movement time	H	-0.24 (P=0.35)
	Sit & stand % of movement	H	-0.48 (P=0.05)

The evaluation of how well the MSM was able to score bradykinesia and hypokinesia. The values of bradykinesia and hypokinesia features were compared to the overall bradykinesia UPDRS score (UPDRS 31) given by the physician. The between-subject Spearman rank correlation between both values was computed. Correlations printed in black were significant, i.e. P-value<0.05. Correlations printed in grey were not significant. B = Bradykinesia; H = Hypokinesia

7.4. Discussion

Currently, motor symptoms of PD patients are assessed by the use of short subjective tests performed in the hospital, such as the UPDRS. As this approach has some downsides, a new evaluation system would be beneficial. This paper presents a novel monitor to follow PD patients in their daily lives. Current objective PD monitors only assess general aspects of tremor, bradykinesia, and hypokinesia. The advanced PD monitor described in this paper assesses a wide range of aspects related to tremor, bradykinesia, and hypokinesia in order to gain a complete motor assessment of the patient. To accomplish this thorough analysis, an AC was incorporated into the PD monitor. Another advantage of the AC lies in the fact that it enables direct implementation of our PD monitor into an ambulatory environment. Although not further explored in this paper, the AC could eventually also be used to gain knowledge about the time spend on different activities during the entire day. The monitor uses a setup of four sensors worn on the thigh, wrist, and foot of the affected side and on the trunk. This was the minimal number of sensors required to accomplish the proposed analysis.
The inclination estimate and activity classification proved accurate. Subsequent,

tremor analysis comprised the evaluation of rest tremor in the arm, thigh, and trunk and the evaluation of kinetic tremor in the arm. The validity of the PD monitor in quantifying arm rest and kinetic tremor was demonstrated by the significantly high correlation with corresponding UPDRS scores. Differences between rest tremor in the arm, thigh, and trunk as well as differences between rest and kinetic tremor within individual patients were observed. This underlines the importance of assessing different aspects of tremor, which is accomplished in our PD monitor.

The three aspects of bradykinesia and hypokinesia that were analyzed (arm movement, standing up, and walking) included features with a significant correlation to UPDRS item 31 score for overall bradykinesia and hypokinesia. However, whereas multiple bradykinesia parameters were correlated, none of the hypokinesia parameters were correlated. One reason for this might be that item 31 not solely quantifies hypokinesia, but also bradykinesia. This is an apparent advantage of our PD monitor, which makes a clear distinction between both symptoms.

After the accuracy of the motor symptom quantification was established, it was investigated whether the monitor could be used to optimize the treatment of PD. In the DBS patients, three conditions were analyzed: stimulator on, stimulator on with a stimulation amplitude at 80%, and stimulator off. The ability to distinguish the severity of tremor, bradykinesia, and hypokinesia at different DBS settings was evaluated. First, the PD monitor found the expected trends, i.e. the symptom worsened as the treatment level reduced. Second, it was shown that the values of rest tremor differed significantly between conditions. However, kinetic tremor, bradykinesia, and hypokinesia related parameters did not differ significantly between conditions. Still the results showed that the UPDRS test was not able to find any significant difference in symptoms severity between the conditions, whereas our PD monitor was. Therefore, our PD monitor proves to be a useful tool in optimizing treatment. Furthermore, the lack of significant differences can be explained by inter-individual differences in the severity of the disease, as well as differences in the response to DBS. The different responses to DBS are not only the result of differences in the way Parkinson is manifested in the patients, but may also be caused by inter-individual variations of the electrode position causing activation of different areas in the somatotopically organized subthalamic nucleus (Nambu et al. 1996). Therefore, the patients cannot be considered as a homogeneous group. This is also found in our results, as not all individual patients followed the expected trends of worsening symptoms with reducing treatment level. Finally, Krack et al. (Krack et al. 2002) argued that it could take several hours and even days before the effect of changes in DBS settings on bradykinesia stabilize. We chose to measure patients during a

single day in order to circumvent day-to-day fluctuations. In addition, we limited our total measurement time to three hours, thereby avoiding fatigue in the PD patients. Therefore, our experiments started 15 to 30 minutes after adjustment of DBS, even though the effect of changing the settings on bradykinesia might not have been fully stable. This may have negatively influenced our results on bradykinesia evaluation.

Dyskinesia, which has been studied before by Keijsers et al. (Keijsers et al. 2002) and Hoff et al. (Hoff et al. 2001), is not considered in this paper. Nonetheless, this is an important aspect that can be used to identify on and off-periods. Dyskinesia detection is also essential because bradykinesia cannot be quantified during a period of dyskinesia. For these reasons, the inclusion of dyskinesia detection in the PD monitor is an important next step in the development of the monitor. Another symptom not yet assessed by our monitor is freezing of gait, which would be classified as standing still by our current algorithm. We are currently performing studies to resolve this issue. A last topic not addressed in this paper, is the test-retest reliability. This is another essential next step before final implementation of the PD monitor.

In conclusion, this paper shows the PD monitor's accuracy in a thorough analysis of tremor, bradykinesia, and hypokinesia that can eventually be carried out in an ambulatory environment. Furthermore, it demonstrates that the monitor can be used to evaluate the PD motor symptoms in order to optimize treatment.

References

Bao, L. and S. Intille (2004). "Activity recognition from user-annotated acceleration data." Pervasive Computing: 1-17.

Bouten, C. V., K. R. Westerterp, M. Verduin and J. D. Janssen (1994). "Assessment of energy expenditure for physical activity using a triaxial accelerometer." Med Sci Sport Exer 26(12): 1516-1523.

de Klerk, D. G. M., J. P. P. van Vugt, J. A. G. Geelen and T. Heida (2008). A longterm monitor including activity classification for motor assessment in Parkinson's disease patients. Proc.4th Eur. Conf. IFMBE, Antwerp, Belgium.

Deuschl, G., J. Raethjen, R. Baron, M. Lindemann, H. Wilms and P. Krack (2000). "The pathophysiology of parkinsonian tremor: a review." J Neurol 247: 33-48.

Dunnewold, R. J. W., J. I. Hoff, H. C. J. van Pelt, P. Q. Fredrikze, E. A. H. Wagemans and B. J. J. van Hilten (1998). "Ambulatory quantitative assessment of body position, bradykinesia, and hypokinesia in Parkinson's disease." J Clin Neurophysiol 15(3): 235-242.

Dunnewold, R. J. W., C. E. Jacobi and J. J. van Hilten (1997). "Quantitative assessment of bradykinesia in patients with parkinson'sdisease." J Neurosc Meth 74(1): 107-112.

Fahn, S. and R. L. Elton (1987). Unified Parkinson's Disease Rating Scale development Committee: Unified Parkinson's Disease Rating Scale. Recent developments in Parkinson's disease. S. Fahn, C. D. Marsden and D. Calne. New York, Macmillan**:** 153-164.

Findley, L. J., M. A. Gresty and G. M. Halmagyi (1981). "Tremor, the cogwheel phenomenon and clonus in Parkinson's disease." J Neurol Neurosurg Psychiatry 44(6): 534-546.

Hoff, J., E. A. Wagemans and J. J. van Hilten (2001). "Ambulatory objective assessment of tremor in Parkinson's disease." Clin. Neuropharmacol. 24(5): 280/283.

Hoff, J. I., E. A. H. Wagemans and J. J. van Hilten (2001). "Accelerometric assessment of levodopa-induced dyskinesias in Parkinson's disease." Mov. Disord. 16(1): 58-61.

Keijsers, N. L., M. W. Horstink and S. C. Gielen (2002). "Automatic assessment of levodopa-induced dyskinesias in daily life by neural networks." Mov. Disord. 18(1): 70-80.

Krack, P., V. Fraix, A. Mendes, A. L. Benabid and P. Pollak (2002). "Postoperative management of subthalamic nucleus stimulation for Parkinson's disease." Mov. Disord. 17(S3): S188-S197.

Kraus, P. H., M. R. Lemke and H. Reichmann (2006). "Kinetic tremor in Parkinson's disease–an underrated symptom." J Neural Transm 113: 845-853.

Louis, E. D., G. Levy, L. J. Côte, H. Mejia, S. Fahn and K. Marder (2002). "Diagnosing Parkinson's disease using videotaped neurological examinations: validity and factors that contribute to incorrect diagnose." Mov. Disord. 17(3): 513-517.

Luinge, H. J. and P. H. Veltink (2004). " Inclination measurement of human movement using a 3-D accelerometer with autocalibration." IEEE Trans Neural Syst Rehabil Eng 12(1): 112-121.

Luinge, H. J., P. H. Veltink and C. T. M. Baten (2007). "Ambulatory measurement of arm orientation." J Biomech 40(1): 78-85.

Mackey, A., P. Hewart, S. Walt, M. Moreau and S. Stott (2006). "Reliability and validity of an activity monitor (IDEEA®) in a paediatric population." Gait Posture 24: S34-S35.

Morris, M. E. (2000). "Movement disorders in people with Parkinson's disease: A model for physical therapy." Phys. Ther. 80: 578-597.

Najafi, B., K. Aminian, A. Paraschiv-Ionescu, F. Loew, C. J. Bula and P. Robert (2003). "Ambulatory system for human motion analysis using a kinematic sensor: monitoring of daily physical activity in the elderly. Biomedical Engineering, IEEE Transact." IEEE Trans Biomed Eng 50(6): 711-723.

Nambu, A., M. Takada, M. Inase and H. Tokuno (1996). "Dual somatotopical representations in the primate subthalamic nucleus: evidence for ordered but reversed body-map transformations fromt he primary motor cortex and supplementary motor area." J. Neurosci. 16: 2671-2683.

Rangayyan, R. M. (2002). Biomedical Signal Analysis - A Case-study Approach. New York, Wiley-Interscience.

Russel, S. J. and P. Norvig (1995). Learning from observations. Artificial intelligence - A modern approach. NJ, Upper Saddle River.

Sabatini, A. M., C. Martelloni, S. Scapellato and F. Cavallo (2005). "Assessment of walking features from foot inertial sensing." IEEE Trans Biomed Eng 52(3): 486-494.

Salarian, A. (2006). Ambulatory monitoring of motor functions in patients with Parkinson's disease using kinematic sensors, Ecole polytechnique federale de Lausanne.

Schoffer, K. L., V. Patterson, S. J. Read, R. D. Henderson, J. D. Pandian and J. D. O'Sullivan (2005). "Guidelines for filming digital camera video clips for the assessment of gait and movement disorders by teleneurology." J Telemed Telecare 11(7): 368-371.

Someren, E. J. W., M. Pticek, J. D. Speelman, P. R. Schuurman, R. Esselink and D. F. Swaab (2006). "New actigraph for long-term tremor recording." Mov. Disord. 21(8): 1136-1143.

Veltink, P. H., H. B. J. Bussman, W. de Vries, W. L. J. Martens and R. C. van Lummel (1996). "Detection of static and dynamic activities using uniaxial accelerometers." IEEE Trans Rehab Eng 4(4): 375-385.

Zhang, K., P. Werner, M. Sun, F. X. Pi-Sunyer and C. N. Boozer (2003). "Measurement of human daily physical activity." Obes Res 11(1): 33-40.

Chapter 8

General discussion

In this thesis, we focused on the improvement of deep brain stimulation (DBS) as a surgical treatment for Parkinson's disease (PD) patients. We hypothesize that DBS can be improved by targeted stimulation in the motor region of the subthalamic nucleus (STN), avoiding stimulation of the subthalamic limbic and associative regions. We believe that this will improve therapeutic benefits on motor symptoms and reduce the cognitive and limbic alterations, which are currently experienced by about half of the PD patients receiving DBS in the STN (Temel et al. 2006). To assess whether motor symptoms are improved by new treatment methods, we propose an objective and ambulant approach for the detailed assessment of PD motor symptoms.

8.1. Cortically evoked responses in the STN

One approach to locate the STN motor area is through sensing of the neural activity while performing motor cortex stimulation (MCS). In chapter 2 and 3, we showed that this is feasible, since both the unit activity and the local field potential (LFP) in the STN showed a distinctive pattern as a response to MCS. However, certain pitfalls were also evident. First of all, part of the subject group experienced epileptic seizures as a result of MCS. Second, in only one out of five patients a subthalamic response after MCS was visible.

We showed that a typical pattern in the unit activity response is present in the dorsolateral region (chapter 2), which is believed to be the region for motor function (Parent and Hazrati 1995; Hamani et al. 2004; Temel et al. 2005). The evoked LFPs were less focal than the unit activity (chapter 3), which is not surprising as LFPs represent activity of a group of neurons as opposed to the unit activity representing activity of a single neuron. However, as the measuring electrodes were spaced quite far apart, i.e. 2 mm from each other, we did expect the LFP to have a high enough spatial resolution. Despite the wide spacing between the electrodes in our measurement setup, the LFPs had an insufficient resolution. Therefore, measuring LFPs after MCS is not advisable for our purpose in the current paradigm.

Although our first results were promising, they also demonstrated that the approach involving MCS requires extensive further research and major adjustments before it can be put into practice. We propose to first assess how MCS can be applied safely, like it is applied in the treatment of central

neuropathic pain (Canavero and Bonicalzi 2002), how MCS can be applied more effectively and how STN responses can be recorded and interpreted optimally. Considering the first point, a safer approach to apply MCS should be feasible, as seizures also occur in other surgical procedures, but with a lower incidence, 1.2% (Szelenyi et al. 2007). We believe that, in future, the seizures can be avoided by charge-balanced stimulation and a lower current density during stimulation. Secondly, MCS can be applied more effectively by interpreting results of the MCS model (chapter 4). When considering chronic MCS for the treatment of PD, various stimulation protocols have been proposed in chapter 4. The optimal stimulation protocol has yet to be established through experimental studies. Considering acute MCS to locate the STN sensorimotor area during stereotatic surgery, the results indicate the following. To activate the hyperdirect and indirect pathway, pyramidal tract (PT) type (Giuffrida et al. 1985) and intratelencephalic (IT) type (Ballion et al. 2008; Mathai and Smith 2011) pyramidal axons should be activated respectively. It is important to avoid activation of the Basket cell axons, as those inhibit pyramidal neurons. The model predicts that PT and IT type pyramidal axons can be selectively targeted, while avoiding Basket cell axon activation, by using anodal rather than cathodal and bipolar stimulation. As we used cathodal and bipolar stimulation during the experiments described in chapter 2 and 3, there is room left for improvement on this part. If we want to activate the hyperdirect or indirect pathway separately, we have to use a large contact size and epidural stimulation for the activation of the PT type pyramidal axons and thus the hyperdirect pathway. A smaller contact size and subdural stimulation favor activation of the IT type pyramidal axons and thus the indirect pathway, but still PT type axons are activated in larger quantities with these parameters. Furthermore, it should be noted that subdural stimulation is undesirable because of the increased risk for seizures associated with it in comparison to epidural stimulation (Lefaucheur 2008). At present, a proper method to achieve selective stimulation of the indirect pathway has yet to be determined. Note that, the existence of the hyperdirect pathway has never been confirmed in human (Marani et al. 2008) and this research has also failed to demonstrate the existence of this pathway. Nonetheless, recently Brunenberg et al. (Brunenberg et al. 2012) performed high angular resolution diffusion imaging confirming the existence of the hyperdirect pathway in human. Another option to achieve safer but effective cortical stimulation is transcranial magnetic

stimulation (TMS). This has been shown to evoke subthalamic responses in a previous study (Strafella et al. 2004). An advantage of this approach is the fact that it is non-invasive. On the other hand, this approach lacks focality and spatial resolution (Molina-Luna et al. 2007). In an initial stage, a high resolution is not required and TMS could be used to optimize sensing and interpretation of the STN response signal.

To optimize sensing, good measurement equipment is important. The current recording electrodes should be suitable for the measurement of both unit activity and LFPs (Nelson and Pouget 2010). However, recent advancements in the development of stimulation electrodes provide another possibility, namely a new high resolution DBS electrode consisting of 64 contacts, namely eight rings of four contacts along the electrode (Martens et al. 2011)(Fig. 1). This enables the electrode to steer the stimulation in different directions and also provides a higher resolution along the electrode. Thereby, this electrode enables a more specific targeting of certain subthalamic regions, such as the area involved in motor function, even sub regions that can be allocated to different body parts (Nambu et al. 1996) might be stimulated selectively. In this regard, high resolution sensing could also become an important aspect as this could help to accurately locate different STN regions. Excitingly, this electrode also opens up opportunities for measuring the LFP in a higher resolution and in different directions. With this new electrode, techniques applying current source density (CSD) analysis on LFPs as described in chapter 5 come closer. In this chapter, we showed that the CSD analysis allows us to identify areas of neuronal input into the STN. This approach appeared to be well able to find and spatially distinguish these sources and sinks of the inputs in the rat. Apart from the physiological meaning, another important advantage of using the CSD is the fact that it has a higher resolution than LFPs. From chapter 3, we concluded that the spatial resolution of the LFP response was too low for our purpose. The CSD with its higher resolution gives us the opportunity of using the LFP measurements. In future, the CSD approach could be used to study the sources and sinks of neuronal activity, which could be useful to define the optimal target location for the DBS electrode. In that regard, it has to be determined which location relative to these sources and sinks provides the optimal clinical benefit for the patient. We should, however, consider that the 64 contact electrode design does not give the same 3D measurement grid as we obtained in the rat (chapter 5). Therefore,

two possibilities exist to apply the CSD method with this DBS electrode. The first option is using similar techniques but CSD analysis in which the grid consists of each of the four columns of 16 contacts below each other as a grid. A second option is to develop a new mathematical procedure to obtain the CSD based on the approach described in chapter 5. Modeling approaches could determine how neural activity from a source on a particular location would be represented by the different contacts. As each contact measures activity from a different direction, one could use the combined information of several contacts to reconstruct the sources of activity.

Figure 1. The design of the 64 contact DBS electrode (Sapiens Steering Brain Stimulation B.V., Eindhoven, The Netherlands).

8.2. Spontaneous subthalamic activity in human

A second approach to locate the STN motor area in human is by the recording of spontaneous activity. It has previously been shown that the beta power is elevated in the dorsolateral STN, which supposedly is the area for motor function (Parent and Hazrati 1995; Hamani et al. 2004; Temel et al. 2005). Knowledge on gamma oscillations in the STN is a less explored phenomenon compared to beta oscillations (Jenkinson et al. 2012). A previous study showed an increased LFP activity in the gamma band in the zona incerta, which is found dorsal to the STN, and the dorsal part of the STN (Trottenberg et al. 2006). The gamma oscillations were found in 8 out of 15 STNs. In chapter 6, we describe results of

neural beta and gamma activity in the STN. We confirmed that the LFP beta power is elevated in the STN sensorimotor area and also found that this elevation is mainly located in the high beta band (20-30 Hz). Furthermore, we found an elevated power in the LFP gamma band inside the STN as opposed to outside the STN, which was most prominent in the higher frequency range of the gamma band (60-80 Hz). Unlike Trottenberg et al. (Trottenberg et al. 2006), we did not see increased neuronal gamma activity in the zona incerta and we saw an increase throughout the entire STN and not just the dorsal part. The elevation of neuronal gamma power was present in all STNs, which indicates its potential use for discriminating the STN as a whole. As the beta oscillations were elevated within the sensorimotor area, this feature would be useful for the discrimination of the sensorimotor area within the STN. Though, it should be noted that this elevation was only present in about 70% of the STNs. Therefore, the cortically evoked subthalamic potentials as described in chapter 2-5 could offer an alternative solution for identifying the sensorimotor area within the STN.

8.3. Assessing motor improvement

In chapter 7, we describe an objective and ambulant approach for an extensive and detailed assessment of motor function. Such tools have been developed before (Dunnewold et al. 1997; Hoff et al. 2001; Salarian 2006; Someren et al. 2006), but these lack the ability of performing a motor assessment on a broad range of individual aspects. Essentially, our approach offers the first means to simultaneously assess different PD symptoms separately while distinguishing between several body parts using one ambulant system. As the STN is functionally segregated, the placement of the DBS electrode can have a differential effect on different aspects of motor function. Therefore, a tool that is able to assess each aspect individually offers an important additional feature.

8.4. Conclusions and direction for future research

Optimizing DBS surgery

The current DBS procedure involves awake stereotactic surgery when placing and testing the DBS electrode. In the future, it would be desirable to achieve a shorter operation time and eventually a procedure which does not require the

patient to be awake would be ideal. The procedure time could be shortened considerably if micro electrode recordings would not be required. The recently developed DBS electrode (Martens et al. 2011), described in section 8.1, could eventually lead to the exclusion of micro electrode recordings from the procedure. This novel DBS electrode offers the possibility of high resolution stimulation and recording of LFPs steered in multiple directions. From the studies in this thesis, we can conclude that two good options exist to interpret the subthalamic LFPs to locate the STN sensorimotor area: 1. CSD analysis on cortically evoked subthalamic LFPs could be performed. 2. Oscillations of spontaneous LFP activity could be assessed in the gamma band to distinguish the STN from other brain areas and oscillations in the LFP beta band could discriminate the STN sensorimotor area. The advantage of using spontaneous LFP activity is that is does not require MCS, which prolongs surgery time and induces additional risks due to the extra burr hole and cortical stimulation. On the other hand, a cortical electrode configuration could also be used for additional stimulation to optimize the treatment, or for sensing to create a closed-loop DBS system. The advantage of using MCS and CSD analysis of the evoked LFPs is that this provides high resolution spatial information on the neuronal input activity in areas with motor function. We believe that this latter approach offers a higher spatial accuracy. This is especially important if we would like to achieve a surgical procedure that does not require the patient to be awake, as in that case specific information on the motor improvement of patients is lacking. Furthermore, after surgery patients should be monitored with the novel objective ambulant motor assessment system described in chapter 7. Using the feedback of this monitor, DBS could be fine-tuned more specifically to improve certain motor functions.

The relation between subthalamic neuronal synchronization and PD symptoms

In this thesis, we generally focused on the spatial extent of the neural activity in the STN. Another aspect that reserves attention is the functional meaning of the neuronal activity. In particular, the relation between oscillations in the LFPs and PD symptoms could be investigated more extensively. It has been suggested that alpha and beta oscillations are antikinetic and pathological. Oscillations in the alpha band have been linked to rest and kinetic tremor, while beta oscillations are believed to play a role in bradykinesia and rigidity (Brown 2003; Ray et al.

2008). It has been suggested that dopaminergic therapy induces a shift of the neural activity power from the beta to the gamma frequency band (Cassidy et al. 2002; Williams et al. 2002; Alegre et al. 2005; Fogelson et al. 2005; Androulidakis et al. 2007) and that there is a reciprocal relationship between subthalamic LFP activity at 5-32 Hz and 65-85 Hz (Fogelson et al. 2005). In concordance with this, gamma oscillations have been suggested to be prokinetic and physiological rather than pathological. In this thesis, we found that the presence of gamma band LFP activity is elevated inside the STN and throughout the entire STN (chapter 6). This confirms that oscillations in this frequency band play a role in subthalamic processes. As the gamma oscillations are present throughout the STN, we believe that gamma oscillations play a role in motor function as well as associative and/or limbic function. A better understanding of the oscillations in neuronal activity and the patterns of neuronal activity in relation to PD symptoms could offer means to improve DBS. Stimulation could be applied more specifically to modulate brain activity related to certain PD symptoms. Stimulation parameters, like frequency, stimulation pattern (Hess et al. 2013), waveforms could be adjusted, even on an individual patient basis. Furthermore, a better understanding of the neuronal activity would also be useful in closed-loop DBS systems (Tass et al. 2012), as in these systems brain activity could be measured and DBS adjusted accordingly. Gaining insight on the meaning of neuronal activity could eventually even open up doors for patients who are at present not eligible for DBS, such as patients suffering from akinesia.

The relation between subthalamic subareas and PD symptoms

Numerous studies have reported on the functional division of the subthalamic nucleus into three areas, i.e. the motor, limbic and associative area (Parent and Hazrati 1995; Hamani et al. 2004; Temel et al. 2005; Lambert et al. 2012). Others even attempted to make a more detailed division of subthalamic regions into areas corresponding to different body parts (Nambu et al. 1996; Rodriguez-Oroz et al. 2001; Theodosopoulos et al. 2003) and areas related to different symptoms (Butson et al. 2011). Using probabilistic analysis of activation volumes during DBS, Butson et al. (Butson et al. 2011) found that optimal stimulation areas to treat rigidity are located anterior to optimal areas for bradykinesia treatment, although the sample size was small and analyses should be performed over a larger group to make definite conclusions. Another important finding was

that optimal stimulation sites for both bradykinesia and rigidity were located outside of the STN. This suggests that activation of the cortical afferents or lenticular fasciculus might be the real targets for DBS.

The detailed division of STN areas opens up opportunities to specifically target certain symptoms and certain body parts. In this regard, MCS (chapter 2 and 3) could provide means to differentiate areas in high detail. One could, for example, stimulate the MC hand area which is expected to result in a response in the subthalamic hand area. In this regard, it is also important to know which neural elements are being stimulated at a cortical level, which can be studied by the model proposed in chapter 4. Additionally, accurate sensing in the STN is also important and methods described in chapter 5 could be important in this respect.

An increase in beta band power was found to distinguish STN sensorimotor area from the other functional areas of the STN (chapter 6). However, the electrodes used for LFP recording were not direction specific and were differently shaped from the electrodes used for stimulation, which makes accurate identification of the sensorimotor area with respect to the final electrode difficult. In this regard, the next step could be the combination of local sensing and selective stimulation, which can be achieved by the novel electrode design introduced by Martens et al. (Martens et al. 2011) .

Once the high-resolution DBS electrode is placed, a tool as presented in chapter 7 could provide a detailed analysis of the PD symptoms, while discriminating different body parts, in order to optimize stimulation parameters and study the improvement of each aspect separately.

Network perspectives

To optimize DBS it is important to understand the underlying mechanisms. Currently, it is thought that DBS interacts with the diseased network to modulate and thereby eliminate pathological neural activity (McIntyre and Hahn 2010). In view of different approaches to understand DBS, McIntyre and Hahn conclude that DBS is associated with reduced bursting activity, reduced variability in spiking and overriding of disruptive oscillations.

Li et al. (Li et al. 2007) showed that DBS induces antidromic activation of layer V pyramidal cells, i.e. PT type cells, which triggered a damping oscillation of cortical LFPs with a resonant frequency around 120 Hz. This suggests that

activation of the PT type cells could be one of the most important reasons for the clinical effectiveness of DBS. In that case, one could also consider MCS instead of DBS to treat PD (Canavero and Paolotti 2000; Drouot et al. 2004; Arle and Shils 2008; Fasano et al. 2008; Cioni et al. 2009; Gutierrez et al. 2009; Meglio and Cioni 2009). Selective stimulation of PT type axons could be the key for successful MCS. As described in chapter 4, selective stimulation of PT type axons is achieved by anodal epidural stimulation using large contact size stimulation electrodes.

Recently, using fMRI in human Kahan et al. (Kahan et al. 2012) found that during voluntary movement, DBS reverses the effective connectivity between regions of the cortex and thalamus. As observed from the analysis of the data recorded during ambulatory monitoring, DBS has a differential impact on different PD motor symptoms. Furthermore, a change in the settings of stimulation results in gradual changes of the symptoms with different time scales. Network perspectives have not been considered in this study. However, the changes in network connectivity resulting from pathology and those resulting from continuous stimulation need to be taken into account in order to optimize DBS. Based on a modeling study it was suggested that a network may learn or unlearn pathological synaptic interactions dependent on the applied stimulation protocol (Tass and Majtanik 2006). It has been proposed that by multi-site coordinated reset, a network may be desynchronized and it enables the network to unlearn pathologically strong synaptic interactions. Multi-site DBS electrodes may provide a means to apply such coordinated reset protocols.

Conclusion

In order to optimize DBS many different aspects are of importance. First of all, the pathological neural activity needs to be understood in more detail. Not only at the level of a single neuron, but also at the level of neural activity in the entire network. Second, the way DBS can modulate this pathological neural activity needs to be investigated. In this regard, the pattern of stimulation will be of major importance. Third, the spatial distribution of the functional areas is of interest. This will give clues to which area(s) should be stimulated to most effectively suppress the different symptoms of the disease. In this thesis, we investigate different approaches to locate the functional areas of the STN. When we are able to locate the functional areas, selective stimulation of these specific

areas becomes important. To achieve selective stimulation, modeling studies of neural activation, such as presented in chapter 4, can provide insight into how certain areas can be targeted specifically. In addition, these computational models can be used to design novel electrode configurations that increase stimulation selectivity.

References

Alegre, M., F. Alonso-Frech, M. C. Rodriguez, J. Guridi, I. Zamarbide, M. Valencia, M. Manrique, J. A. Obeso and J. Artieda (2005). "Movement-related changes in oscillatory activity in the human subthalamic nucleus: ipsilateral vs. contralateral movements." Eur. J. Neurosci. 22: 2315-2324.

Androulidakis, A. G., A. A. Kühn, C. C. Chen, P. Blomstedt, F. Kempf, A. Kupsch, G. H. Schneider, L. Doyle, P. Dowsey-Limousin, M. I. Hariz and P. Brown (2007). "Dopaminergic therapy promotes lateralized motor activity in the subthalamic area in Parkinson's disease." Brain 130: 457-468.

Arle, J. E. and J. L. Shils (2008). "Motor Cortex Stimulation for Pain and Movement Disorders." Neurotherapeutics 5: 37-49.

Ballion, B., N. Mallet, E. Bézard, J. L. Lanciego and F. Gonon (2008). "Intratelencephalic corticostriatal neurons equally excite striatonigral and striatopallidal neurons and their discharge activity is selectively reduced in experimental parkinsonism." Eur. J. Neurosci. 27(9): 2313-2321.

Brown, P. (2003). "Oscillatory nature of human basal ganglia activity: relationship to the pathophysiology of Parkinson's disease." Mov. Disord. 18: 357-363.

Brunenberg, E. L. J., P. Moeskops, W. H. Backes, C. Pollo, L. Cammoun, A. Vilanova, M. L. F. Janssen, V. Visser-Vandewalle, B. M. ter Haar Romeny, J. Thiran and B. Platel (2012). "Structural and Resting State Functional Connectivity of the Subthalamic Nucleus: Identification of Motor STN Parts and the Hyperdirect Pathway." PloS One 7(6): e39061.

Butson, C. R., S. E. Cooper, J. M. Henderson, B. Wolgamuth and C. C. McIntyre (2011). "Probablistic analysis of activation volumes during deep brain stimulation." NeuroImage 54: 2096-2104.

Canavero, S. and V. Bonicalzi (2002). "Therapeutic Extradural Cortical Stimulation for Central and Neuropathic Pain: A Review." Clin. J. Pain 18(1): 48-55.

Canavero, S. and R. Paolotti (2000). "Extradural motor cortex stimulation for advanced Parkinson's disease: Case report." Mov. Disord. 15(1): 169-171.

Cassidy, M., P. Mazzone, A. Oliviero, A. Insola, P. Tonali, V. Di Lazzaro and P. Brown (2002). "Movement-related changes in synchronization in the human basal ganglia." Brain 125: 1235-1246.

Cioni, B., A. Bentivoglio, C. De Simone, A. Fasano, C. Piano, D. Policicchio, V. Perotti and M. Meglio (2009). Invasive cortical stimulation for Parkinson's disease and movement disorders. New York, Nova Science Publishers, Inc.

Drouot, X., S. Oshino, B. Jarraya, L. Besret, H. Kishima, P. Remy, J. Dauguet, J. P. Lefaucheur, F. Dolle, F. Conde, M. Bottlaender, M. Peschanski, Y. Keravel, P. Hantraye and S. Palfi (2004). "Functional recovery in a primate model of parkinson's disease following motor cortex stimulation." Neuron 44: 769-778.

Dunnewold, R. J. W., C. E. Jacobi and J. J. van Hilten (1997). "Quantitative assessment of bradykinesia in patients with parkinson'sdisease." J Neurosc Meth 74(1): 107-112.

Fasano, A., C. Piano, C. De Simone, B. Cioni, D. Di Giuda, M. Zinno, A. Daniele, M. Meglio, A. Giordano and A. Bentivoglio (2008). "High frequency extradural motor cortex stimulation transiently improves axial symptoms in a patient with Parkinson's disease." Mov. Disord. 23(13): 1916-1919.

Fogelson, N., A. Pogosyan, A. A. Kühn, A. Kupsch, G. van Bruggen, H. Speelman, M. Tijssen, A. Quartarone, A. Insola, P. Mazzone, V. Di Lazzaro, P. Limousin and P. Brown (2005). "Reciprocal interactions between oscillatory activities of different frequencies in the subthalamic region of patients with Parkinson's disease." Eur. J. Neurosci. 22: 257-266.

Giuffrida, R., G. Li Volsi, G. Maugeri and V. Percivalle (1985). "Influences of pyramidal tract on the subthalamic nucleus in the subthalamic nucleus of the cat." Neurosci. Lett. 54: 231-235.

Gutierrez, J. C., F. J. Seijo, M. A. Alcarez Vega, F. Fernandez Gonzalez, B. Lozano Aragoneses and M. Blazquez (2009). "Therapeutic extradural cortical stimulation for Parkinson's diseease: Report of six cases and review of the literature." Clin. Neurol. Neurosurg. 111: 703-707.

Hamani, C., J. A. Saint-Cyr, J. Fraser, M. Kaplitt and A. M. Lozano (2004). "The subthalamic nucleus in the context of movement disorders." Brain 127(1): 4-10.

Hess, C. W., D. E. Vaillancourt and M. S. Okun (2013). "The temporal pattern of stimulation may be important to the mechanism of deep brain stimulation." Exp Neurol In press.

Hoff, J., E. A. Wagemans and J. J. van Hilten (2001). "Ambulatory objective assessment of tremor in Parkinson's disease." Clin. Neuropharmacol. 24(5): 280/283.

Jenkinson, N., A. A. Kühn and P. Brown (2012). "Gamma oscillations in the human basal ganglia." Exp Neurol.

Kahan, J., L. Mancini, M. Urner, K. Friston, M. Hariz, E. Holl, M. White, D. Ruge, M. Jahanshahi, T. Boertien, T. Yousry, J. S. Thornton, P. Limousin, L. Zrinzo and T. Foltynie (2012). "Therapeutic subthalamic nucleus deep brain stimulation reverses cortico-thalamic coupling during voluntary movements in Parkinson's disease." PloS One 7(12): e50270.

Lambert, C., L. Zrinzo, Z. Nagy, A. Lutty, M. Hariz, T. Foltynie, B. Draganski, J. Ashburner and R. Frackowiak (2012). "Confirmation of functional zones within the human subthalamic nucleus: Patterns of connectivity and sub-parcellation using diffusion weighted imaging." Neuroimage 60: 83-94.

Lefaucheur, J. P. (2008). "Principles of therapeutic use of transcranial and epidural cortical stimulation " Clin. Neurophysiol. 119(10): 2179-2184.

Li, S., G. W. Arbuthnott, M. J. Jutras, J. A. Goldberg and D. Jaeger (2007). "Resonant antidromic cortical circuit activation as a consequence of high-frequency subthalamic deep-brain stimulation." J Neurophysiol 98: 3525-3537.

Marani, E., T. Heida, E. A. J. F. Lakke and K. G. Usunoff (2008). The subthalamic nucleus. Part I: Development, Cytology, Topography and Connections. Berlin, Springer-Verlag.

Martens, H. C., E. Toader, M. M. J. Decre, D. J. Anderson, R. Vetter, D. R. Kipke, K. B. Baker, M. D. Johnson and J. L. Vitek (2011). "Spatial steering of deep brain stimulation volumes using a novel lead design." Clin. Neurophysiol. 122(3): 558-566.

Mathai, A. and S. Smith (2011). "The corticostriatal and corticosubthalamic pathways: two entries, one target. So what?" Front. Syst. Neurosci. 5(64).

McIntyre, C. C. and P. J. Hahn (2010). "Network perspectives on the mechanisms of deep brain stimulation." Neurobiol. Dis. 38: 329-337.

Meglio, M. and B. Cioni (2009). Motor cortex stimulation for Parkinson's disease. Textbook of stereotactic and functional neurosurgery. A. M. Lozano, P. Gildenberg and R. Tasker. Berlin Heidelberg, Springer. 7: 1679-1690.

Molina-Luna, K., M. M. Buitrago, B. Hertler, M. Schubring, F. Haiss, W. Nisch, J. B. Schulz and A. R. Luft (2007). "Cortical stimulation mapping using epidurally implanted thin-film microelectrode arrays." J. Neurosci. Methods 161(1): 118-125.

Nambu, A., M. Takada, M. Inase and H. Tokuno (1996). "Dual somatotopical representations in the primate subthalamic nucleus: evidence for ordered but reversed body-map transformations fromt he primary motor cortex and supplementary motor area." J. Neurosci. 16: 2671-2683.

Nelson, M. J. and P. Pouget (2010). "Do electrode properties create a problem in interpreting local field potential recordings?" J. Neurophysiol. 103: 2315-2317.

Parent, A. and L. Hazrati (1995). "Functional anatomy of the basal ganglia. II. The place of the subthalamic nucleus and external pallidum in basal ganglia circuitry." Brain Res. Rev. 20: 128-154.

Ray, N. J., N. Jenkinson, S. Wang, P. Holland, J. S. Brittain, C. Joint, J. F. Stein and T. Aziz (2008). "Local field potential beta activity in the subthalamic nucleus of patients with Parkinson's disease is associated with improvements in bradykinesia after dopamine and deep brain stimulation." Exp Neurol 213: 108-113.

Rodriguez-Oroz, M. C., M. Rodriguez, J. Guridi, K. Mewes, V. Chockkman, J. L. Vitek, M. R. DeLong and J. A. Obeso (2001). "The subthalamic nucleus in Parkinson's disease: somatotopic organization and physiological characteristics." Brain 124: 1777-1790.

Salarian, A. (2006). Ambulatory monitoring of motor functions in patients with Parkinson's disease using kinematic sensors, Ecole polytechnique federale de Lausanne.

Someren, E. J. W., M. Pticek, J. D. Speelman, P. R. Schuurman, R. Esselink and D. F. Swaab (2006). "New actigraph for long-term tremor recording." Mov. Disord. 21(8): 1136-1143.

Strafella, A. P., Y. Vanderwerf and A. F. Sadikot (2004). "Transcranial magnetic stimulation of the human motor cortex influences the neuronal activity of subthalamic nucleus " Eur. J. Neurosci. 20(8): 2245-2249.

Szelenyi, A., B. Joksimovic and V. Seifert (2007). "Intraoperative risk of seizures associated with transient direct cortical stimulation in patients with symptomatic epilepsy." J. Clin. Neurophysiol. 24: 39-43.

Tass, P. A. and M. Majtanik (2006). "Long-term anti-kindling effects of desynchronizing brain stimulation: a theoretical study." Biol Cybern 94: 58-66.

Tass, P. A., L. Qin, C. Hauptmann, S. Dovero, E. Bezard, T. Boraud and W. G. Meissner (2012). "Coordinated reset has sustained aftereffects in Parkinsonian monkeys." Ann Neurol 72(5): 816-820.

Temel, Y., A. Blokland, W. M. Steinbusch and V. Visser-Vandewalle (2005). "The functional role of the subthalamic nucleus in cognitive and limbic circuits." Prog. Neurobiol. 76: 393-413.

Temel, Y., A. Kessels, S. Tan, A. Topdag, P. Boon and V. Visser-Vandewalle (2006). "Behavioural changes after bilateral subthalamic stimulation in advanced Parkinson disease: A systematic review." Parkinsonism & Related Disorders 12(5): 265-272.

Theodosopoulos, P. V., W. J. Marks, C. Christine and P. A. Starr (2003). "Locations of movement-related cells in the human subthalamic nucleus in Parkinson's disease." Mov. Disord. 18: 791-798.

Trottenberg, T., N. Fogelson, A. A. Kühn, A. Kivi, A. Kupsch, G. H. Schneider and P. Brown (2006). "Subthalamic gamma activity in patients with Parkinson's disease." Exp Neurol 200: 56-65.

Williams, D., M. Tijssen, G. van Bruggen, A. Bosch, A. Insola, V. Di Lazzaro, P. Mazzone, A. Oliviero, A. Quartarone, H. Speelman and P. Brown (2002). "Dopamine-dependent changes in the functional connectivity between basal ganglia and cerebral cortex in humans." Brain 125: 1558-1569.

List of acronyms

PD	Parkinson's disease
BG	Basal ganglia
STN	Subthalamic nucleus
GPi	Globus pallidus internus
GPe	Globus pallidus externus
SNr	Substantia nigra pars reticulate
DBS	Deep brain stimulation
LFP	Local field potential
UPDRS	Unified Parkinson's disease rating scale
MCS	Motor cortex stimulation
CSD	Current source density
TMS	Transcranial magnetic stimulation
PSTH	Peristimulus time histogram
MEP	Motor evoked potential
MER	Micro electrode recordings
MC	Motor cortex
PT	Pyramidal tract
IT	Intratelecenphalic
iCSD	Inverse current source density
CG	Cingulate gyrus
CGS	Cingulate gyrus stimulation
MRI	Magnetic resonance imaging
CT	Computed tomography
PSD	Power spectral density
AC	Activity classifier
MSM	Motor symptom monitor
AAM	Active arm movement

Summary

Deep brain stimulation (DBS) of the subthalamic nucleus (STN) alleviates motor symptoms in Parkinson's disease (PD) patients. However, some patients suffer from cognitive and emotional changes. We hypothesize that by identifying the motor part of the STN, the stimulation field can be positioned such that current spread to the cognitive and limbic territories is prevented therewith reducing side effects. In this thesis, methods to identify the motor part of the STN during DBS surgery will be assessed in order to reduce stimulation-induced behavioral side effects and to optimize the therapeutic benefit. In chapter 2-5, the use of motor cortex stimulation (MCS) to locate the STN motor area is investigated and in chapter 6 a method utilizing spontaneous oscillations in the local field potentials (LFPs) is assessed. To determine the therapeutic benefit of DBS, chapter 7 introduces an advanced ambulant method to quantify motor improvement.

MCS to locate the STN motor area

In chapter 2 and 3, the use of MCS to locate the STN motor area is assessed during DBS surgery. We expect that MCS evokes a spatially specific response within the STN, which identifies the STN motor area. We describe the results of subthalamic neuronal responses to stimulation of the motor cortex (MC) hand area and evaluate the safety of this novel technique. When studying the responses in the unit activity we found that responses differed between regions within the STN. Unit activity is generally considered as a measure of the output activity. To gain more insight into the neuronal input into the STN, we also studied cortically evoked subthalamic LFPs. We show that the cortically evoked LFPs follow a certain temporal and spatial pattern. The significant peaks of the evoked LFPs coincide with the timing of some of the inhibitions and excitations present in the unit responses. In conclusion, we saw that MCS evokes responses in the unit activity specifically within certain areas of the STN. The spatial resolution of responses measured in the LFP to MCS is not high enough to identify the STN motor region. However, this might be improved by the development of novel DBS electrodes. In order to safely use MCS evoked responses during DBS surgery the current density should be lowered or biphasic pulses should be used to prevent seizures.

Based on these first findings, two aspects were investigated in more detail in chapter 4 and 5: Stimulation of the MC and sensing of the STN response. To evaluate what happens at a neuronal level during MCS, a MCS model with a 3D

representation of several axonal populations was developed in chapter 4. The model focuses on selective stimulation of certain neuronal populations in the MC in relation to chronic stimulation for PD. It can, however, also be used for the purpose to improve selective stimulation of the cortical neuronal populations evoking the STN response. The MC is connected to the STN through the hyperdirect pathway, which originates from pyramidal tract (PT) type axons, and the indirect pathway, which originates from intratelencephalic (IT) type axons. To evoke a subthalamic response with MCS, those axon types should be activated while the activation of inhibiting Basket cell axons should be avoided. The model predicts that PT and IT type pyramidal axons can be selectively targeted by using anodal rather than cathodal and bipolar stimulation, during which PT type axons are activated in relatively larger quantities than IT type axons. As we used cathodal and bipolar stimulation during the experiments described in chapter 2 and 3, there is room left for improvement on this part.

To interpret the subthalamic response to MSC, we assess an approach enabling computation of the sources and sinks of the neuronal input in the STN in chapter 5. This approach involves the inverse current source density (iCSD) method to estimate the CSD from cortically evoked LFPs in the STN. We assess this new approach by studying the cortically evoked potentials in a three dimensional grid in anesthetized rats. The analysis showed that the sink corresponding to the direct input from the MC was located medial to the source of the globus pallidus input. Furthermore, the inputs of the paths evoking the long inhibitory period after MCS and cingulate gyrus stimulation are located in the same STN area. CSD analysis of our experiments resulted in clear and well discriminable sources and sinks of the neuronal input activity in the STN. Therefore, the method could also be applicable to the human experiments described in chapter 2 and 3, although a novel electrode design and an adaptation to the method would be required in that case.

Measuring spontaneous subthalamic activity to locate the STN motor area

In chapter 6, we evaluated the spatial distribution of beta and gamma LFP activity in the STN and assessed its potential use to locate the STN and STN sub-areas during DBS surgery. Unit activity and LFPs were measured simultaneously in 25 PD patients undergoing DBS surgery. The beta and gamma oscillations were assessed in the sensorimotor and non-sensorimotor STN and areas outside

of the STN. We found a pronounced increase in LFP power within the gamma band throughout the entire STN. LFPs in the beta frequency band had a significantly higher power in the sensorimotor STN compared to the non-sensorimotor STN. From these data, we can conclude that LFP gamma oscillations may provide a useful tool for locating the borders of the STN, and LFP beta oscillations could be used to locate the dorsolateral sensorimotor area within the STN.

Evaluation of the therapeutic benefit of deep brain stimulation

Ambulatory monitoring of motor symptoms in PD can improve our therapeutic strategies. Especially for patients receiving DBS, it would be useful to study symptoms separately while distinguishing between several body parts: As the STN is functionally segregated, the placement of the DBS electrode can have a differential effect on several aspects of motor function. Therefore, a tool that is able to assess each aspect individually offers an important additional feature. Previously published monitors usually assess only one or a few basic aspects of the cardinal motor symptoms in a laboratory setting. Chapter 7 describes a novel ambulatory monitoring system that provides a complete motor assessment by simultaneously analyzing current motor activity of the patient (e.g. sitting, walking) and the severity of many aspects related to tremor, bradykinesia, and hypokinesia.

The monitor consists of a set of four inertial sensors and is assessed in seven healthy controls and six PD patients treated with STN DBS. The monitor proved very accurate in discriminating between several motor activities. Monitor output correlated well with blinded UPDRS ratings for different DBS amplitudes. The combined analysis of motor activity and symptom severity by our PD monitor brings true ambulatory monitoring of a wide variety of motor symptoms one step closer.

Samenvatting

Diepe hersenstimulatie van de subthalamische kern zorgt voor de vermindering van motororische symptomen bij de ziekte van Parkinson. Sommige patiënten hebben echter last van cognitieve en emotionele bijwerkingen. Onze hypothese is dat door het motor gedeelte in de STN te identificeren, men het stimulatie veld dusdanig kan positioneren dat stroomspreiding in de gebieden verantwoordelijk voor cognitieve en limbische functies voorkomen kan worden. Methodes hiervoor zullen in dit proefschrift worden onderzocht om stimulatie-geïnduceerde bijwerkingen te reduceren en de therapeutische effectiviteit the optimaliseren. Om het subthalmische motor gebied te identificeren wordt in hoofdstuk 2-5 het gebruik van motor cortex (MC) stimulatie (MCS) onderzocht en in hoofdstuk 6 het gebruik van spontane oscillaties in de locale veldpotentialen (LFPs). Om het therapeutische effect van diepe hersenstimulatie te bepalen wordt in hoofdstuk 7 een geavanceerde, ambulante methode om motorische verbetering te kwantificeren geïntroduceerd.

MCS om het motorische gebied in de STN te lokaliseren

In hoofdstuk 2 en 3 wordt het gebruik van MCS om het motorische gebied in de STN te lokaliseren onderzocht tijdens DBS chirurgie. We verwachten dat MCS een spatieel specifieke respons binnen de STN veroorzaakt, welke gebruikt kan worden om het motorische gebied van de STN te identificeren. We beschrijven resultaten van subthalamische neuronale responsies op stimulatie van het hand gebied in de MC. Ook de veiligheid van deze nieuwe techniek wordt geëvalueerd. Aan de hand van metingen aan het vuurgedrag van de neuronen hebben we een verschil in responsie bij verschillende STN gebieden gevonden. Het vuurgedrag wordt over het algemeen beschouwd als de output van neuronale activiteit. Om meer inzicht te verkrijgen in de neuronale input hebben we ook de corticaal opgewekte LFPs bestudeerd. De responsies zichtbaar in het LFP bleken een specifiek temporeel en spatieel patroon te volgen. De significante pieken in de corticaal opgewekte LFPs komen qua timing overeen met de significante inhibities en excitaties die zichtbaar waren in het vuurgedrag van de neuronen. We kunnen concluderen dat in bepaalde STN gebieden MCS specifieke veranderingen opwekt in het vuurgedrag van de neuronen. De spatiële resolutie van corticaal opgewekte LFP responsies is in tegenstelling tot het vuurgedrag van de neuronen niet hoog genoeg om het motor gebied in de STN te kunnen identificeren. Dit zou echter nog verbeterd kunnen worden door de ontwikkeling

van nieuwe DBS elektrodes. Om MCS veilig toe te kunnen passen tijdens DBS chirurgie en een epileptisch insult te voorkomen moet de stroomdichtheid verlaagd worden of kunnen er bifasische pulsen gebruikt worden.
Naar aanleiding van deze bevindingen zijn in hoofdstuk 4 en 5 twee aspecten in meer detail onderzocht: Stimulatie van de MC en meting van de STN responsie. In hoofdstuk 4 is onderzocht wat er gebeurt op neuronaal niveau tijdens MCS. Voor dit doel is een MCS model met een 3D representatie van verscheidene axonale populaties ontwikkeld. Het model is gericht op selectieve stimulatie bij chronische stimulatie voor de behandeling van de ziekte van Parkinson. Het kan echter ook gebruikt worden om selectieve stimulatie te verkrijgen van corticale neuronale populaties die de responsie in de STN veroorzaken. De connectie tussen de MC en de STN bestaat uit een hyperdirect pad, welke zijn oorsprong heeft in pyramidal tract (PT) axonen, en het indirect pad, welke zijn oorsprong heeft in intratelencephalic (IT) axonen. Deze axonen moeten worden gestimuleerd om een responsie in de STN te veroorzaken met MCS. Daarbij moet stimulatie van de inhiberende Basket cell axonen voorkomen worden. Het model voorspelt dat PT en IT axonen selectief kunnen worden gestimuleerd met behulp van anodale stimulatie. Hierbij worden naar verhouding meer PT dan IT axonen geactiveerd. Gedurende de experimenten in hoofdstuk 2 en 3 hebben we cathodale en bipolaire stimulatie gebruikt, dus hier liggen verbeterpunten.
In hoofdstuk 5 onderzoeken we een methode om de stroombronnen en stroomputten van de neuronale input in de STN te kunnen bepalen. Dit biedt ons de mogelijkheid om de subthalamische responsie ten gevolge van MSC beter te kunnen interpreteren. Deze methode maakt gebruikt van de “inverse current source density” (iCSD) aanpak om de CSD van corticaal opgewekte subthalamisch LFPs te kunnen schatten. We hebben deze methode onderzocht in ratten, waarbij we corticaal opgewekte potentialen in een 3D raster hebben gemeten. De analyse laat zien dat de stroomput behorende bij de directe input vanuit de MC mediaal ligt ten opzichte van de stroombron behorende bij de globus pallidus input. Ook lieten de resultaten zien dat de input van de paden welke de lange inhibitoire periode veroorzaken na MCS en cortex cingularis stimulatie in hetzelfde subthalamische gebied liggen. CSD analyse van onze experimenten resulteerde in duidelijke onderscheidbare stroombronnen en –putten van de neuronale input in de STN. Daarom zou de iCSD methode ook bruikbaar kunnen zijn in experimenten tijdens DBS chirurgie zoals beschreven in

hoofdstuk 2 en 3, hoewel een nieuw elektrode design en modificatie van de methode in dat geval wel essentieel zijn.

Metingen aan spontane subthalamische activiteit om het motorische gebied in de STN te kunnen lokaliseren

In hoofdstuk 6 hebben we de spatiële distributie van beta en gamma LFP activiteit in de STN geëvalueerd, waarbij we voornamelijk de bruikbaarheid hiervan om de STN en subgebieden in de STN te kunnen lokaliseren hebben onderzocht. In 25 patiënten die DBS chirurgie ondergingen hebben we het vuurgedrag en de LFPs simultaan gemeten. Oscillaties in de beta en gamma activiteit zijn onderzocht in sensorimotorische en non-sensorimotorische STN gebieden en gebieden buiten de STN. Het LFP vermogen in de gamma frequentie band was verhoogd in de gehele STN, terwijl LFPs in the beta frequentie band een significant hoger vermogen hadden in het sensorimotorische gebied ten opzichte van het non-sensorimotorische gebied in de STN. We kunnen concluderen dat LFP gamma oscillaties bruikbaar zijn om STN grenzen te kunnen lokaliseren, terwijl de LFP beta oscillaties bruikbaar zijn om het dorsolaterale sensorimotorische gebied binnen de STN te kunnen bepalen.

Evaluatie van de motorische vooruitgang ten gevolge van diepe hersenstimulatie

Het ambulant monitoren van motor symptomen kan therapieën ten behoeve van PD verbeteren. Zeker in het geval van DBS patiënten zou het nuttig zijn om symptomen apart te kunnen bestuderen terwijl verschillende lichaamsdelen ook onderscheiden worden: Aangezien de STN functioneel gesegregeerd is, kan de plaatsing van de DBS electrode een verschillend effect hebben op verscheidene motorische functies. Daarom is een apparaat wat de verschillende aspecten individueel kan beoordelen belangrijk. Eerder gepubliceerde monitors bestuderen over het algemeen een paar basis motorische symptomen in een laboratorium omgeving. Hoofdstuk 7 beschrijft een nieuw ambulant meetsysteem welke een complete motorische evaluatie biedt door simultaan de huidige motorische activiteit (bijvoorbeeld zitten of liggen) en de ernst van meerdere aspecten gerelateerd aan tremor, bradykinesie en hypokinesie te onderzoeken.
De monitor bestaat uit vier inertiële sensoren en is onderzocht in zeven gezonde controlepersonen en zes PD patiënten die behandeld worden met STN DBS. De monitor kon motorische activiteiten met een hoge nauwkeurigheid

onderscheiden. De output van de monitor correleerde goed met geblindeerde UPDRS scores voor verschillende DBS stimulatie niveaus. De gecombineerde analyse van motorische activiteit en de ernst van PD symptomen brengt echte ambulante monitoring van een breed scala aan motorische symptomen een stap dichterbij.

Dankwoord

Het is zover, het proefschrift is bijna af. Na een aantal jaren hard, maar vooral ook met erg veel plezier werken is het resultaat klaar. Natuurlijk heb ik dit niet alleen kunnen doen en hierbij hulp gehad van een aantal mensen.
Uiteraard wil ik beginnen met het bedanken van mijn dagelijks begeleidster en assistent-promotor Ciska Heida. Ciska, bedankt voor de afgelopen jaren. Ik heb onze samenwerking altijd als erg prettig ervaren. Je had altijd veel goede tips bij de analyse van de data. Ook wist je vaak net de goede punten uit mijn artikelen te halen om ze met een kleine wijziging enorm te verbeteren. We hebben ook heel wat reizen samen naar Maastricht afgelegd. De ritten waren vaak erg gezellig en gelukkig konden we over veel meer dan alleen werk praten.
Ook wil ik graag mijn promotor, Peter Veltink, bedanken. Ik heb ontzettend veel aan je gehad bij het reviewen van de artikelen. Ook het opstellen van een goed promotie-plan zag jij als belangrijk punt en dat heeft me erg geholpen om richting te geven aan vier jaar promotie.
Gedurende mijn gehele promotie heb ik een nauwe samenwerking gehad met Mark Janssen, Veerle Visser-Vandewalle en Yasin Temel van het academisch ziekenhuis Maastricht. Bedankt voor de goede samenwerking. Mark, jou wil ik in het bijzonder bedanken. We hebben bij een aantal studies heel nauw samengewerkt en daarbij hebben we naar mijn mening ontzettend veel aan elkaar gehad. Jij kon mij helpen met het klinische en experimentele gedeelte en ik jou met analyse technieken. De communicatie verliep altijd erg goed en ik kan me nog herinneren dat we op een zonnige zondagavond heerlijk een biertje op het terrasje hebben gedronken. Bedankt voor deze goede samenwerking.
Tijdens mijn promotie ben ik in contact gekomen met Lo Bour. Het begin van een nauwe en vruchtbare samenwerking. We hebben samen veel metingen gedaan tijdens DBS-operaties in het Amsterdam medisch centrum. Het was erg leuk om zo dicht bij de kliniek te staan. We hebben veel overleg gehad over de analyse van de signalen en daarbij heb ik erg veel aan je expertise gehad.
Ik wil ook graag Hubert Martens van Sapiens steering brain stimulation bedanken. Vooral bij het modelwerk heb jij veel kunnen betekenen. Ik heb zelfs nog een drietal weken in Eindhoven mogen komen werken om het model goed uit te kunnen werken met behulp van jullie ervaring. Bedankt dat je je expertise met mij wilden delen.
To conduct the rat-experiments, I was allowed to use the facilities of Abdelhamid Benazzouz, Université de Bordeaux. Thank you for allowing Mark to perform my experiments in your laboratories and for the useful comments on the resulting paper.

Mijn promotie is uitgevoerd binnen het Braingain project. Ik wil al mijn braingain-collega's bedanken.
De meeste tijd van mijn promotie heb ik uiteraard doorgebracht binnen de vakgroep Biomedische signalen en systemen. Daarom wil ik graag al mijn collega's bedanken voor een ontzettend leuke en gezellige tijd. Het eten van ijsjes bij van der Poel en de lunches bij de faculty club zal ik echt gaan missen.
In het bijzonder wil ik Peter en Eva bedanken. Voor onze promotie hebben we alle drie tegelijkertijd onze master opdracht uitgevoerd, ook binnen BSS. De gezelligheid in het studentenhok heeft zich uiteraard voortgezet tijdens ons promotie project. Toen we al niet meer allemaal op de vakgroep zaten hebben we nog regelmatig van een etentje bij la cucina mogen genieten. Peter, ik heb je regelmatig lastig gevallen met een praatje tijdens werk. Zeker toen ik een tijdje zo'n beetje alleen op mijn kamer zat, moest je er vaak aan geloven. Het was altijd erg gezellig. Eva, wij hebben een hele tijd samen hardgelopen in de pauze. Zelfs een aantal loopjes samen afgelegd. Inmiddels ben ik weer wat minder sportief, maar wie weet kunnen we in de toekomst nog eens samen een loopje doen?
Ook wil ik Esther en Jan bedanken. Toen ik bij BSS begon kwam ik op de kamer bij jullie. Jullie zaten al een hele tijd samen op de kamer, maar ik vond het gelijk leuk om er bij te komen. We hebben altijd erg gezellig kunnen kletsen en heel wat weetjes uitgewisseld.
Mijn nieuwe kamergenoten wil ik ook bedanken. Lamia en Josien, bedankt voor de gezelligheid op de kamer. Ook Heidi wil ik graag bedanken voor de leuke momenten als collega's binnen BSS.
Bij het doen van mijn onderzoek heb ik hulp gehad van een aantal studenten. Ten eerste mijn master-studenten Kees en Evita. Kees, bedankt voor het uitwerken van de CSD analyse methode. Evita, bedankt voor het uitvoeren van vele metingen in het AMC en uitwerken daarvan. Jullie zijn nu beide promovendus geworden, erg leuk om te horen! Heel veel succes daarbij. Ook mijn bachelor-studenten Tamar en Matthijs wil ik bedanken voor hun bijdrage aan mijn onderzoek.
Naast mijn promotiewerk hebben een heel aantal vriendinnen gelukkig kunnen zorgen voor de broodnodige afleiding. In het bijzonder wil ik noemen: Marjolein, Danielle, Daphne en Esther bedankt voor alle gezelligheid.
Mijn familie verdient natuurlijk ook een plaats in het dankwoord. Papa, jij bent als doctor een inspiratie voor me geweest. Mama, jij hebt me altijd gesteund door dik en dun. Myrto en Ruben, ondanks dat we ver uit elkaar wonen, hebben we het altijd gezellig als we elkaar weer zien en spreken we elkaar nog vaak via MSN wat ook voor de welkome afleiding heeft gezorgd tijdens mijn promotie.
Ten slotte, wil ik mijn man Ardjan en onze dochter Jinte, die tijdens mijn promotie ons leven heeft verrijkt, bedanken. Ardjan, bedankt voor je steun

gedurende de hele promotie. Dat was niet altijd makkelijk, maar gelukkig begrijpen we elkaar aangezien we beiden in dit traject zitten. Bedankt, dat je er altijd voor me bent en voor alle liefde die je geeft. Ik ben nog elke dag blij dat we er voor elkaar kunnen zijn om van elkaar kunnen blijven houden.

Biography

Daphne Zwartjes was born on August 25th 1983 in Nijmegen, the Netherlands. Daphne holds an MSc degree in Biomedical Engineering. She studied Biomedical Engineering from 2002-2008. Her master assignment was called: "The development of a monitoring system to assess movement control in patients with Parkinson's disease". In 2008, she received her Master degree and started her PhD at the department of Biomedical systems and systems.
Her PhD research, 2008-2013, focuses on deep brain stimulation in Parkinson's disease. The aim was to develop methods for more accurate and more selective targeting of the motor area of the subthalamic nucleus. Her work is part of the BrainGain project.
Currently, Daphne works as a project manager within Demcon Advanced Mechatronics. Demcon is a company specialized in high-tech mechatronic systems and products with a focus on research, development and production.

List of publications

Journal articles

Zwartjes, D.G.M., Heida, T., van Vugt, J.P.P., Geelen, J.A.G. and Veltink, P.H., Ambulatory monitoring of activities and motor symptoms in Parkinson's disease. IEEE T Bio-Med Eng, 2010. **57**(11): p. 2778-2786.

*Zwartjes, D.G.M., *Janssen, M.L.F., Heida, T., Van Kranen-Mastenbroek, V., Bour, L.J., Temel, Y., Visser-Vandewalle, V. and Veltink, P.H., Cortically evoked potentials in the human subthalamic nucleus. Neurosci Lett, **539**: p. 27-31.

Zwartjes, D.G.M., Heida, T., Feirabend, H.K.P., Janssen, M.L.F., Visser-Vandewalle, V., Martens, H.C.F. and Veltink, P.H., Motor cortex stimulation for Parkinson's disease: a modeling study. J Neural Eng, **9**(5): 056005

*Janssen, M.L.F., *Zwartjes, D.G.M., Temel, Y., Van Kranen-Mastenbroek, V., Duits, A., Bour, L.J., Veltink, P.H., Heida, T., Visser-Vandewalle, V., Subthalamic neuronal responses to cortical stimulation. Mov Disord 2012. **27**(3): p. 435-438.

Janssen, M.L.F., Zwartjes, D.G.M., Tan, S.K.H., Vlamings, R., Jahanshahi, A., Heida, T., Hoogland, G., Steinbusch, H.W.M., Visser-Vandewalle, V. and Temel, Y., Mild dopaminergic lesions are accompanied by robus changes in subthalamic nucleus activity. Neurosci Lett, 2012. **508**(2), p. 101-105.

Zwartjes, D.G.M., Janssen, M.L.F., van Dijk, K.J., Temel, Y., Visser-Vandewalle, V., Veltink, P.H., Benazzouz, A. and Heida, T., Current source density analysis of cortically evoked potentials in the rat Subthalamic Nucleus.

Zwartjes, D.G.M., Heida, T., Wiegers, E.C., Verhagen, R., de Bie, R.M.A., Contarino, M.F., van den Munckhof, P., Schuurman, P.R., Veltink, P.H., Martens, H.C.F. and Bour, L.J., Different spatial distribution of neural beta and gamma activity of the subthalamic nucleus in Parkinson's disease.

*Both authors contributed equally to this manuscript.

Conference contributions

Zwartjes, D.G.M., Heida, T. and Veltink, P.H., Motor cortex stimulation: The significance of modelling axon collaterals. The 3rd Dutch BME conference, Egmond aan Zee, 2011.

Janssen, M.L.F., Zwartjes, D.G.M., Temel, Y., van Kranen-Mastenbroek, V., Magill, P., Vektink, P.H., Heida, T. and Visser-Vandewalle, V., Subthalamic responses to motor cortex stimulation: Selective targeting of the subthalamic motor area. 40th annual meeting Society for Neuroscience, San Diego, 2010.

de Klerk, D.G.M., Heida, T., Modeling motor cortex stimulation to excite the Subthalamic nucleus via different pathways in human, INS congress, Seoul, 2009.

Martens, H., Toader, E., de Klerk, D.G.M., Neurostimulation safety limits: A modeling study. 4th Ann. Symp. IEEE-EMBS Benelux Chapter Proceedings, Enschede, 2009.

de Klerk, D.G.M., van Vugt, J.P.P., Geelen, J.A.G. and Heida, T., A long-term monitor including activity classification for motor assessment of Parkinson's disease patients, 4th European Conference IFMBE Proceedings, Antwerp, vol. 22, p.p. 1706-1709, 2008.